

Displacement of Oil by Carbon Dioxide

Annual Report
for the period
October, 1980 - September, 1981

F.M. Orr, Jr. and J.J. Taber
Principal Investigators
New Mexico Petroleum Recovery Research Center
Socorro, New Mexico

Contributors:

R.E. Bretz
B.T. Campbell
M.L. Graham
C.M. Jensen
C.L. Lien
M.T. Pelletier
M.K. Silva

L.A. Noll
Technical Project Officer
Bartlesville Energy Technology Center
Bartlesville, Oklahoma

Prepared for the Department of Energy
Under Contract No. DE-AS19-80BC10331

81-49

November 1981

NOTICE

This report was prepared as an account of work sponsored by an agency of the United States Government. Neither the United States Government nor any agency thereof, nor any of their employees, makes any warranty, express or implied, or assumes any legal liability or responsibility for the accuracy, completeness, or usefulness of any information, apparatus, product, or process disclosed, or represents that its use would not infringe privately owned rights. Reference herein to any specific commercial product, process, or service by trade name, trademark, manufacturer, or otherwise, does not necessarily constitute or imply its endorsement, recommendation, or favoring by the United States Government or any agency thereof. The views and opinions of authors expressed herein do not necessarily state or reflect those of the United States Government or any agency thereof.

TABLE OF CONTENTS

	<u>PAGE</u> <u>NO.</u>
LIST OF TABLES	i
LIST OF FIGURES	ii
ABSTRACT	viii
1. Introduction	1
2. Displacement Experiments	3
2.1 Literature Review	3
Single Phase Displacements	3
Multiphase Displacements	14
2.2 Results of Displacement Experiments	16
2.3 Conclusions	34
3. Supporting Measurements: Phase Behavior and Fluid Properties of CO ₂ -Crude Oil Mixtures	38
3.1 Volumetric Behavior of CO ₂ -Crude Oil Mixtures	38
Maljamar Recombined Reservoir Fluid	38
Wasson Stock Tank Oil	47
3.2 Phase Compositions and Fluid Properties: Measurement by the Continuous Multiple Contact Experiment	50
Experimental Apparatus	50
Measurement of Phase Viscosities	62
CMC Displacements in Binary Systems	65
CMC Displacement Results: CO ₂ -Separator Oil Systems	78
CMC Displacement Results: CO ₂ -Maljamar Recombined Reservoir Fluid	90
3.3 Conclusions	93

LIST OF TABLES

	<u>PAGE NO.</u>
Table 2.1 Properties of Core Materials	19
Table 2.3 Summary of Miscible Displacements	26
Table 3.1 Composition of Maljamar Solution Gas, Separator Oil and Recombined Reservoir Fluid	39
Table 3.2 Operating Conditions and Fluid Properties for Continuous Multiple Contact Displacements of Decane by CO ₂ at 160°F	72
Table 3.3 Volume Change on Mixing of CO ₂ with Decane at 160°F	74
Table 3.4 Comparison of Instantaneous and Averaged Compositions for CO ₂ and C ₁₀ at 1250 psia, 160°F	76

	PAGE <u>NO.</u>
4. Interpretation of Experiments and Application to Field Problems	97
4.1 Effect of Solution Gas on Local CO ₂ -Crude Oil Displacement Efficiency	97
4.2 Two-Dimensional Simulation of CO ₂ Flood Performance	103
4.3 Conclusions	107
5. Summary	108
Acknowledgement	110
References	111
Research Presentations	116
Research Participants	118

LIST OF FIGURES

	<u>PAGE NO.</u>
Figure 2.1 Dependence of dispersion coefficients on flow velocity for sandstone samples	7
Figure 2.2 Dependence of mass transfer coefficients on flow velocity for sandstone samples	8
Figure 2.3 Dependence of dispersion coefficients on flow velocity for carbonate core samples	9
Figure 2.4 Dependence of mass transfer coefficients on flow velocity for carbonate core samples	10
Figure 2.5 Dependence of flowing fraction on flow velocity for carbonate core samples	11
Figure 2.6 Dependence of flowing fraction on flow velocity for carbonate core samples	13
Figure 2.7 Schematic of equipment used to perform miscible core floods	17
Figure 2.8 Schematic of equipment used to prepare cores for simultaneous miscible displacements in two flowing phases	18
Figure 2.9 Viscosities of ethylbenzene and ethylbutyrate at various temperatures	22
Figure 2.10 Densities of ethylbenzene and ethylbutyrate at various temperatures	23
Figure 2.11 Viscosity of mixtures of ethylbenzene and ethylbutyrate at 25°C	24
Figure 2.12 Densities of mixtures of ethylbenzene and ethylbutyrate at 25°C	25
Figure 2.13 Compositions of fluids produced during miscible displacements of ethylbenzene and ethylbutyrate in Berea sandstone, runs S1A and S1B	27

	<u>PAGE</u> <u>NO.</u>
Figure 2.14 Compositions of fluids produced during miscible displacements of ethylbenzene and ethylbutyrate in Berea sandstone, runs S3A and S3B	28
Figure 2.15 Comparison of least squares fit and effluent compositions for run S1A	29
Figure 2.16 Dependence of the dispersion coefficient on flow velocity for a Berea sandstone core	31
Figure 2.17 Compositions of fluids produced during miscible displacements of ethylbenzene and ethylbutyrate in a San Andres carbonate core, runs C1A and C2A	32
Figure 2.18 Compositions of fluids produced during miscible displacements of ethylbenzene and ethylbutyrate in a San Andres carbonate core, runs C3A and C3B	33
Figure 2.19 Comparison of compositions of fluids produced during stable and unstable miscible displacements of ethylbutyrate and isopropanol, runs S4 and S5	35
Figure 2.20 Compositions of fluids produced during an unstable displacement of isopropanol by ethylbenzene in a San Andres carbonate core, run C4	36
Figure 3.1 Phase behavior of binary mixtures of CO ₂ with Maljamar recombined reservoir fluid at 90°F	40
Figure 3.2 Phase behavior of binary mixtures of CO ₂ with Maljamar separator oil at 90°F	41
Figure 3.3 Volumetric behavior at 90°F of a mixture containing 60.0 mol % CO ₂ -40.0 mol % Maljamar recombined reservoir fluid	43
Figure 3.4 Volumetric behavior at 90°F of a mixture containing 65.0 mol % CO ₂ -35.0 mol % Maljamar recombined reservoir fluid	44

	<u>PAGE</u> <u>NO.</u>
Figure 3.5 Volumetric behavior at 90°F of a mixture containing 85.0 mol % CO ₂ -15.0 mol % Maljamar recombined reservoir fluid	45
Figure 3.6 Volumetric behavior of Maljamar recombined reservoir fluid at 90°F	46
Figure 3.7 Volumetric behavior at 90°F of CO ₂ -crude oil mixtures with and without solution gas	48
Figure 3.8 Phase behavior of binary mixtures of CO ₂ with Wasson stock tank oil at 105°F	49
Figure 3.9 Comparison of the compositions of Maljamar and Wasson crude oils	51
Figure 3.10 Volumetric behavior at 105°F of a mixture containing 14.2 mol % CO ₂ in Wasson stock tank oil	52
Figure 3.11 Volumetric behavior at 105°F of a mixture containing 34.8 mol % CO ₂ in Wasson stock tank oil	53
Figure 3.12 Volumetric behavior at 105°F of a mixture containing 60.4 mol % CO ₂ in Wasson stock tank oil	54
Figure 3.13 Swelling of Maljamar and Wasson crude oils by dissolved CO ₂	55
Figure 3.14 Volumetric behavior at 105°F of a mixture containing 80.0 mol % CO ₂ in Wasson stock tank oil	56
Figure 3.15 Volumetric behavior at 105°F of a mixture containing 90.0 mol % CO ₂ in Wasson stock tank oil	57
Figure 3.16 Volumetric behavior at 105°F of a mixture containing 95.0 mol % CO ₂ in Wasson stock tank oil	58
Figure 3.17 Schematic of the apparatus for measurement of phase compositions by continuous multiple contacts	59

	<u>PAGE</u> <u>NO.</u>
Figure 3.18 High pressure cell for a vibrating quartz crystal viscometer	61
Figure 3.19 Schematic of the apparatus for evaluation of electrode coatings	64
Figure 3.20 Density of CO ₂ -C ₁₀ mixtures at 1250 psia and 160°F	67
Figure 3.21 Comparison of predicted and experimental rates of production of CO ₂ and C ₁₀ during a CMC displacement at 1250 psia and 160°F	69
Figure 3.22 Comparison of predicted and experimental cumulative production of CO ₂ and C ₁₀ during a CMC displacement at 1250 psia and 160°F	70
Figure 3.23 Phase composition for the CO ₂ -C ₁₀ system in two-phase region	71
Figure 3.24 Density vs. pressure of a CO ₂ -C ₁₀ mixture in two-phase region	71
Figure 3.25 Effect of changing compositions during a sampling period on apparent compositions of the samples	77
Figure 3.26 Predicted overall compositions and vapor phase volume fractions for a CMC displacement of C ₁₀ by CO ₂ at 160°F	79
Figure 3.27 Comparison of weight fractions of liquids in upper and lower samples taken in CMC displacements of Maljamar separator oil at 800, 1200, and 1400 psia and 90°F	80
Figure 3.28 Effect of increasing pressure on weight fractions of hydrocarbon liquids in upper (U) and lower (L) samples	82
Figure 3.29 Smoothed compositions of upper phase gas samples from a CMC displacement of Maljamar separator oil by CO ₂ at 1400 psia and 90°F	83

	<u>PAGE</u> <u>NO.</u>
Figure 3.30 Comparison of compositions of liquid hydrocarbon samples taken before, just after, and well after the appearance of the CO ₂ -rich phase in a CMC displacement of Maljamar separator oil by CO ₂ at 1200 psia and 90°F	85
Figure 3.31 Comparison of compositions of hydrocarbons in upper phase samples taken just after the appearance of the CO ₂ -rich phase	86
Figure 3.32 Pseudo-ternary representation of phase compositions for mixtures of CO ₂ with Maljamar separator oil at 800 psia and 90°F	87
Figure 3.33 Pseudo-ternary representation of phase compositions of mixtures of CO ₂ with Maljamar separator oil at 1200 psia and 90°F	88
Figure 3.34 Pseudo-ternary representation of phase compositions of mixtures of CO ₂ with Maljamar separator oil at 1400 psia and 90°F	89
Figure 3.35 Densities of phases present during CMC displacements of Maljamar separator oil at 800, 1200, and 1400 psia and 90°F	91
Figure 3.36 Comparison of weight fractions of hydrocarbon liquids in upper and lower samples for CMC displacements at 90°F of Maljamar separator oil at 1200 psia and Maljamar recombined reservoir fluid (RRF) at 2500 psia	92
Figure 3.37 Pseudo-ternary representation of phase compositions of mixtures of CO ₂ with Maljamar recombined reservoir fluid at 2500 psig and 90°F	94
Figure 3.38 Pseudo-ternary representation of phase compositions of mixtures of CO ₂ with Maljamar separator oil at 1200 psia and 90°F	95

	<u>PAGE</u> <u>NO.</u>
Figure 4.1 Phase behavior of a CO ₂ -crude oil system with solution gas present	99
Figure 4.2 Phase behavior of a CO ₂ -crude oil system without solution gas	100

ABSTRACT

Progress of a comprehensive research program to quantify factors affecting CO₂ flood displacement efficiency is described. Experimental and theoretical investigations of the interactions of factors such as phase behavior and fluid properties of CO₂-crude oil mixtures, and heterogeneities in reservoir rocks are discussed.

Literature on the interpretation of miscible displacements in one- and two-phase systems is reviewed. Simple displacement experiments to evaluate effects of core heterogeneities and high mobile water saturations are described. Results of miscible displacement experiments with fluids of matched density and viscosity are presented and compared with results of a few displacements in which fluid properties were not matched. Those comparisons clearly indicate that control of viscous fingering is required if short core floods are to be interpreted with reasonable certainty.

Detailed results of investigations of the phase behavior of CO₂-crude oil mixtures are presented. The volumetric behavior of mixtures of CO₂ with dead oils from the Wasson and Maljamar fields are compared with that of a Maljamar recombined reservoir fluid. The results provide the basis for a qualitative analysis of the effects of the presence of solution gas on CO₂ flood performance.

Modifications to improve the continuous multiple contact experiment, which efficiently measures phase compositions and fluid properties, are described. An analysis of the operation of the apparatus is given for binary systems. The theory is compared with experimental results for CO₂-decane displacements, with excellent agreement. Extensive results of experiments to measure compositions and densities of phase present for CO₂-crude oil mixtures are reported.

Finally, formulation of a mathematical model with which the relative importance of factors such as phase behavior, fluid property variations, heterogeneity, and viscous and gravitational instabilities is discussed.

1. INTRODUCTION

CO₂ flooding is a process which operates on a variety of scales. At the pore level, mixing of CO₂, oil and water is controlled partly by diffusion and partly by the convective mixing which results from the motion of phases containing the various components present. That motion is influenced, in turn, by the saturations of the phases and their distribution in the pores, the interfacial tensions between phases and, of course, their densities and viscosities. On a reservoir scale, vertical and horizontal heterogeneity, gravity segregation of injected fluids, and viscous instability will act to reduce the efficiency with which the reservoir is swept. On an intermediate scale, viscous fingering interacts with longitudinal and transverse dispersion as well as with local heterogeneity.

Prediction of the efficiency of a given CO₂ displacement requires some sort of assessment of the relative importance of the various process mechanisms. An ideal predictive scheme would model accurately all the important process mechanisms on all the appropriate scales of the displacement. In principle, then, the relative importance of the individual process mechanisms would emerge from the calculation, and no a priori estimates of the magnitudes of individual effects would be required. In practice, however, such a detailed description of the process or of the structure and properties of the reservoirs is beyond the capabilities of current computational and reservoir description technology. The three types of reservoir simulators - miscible, compositional and hybrid miscible-compositional - currently used to make performance predictions for CO₂ floods reflect that fact. Miscible simulators (Todd and Longstaff 1972) treat CO₂ as completely miscible with oil and therefore, do not model effects of phase behavior and component transfer between phases. Such simulators do, however, attempt to model the effects of viscous fingering through the use of a "mixing parameter." The model is a simple one and is not based on an analysis of the physics of the growth of viscous fingers. Nevertheless, it is the only simulation approach currently available which attempts any treatment of viscous instability on a reservoir scale.

Compositional simulators (McDonald 1971; Nolen 1973; Kazemi et al 1978; Fussell and Fussell 1977; Coats 1979; and Sigmund et al 1979) follow the transport of individual components (or pseudo-components). The distribution of components between phases is calculated using convergence pressure correlations for equilibrium K-values (McDonald 1971; Nolen 1973; and Kazemi et al 1978) or an equation of state (Fussell and Fussell 1977; Coats 1979; and Sigmund et al 1979). Phase viscosities and densities are calculated then from phase compositions. Thus, compositional simulators attempt to represent the details of phase behavior and fluid property variations in a displacement process, but do not account for viscous fingering. In addition, compositional simulations are affected by numerical dispersion which alters the calculated composition path, and hence, the calculated process efficiency.

A hybrid miscible-compositional simulator, such as that described by Todd (1979), does not attempt to calculate component partitioning in as much detail

as the compositional simulators described above. It treats CO₂ as miscible with the oil at pressures above an experimentally determined "minimum miscibility pressure (MMP)", models viscous fingering of CO₂ through a mixing parameter model (Todd and Longstaff 1972), but provides some capability to model component distribution between phases when the local pressure falls below the MMP.

Thus, each of the simulators currently available models only part of the process mechanisms which operate in a CO₂ flood. Improvements to the process models that form the basis for those simulators will require better understanding of the relationships between microscopic and macroscopic aspects of the displacement process. The project described in this report is aimed at improving understanding of several fundamental features of any tertiary CO₂ flood: (1) the efficiency of local mixing of CO₂ and trapped oil droplets, which may be shielded by water; (2) the compositions, densities and viscosities of phases which occur in a CO₂ flood; and (3) the interactions of larger scale flow behavior, gravity segregation and viscous fingering, with local mixing and phase behavior. The approach used here is to make independent measurements of properties which determine process mechanisms, at least where such measurements are possible, and then use the results of those measurements to interpret more complex displacements where several process mechanisms may be operating simultaneously. Thus, the work reported here includes experiments to study effects of pore structure on miscible flood displacement efficiency and separate experiments to study the behavior of CO₂-crude oil mixtures at reservoir conditions.

The experimental portions of this project are reviewed in §2 and §3. In §2, the published literature on trapping (shielding of trapped oil by water), dispersion and dead-end pores is reviewed and initial displacement experiments with fluids of matched density and viscosity are described. In §3, supporting experiments to measure phase behavior and fluid properties of CO₂-crude oil mixtures are described. Results of volumetric phase behavior experiments are reported for two CO₂-crude oil systems, one with and one without solution gas. Additional development work and measurements to validate the continuous multiple contact experiment are reported, as are results of phase compositions and fluid property measurements for Maljamar separator oil at several pressures. Theoretical aspects of the interactions of phase behavior and flow in porous media are discussed in §4. A qualitative assessment of the effect on displacement efficiency of adding solution gas to a dead oil is given. Finally, we return to the question of simulation with a review of options for representation of the interactions of phase behavior, density and viscosity variations in two-dimensional CO₂ floods.

2. DISPLACEMENT EXPERIMENTS

2.1 Literature Review

Single Phase Displacements

Interpretation of displacement experiments from the compositions of produced fluids presents a challenge even for single-phase displacements in linear cores. In miscible displacements, a transition zone develops between the displaced and displacing fluid. As a displacement progresses, the transition zone grows due to molecular diffusion, to mixing caused by nonuniform flow velocities within individual pores (Taylor 1953) and to the mixing which results from differences in flow path length caused by local small-scale heterogeneity in the porous medium. Measurements of the length of that transition zone, say the distance between the 10 and 90 percent concentrations, can be used to calculate a dispersion coefficient (Perkins and Johnston 1963) based on an analogy between molecular diffusion and dispersion (Aronofsky and Heller 1957), which lumps several mixing mechanisms. Thus, the assumption inherent in many interpretations of experimental work on miscible flooding is that flow in a porous rock can be described by convection-diffusion equation of the form

$$\phi \frac{\partial c}{\partial t} + \nabla \cdot (\underline{v} c) - \phi \nabla \cdot D \nabla c = 0 \quad (2.1)$$

where ϕ is the porosity, \underline{v} the Darcy flow velocity, c the local concentration of one component in a binary displacement, and D the dispersion coefficient. Core floods are normally assumed to be one-dimensional, and the velocity is taken as uniform so that

$$\frac{\partial c}{\partial \tau} + \frac{\partial c}{\partial \xi} - \frac{1}{Pe} \frac{\partial^2 c}{\partial \xi^2} = 0, \quad 0 \leq \xi \leq 1 \quad (2.2)$$

where v is the Darcy velocity for flow in the x direction, $\xi = x/L$, $\tau = vt/\phi L$ and $1/Pe = \phi D/vL$, the Peclet number. Thus, in this case, the flow system is characterized by a single parameter, the Peclet number.

The limitations of the simple representation given in equation (2.2) have been reviewed in some detail by Heller (1963). A fundamental assumption inherent in equation (2.2) is that the flow is uniform. Heller demonstrated experimentally and theoretically that the assumption of uniform flow is often not satisfied. He performed a miscible flood in which dyed styrene monomer displaced clear styrene in a Berea sandstone core. After about half a pore volume had been injected, the styrene was polymerized and the core sectioned. There was clear evidence of channeling in a sandstone which is usually assumed

to be relatively uniform. Heller pointed out that the presence of local nonuniformities does not preclude the use of a model of the form given in equation (2.2) as long as the scale over which nonuniformities correlate is small compared to the scale of the displacement. An apparent dispersion coefficient determined for such a porous medium would be larger, however, than that for a truly uniform porous medium. Hence, the apparent longitudinal dispersion coefficient appropriate to a field scale displacement could easily be very different from that measured for laboratory cores.

Nonuniform flow fields can arise from nonuniform fluid properties as well as from nonuniform rock properties. Heller's (1963) derivation of the conditions required for uniform flow illustrates the problem nicely. In vector form, Darcy's law is

$$\nabla p + \frac{\mu}{k} \underline{v} + \rho \underline{g} = 0 \quad (2.3)$$

The curl of equation (2.3) is

$$\frac{\nabla \mu}{k} \times \underline{v} - \frac{\mu}{k^2} \nabla k \times \underline{v} + \frac{\mu}{k} \nabla \times \underline{v} + \nabla \rho \times \underline{g} = 0 \quad (2.4)$$

since $\nabla \times \nabla p = 0$. If the density and viscosity are functions of concentration, then

$$\nabla \times \underline{v} = \left(\frac{\mu'}{\mu} \underline{v} + \frac{\rho' k \underline{g}}{\mu} \right) \times \nabla c + \nabla (\ln k) \times \underline{v} \quad (2.5)$$

where $\mu' = d\mu/dc$, $\rho' = d\rho/dc$, \underline{g} is the gravitational force vector, and \underline{v} is the Darcy velocity. In this form, the contribution of dispersion to the local velocity has been neglected as have variations in porosity. The more general case has also been considered by Heller (1966). If the flow is initially irrotational, as it is in uniform radial or linear displacements, then $\nabla \times \underline{v} = 0$. It will remain so only if the vorticity, $\nabla \times \underline{v}$, vanishes everywhere in the flow. If viscosity and density are independent of concentration, and if permeability does not vary, then each term in equation (2.5) vanishes identically, and the flow will remain uniform. The flow may still remain uniform if there are no permeability variations and if the vector, $\mu'/\mu \underline{v} + \rho'k/\mu \underline{g}$, is aligned with the concentration gradient (Heller 1963, 1966). This will be true, for instance, in slow downward displacements of a viscous, dense fluid by a less viscous, less dense fluid. In that case, gravity forces stabilize an otherwise unstable displacement (Saffman and Taylor 1958; Dumore 1964). Watkins (1978) used gravity segregation to stabilize displacements in CO_2 floods, where phase viscosities and densities are necessarily functions of composition. In the experiments reported below, we use fluids of closely matched density and viscosity to eliminate flow nonuniformities due to variations of fluid properties with composition.

The solution to equation (2.2) for one set of boundary conditions has been given by Aronofsky and Heller (1957). Other boundary conditions have been considered by Aris and Amundson (1957), Brenner (1962), Coats and Smith (1964), and no doubt others. In practice, the solutions do not differ greatly except at early time in the inlet region, and even then, only when the Peclet number is small. The approximate solution

$$\frac{C}{C_0} = \frac{1}{2} \operatorname{erfc} \left\{ \frac{x - vt}{2\sqrt{Dt}} \right\} \quad 0 \leq x \leq L \quad (2.6)$$

where C_0 is the injected concentration (the concentration of i in the porous medium is assumed to be zero until time is zero), and L is the system length, is usually used to determine the dispersion coefficient from effluent composition data (Brigham, Reed, and Dew 1961; Perkins and Johnston 1963).

In the solution given in equation (2.6), the midpoint of the transition zone moves with the displacement velocity v , and the composition profile is symmetric about the midpoint. In standard miscible displacement experiments, the composition profile at a fixed time cannot be observed. Instead, the compositions of fluids passing a fixed point, the core outlet, are measured. A plot of effluent compositions against time (or pore volumes injected) will be slightly asymmetric because the transition zone continues to grow during the time period during which it is produced. In actual displacements, however, observed effluent composition curves are often more asymmetric than can be explained by transition zone growth alone. At the trailing edge of the transition zone, the displaced fluid is recovered more slowly than predicted by equation (2.6). Deans (1963) and Coats and Smith (1964) proposed models to account for the asymmetry. Both models hypothesized that some portion of the porous medium might be stagnant, so that fluid present in such "dead-end pores" would be recovered only by mass transfer into the flowing stream. Deans' model considered mass transfer from dead-end pores, but did not consider effects of longitudinal dispersion in the flowing stream. The model proposed by Coats and Smith accounted for both longitudinal dispersion and mass transfer from dead-end pores. Their model has the form

$$f \frac{\partial c}{\partial \tau} + (1 - f) \frac{\partial c^*}{\partial \tau} + \frac{\partial c}{\partial \xi} - \frac{1}{Pe} \frac{\partial^2 c}{\partial \xi^2} = 0 \quad (2.7)$$

where c is now the concentration in the flowing stream, f the flowing fraction, c^* the concentration in the stagnant volume, $K_m = \phi KL/v$, and K the mass transfer coefficient. At its heart, the Coats-Smith model is an attempt to represent the heterogeneity of the rock. It does so by using two additional parameters, the flowing fraction, f , and the dimensionless mass transfer coefficient, K_m , to describe the flow. Unfortunately, there is no simple way to measure f and K_m independently. Instead, the parameters are determined by history matching effluent composition data.

Multi-variable curve fits of the type required to history match effluent composition data can be difficult to perform because the parameters may not be completely independent. For instance, if the flowing fraction, f , is near one, the calculated results are not sensitive to the value of the mass transfer coefficient, K . In fact, K calculated for large values of K may be very close to that obtained for small values of K and large values of D . Thus, it may be difficult to determine parameters uniquely, especially when the experimental results also exhibit scatter.

Interpretations of miscible displacement experiments based on the Coats-Smith model have been reported for sandstones by Baker (1977); Batycky, Maini, and Fisher (1980); and Spence and Watkins (1980). Figures 2.1 and 2.2 summarize dispersion and mass transfer coefficients reported for Berea sandstone cores. Even the dispersion coefficients (Figure 2.1) show substantial scatter, though a trend of increasing D with increasing velocity is clearly evident. Mass transfer coefficients showed much more scatter, probably because the flowing fractions determined for the sandstone cores were close to one. In fact, Baker (1977) found the flowing fractions to be exactly one for the three displacements conducted in Berea cores and hence reported no mass transfer coefficients. Spence and Watkins (1980) reported flowing fractions ranging from 0.946 to 0.997 for sandstone cores, so again, mass transfer coefficients were probably only weakly determined. Batycky, Maini, and Fisher (1980) also found flowing fractions to be above 0.9 for a Berea core. While several authors have argued that the mass transfer coefficient probably depends on the flow velocity, the data in Figure 2.2 provide little guidance as to the relationship.

Extensive displacement-miscible displacement data for carbonate cores have been reported by Baker (1977); Batycky, Maini, and Fisher (1980); and Spence and Watkins (1980). Dispersion coefficients determined using the Coats-Smith model are collected in Figure 2.3. As for sandstones, a clear dependence on velocity is observed, though at any given velocity the range of coefficients is nearly two orders of magnitude, as might be expected given the variations in heterogeneity from core to core. Mass transfer coefficients for the carbonate cores are reported in Figure 2.4. With some imagination, a velocity dependence can be discerned. Again, the range of values at a given velocity is large. While some of that variation is probably due to differences between cores, it must also reflect the lumping of a variety of physical mechanisms into a single mass transfer coefficient. In addition, the range may be partly due to differences in fitting procedures (Batycky, Maini, and Fisher 1980).

Flowing fractions determined for the various carbonate core samples are plotted against flow velocity in Figure 2.5. Some, but by no means all, of the samples show much lower values of f than are typical for sandstones, but there is no clear dependence of f on flow velocity. Spence and Watkins (1980) argued that the flowing fraction was really a measure of local heterogeneity. In other words, the rock consists of some flow paths, presumably the larger

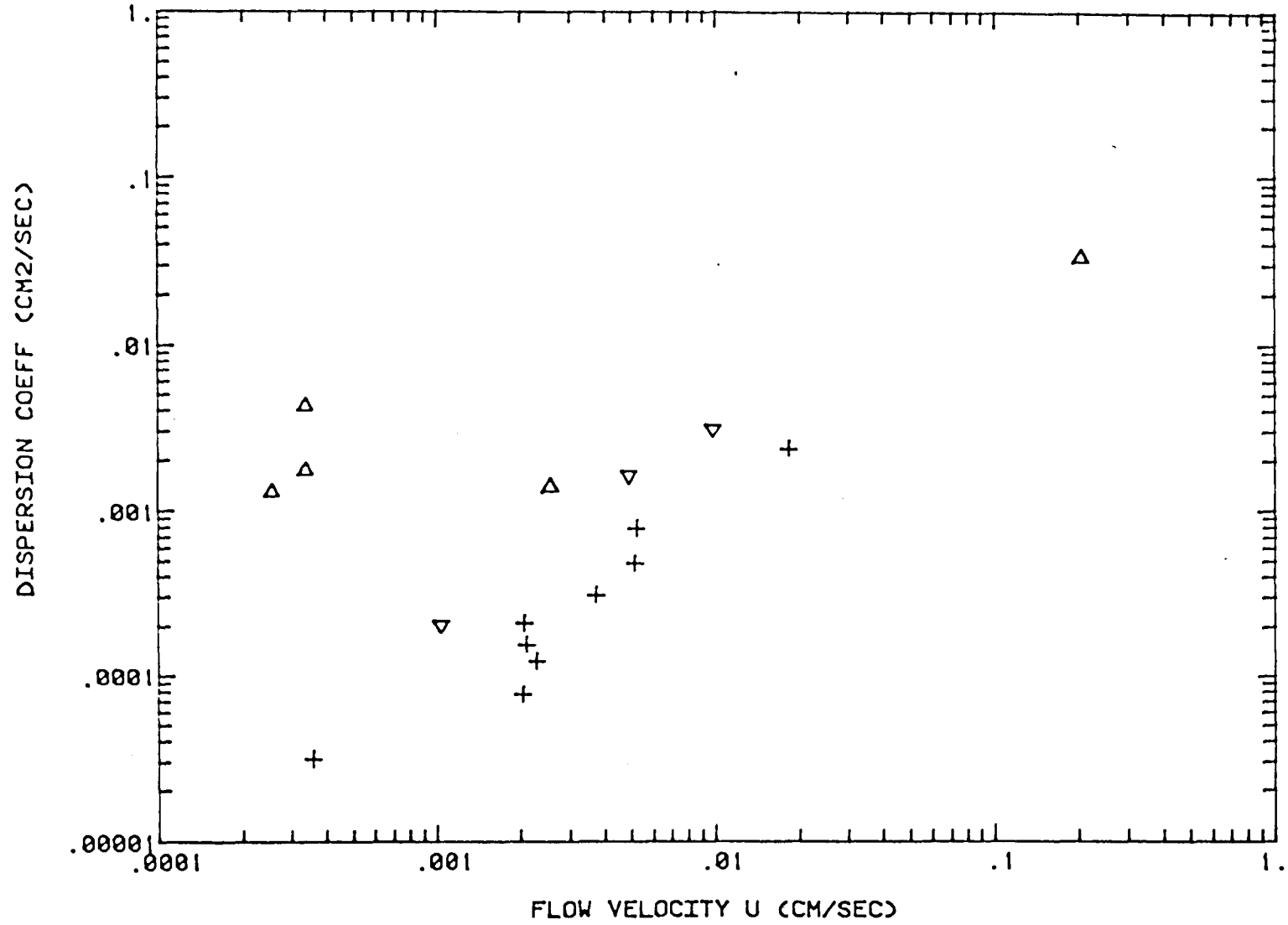


Figure 2.1 Dependence of dispersion coefficients on flow velocity for sandstone samples. Sources of data: Δ Batycky, Maini, and Fisher (1980); + Spence and Watkins (1980); ∇ Baker (1977).

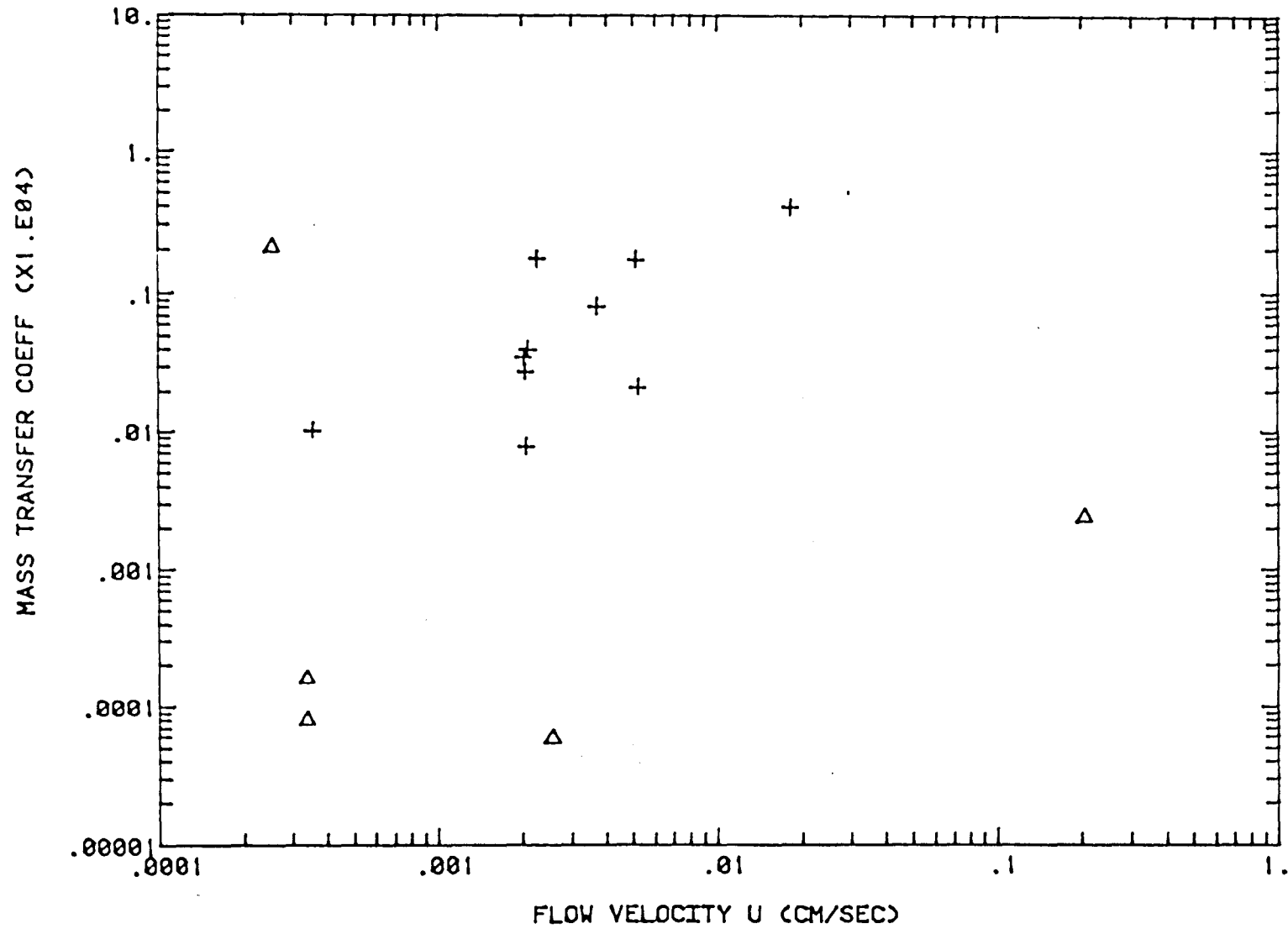


Figure 2.2 Dependence of mass transfer coefficients on flow velocity for sandstone samples. Sources of data: Δ Batycky, Maini, and Fisher (1980); + Spence and Watkins (1980).

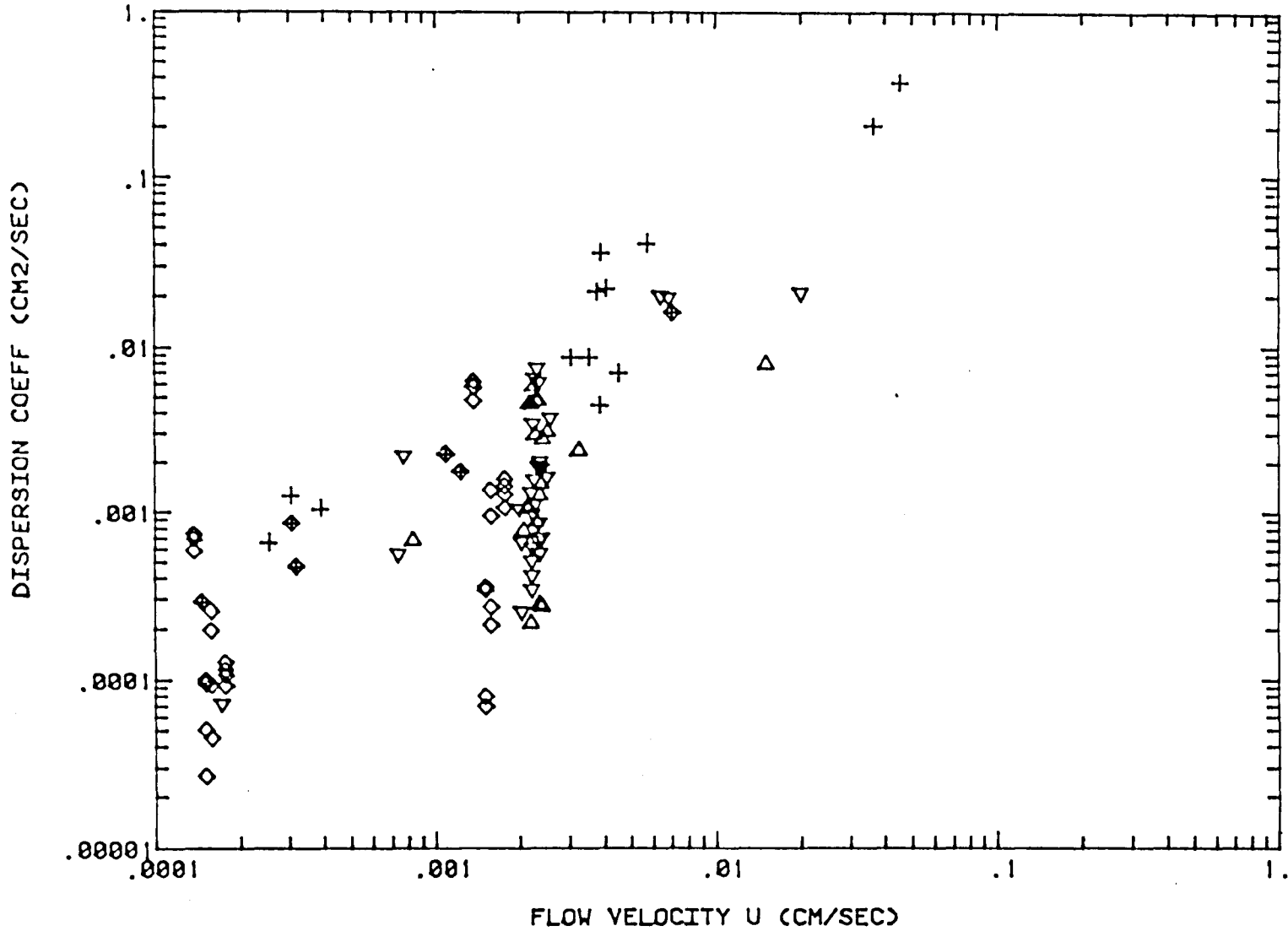


Figure 2.3 Dependence of dispersion coefficients on flow velocity for carbonate core samples. Sources of data: + Batycky, Maini, and Fisher (1980); Δ Spence and Watkins (1980), carbonate A; ∇ Spence and Watkins (1980), carbonate B; \diamond Yellig and Baker (1980); \blacklozenge Baker (1977).

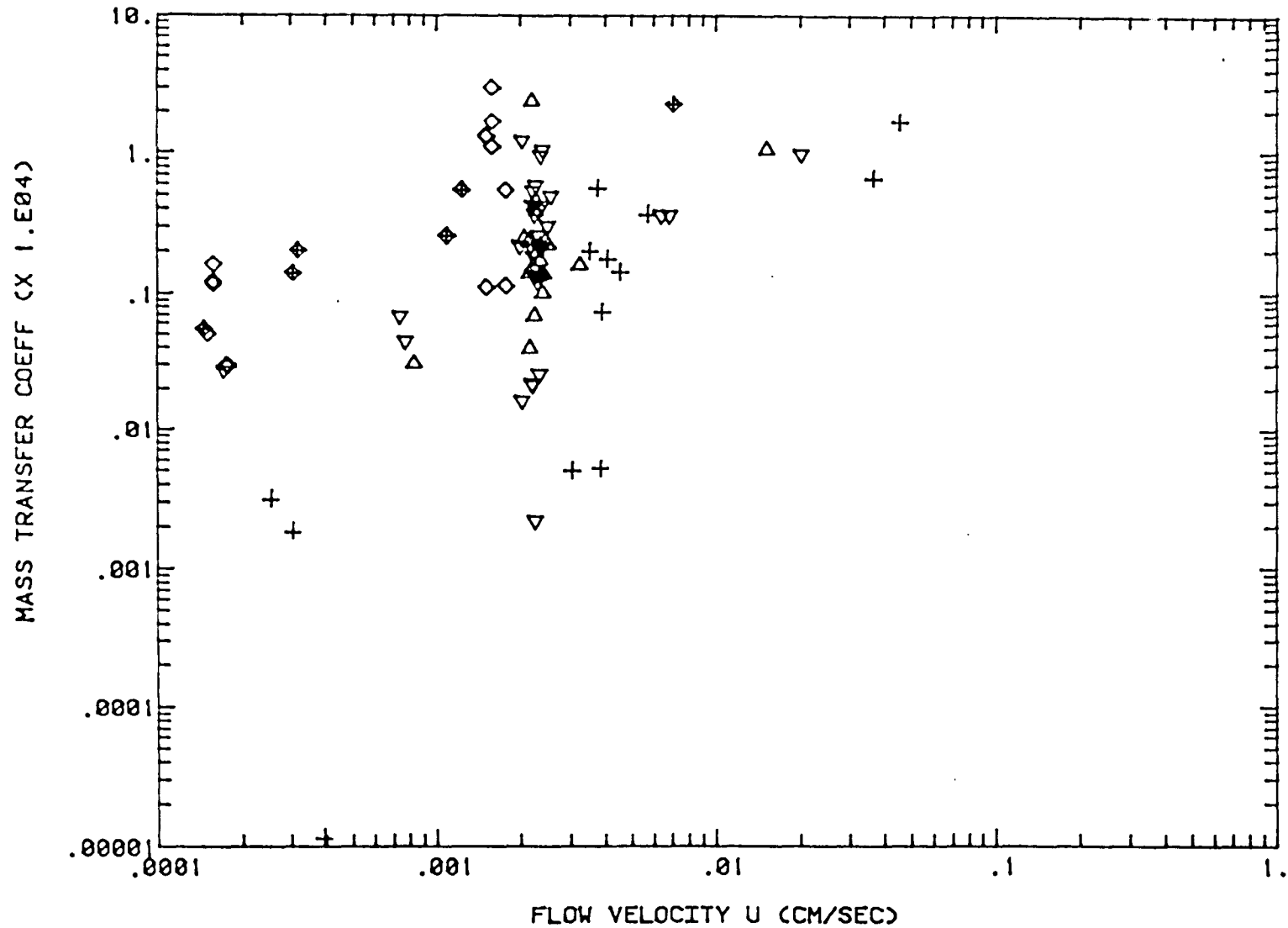


Figure 2.4 Dependence of mass transfer coefficients on flow velocity for carbonate core samples. Sources of data: + Batycky, Maini, and Fisher (1980); Δ Spence and Watkins (1981), carbonate A; ∇ Spence and Watkins (1980), carbonate B; \diamond Yellig and Baker (1980); \blacklozenge Baker (1977).

pores, in which the flow velocity is greater than the overall average velocity and some flow paths in which flow is slower than the average. Thus, in the interpretation given by Spence and Watkins it is not necessary that all of the fluid in the stagnant fraction of the pore volume be motionless, only that it move significantly more slowly than that in the flowing fraction. Analyses of pore size distributions for the cores studied supported their contention: samples with wider pore size distributions showed smaller values of f . Both Spence and Watkins (1980) and Batycky, Maini, and Fisher (1980) reported that for carbonate samples, f declined with increasing velocity. Such behavior is consistent with the idea that there exists a spectrum of flow velocities and that an increase in the displacement velocity increases the flow velocity more in the most permeable flow paths than in the slow flow paths. Thus, in the model interpretation, at high velocities the difference in velocity between slow and fast flow paths is larger and hence, more of the pore space is lumped into the class of slow moving or "stagnant" volume. Unfortunately, data reported so far do not appear to be sufficiently precise to test the hypothesis carefully. Figure 2.6 reports only data for cores in which displacements were performed at more than one velocity. Those data, along with results of the replicated measurements reported by Yellig and Baker (1980) suggest that scatter in the flowing fraction, caused either by experimental error or by problems in fitting the results, is at least as large as any velocity effect.

Comparison of the results shown in Figures 2.1 and 2.2 with those in Figures 2.3-2.5 clearly indicates that miscible displacements are significantly less efficient in carbonate rocks. While questions remain about how the parameters obtained from the model proposed by Coats and Smith are related to the physical characteristics of the rocks and the fluids, that model is the only one in current use which attempts to account for effects of core heterogeneity on laboratory scale displacements. Spence and Watkins presented convincing evidence that efficiency of both secondary and tertiary CO_2 floods in short cores correlates well with the measures of heterogeneity produced by the Coats-Smith model for miscible displacements in the same cores. Thus, the results of such model interpretations have some value as tools for characterization of laboratory core displacements.

Questions also remain about the impact of stagnant volumes on displacements at reservoir scale. Coats and Smith (1964) argued on dimensional grounds that the mass transfer group ($K_m = KL/v$) is large at the displacement lengths and velocities typical of reservoir scales. A large mass transfer coefficient would lead to equalization of concentrations between flowing and nonflowing streams on a time scale which would be short compared to the time required for flow. Stalkup (1970); Spence and Watkins (1980); and Batycky, Maini, and Fisher (1980) used similar arguments and tested their scaling arguments in long core displacements. The experimental results supported the conclusion that mass transfer rate limitations are less important on a field scale. Baker's (1977) analysis of the effect of length differed, however. He derived an effective dispersion coefficient for long displacements which depended on the dimensionless group DK/u^2 , but did not depend on length. In his approach, then, long displacements can be modeled by a simple dispersion model in which the apparent dispersion coefficient is larger than a local dispersion coefficient due to heterogeneity.

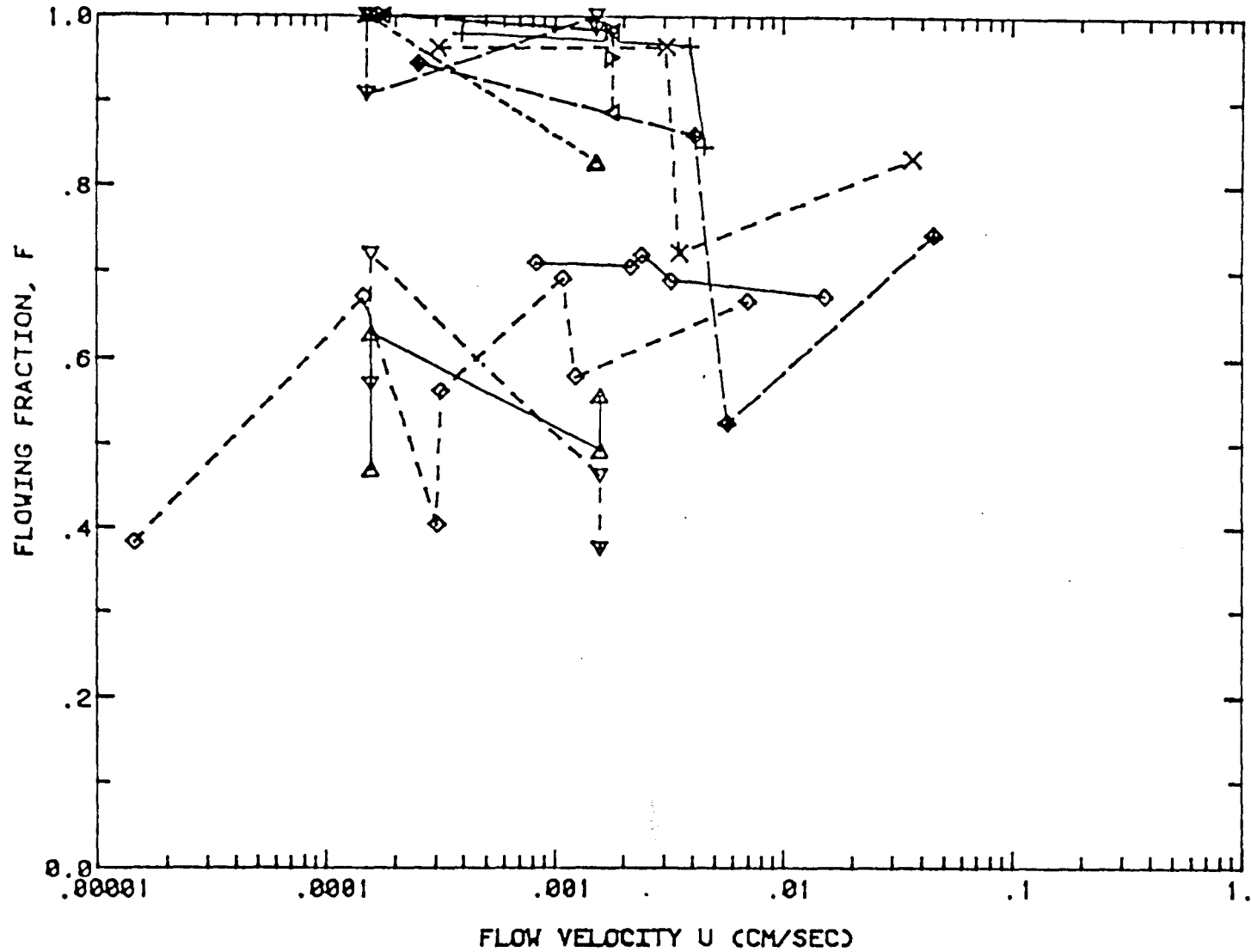


Figure 2.6 Dependence of flowing fraction on flow velocity for carbonate core samples. Data shown are only those for which displacements were performed at different velocities in the same core. Sources of data: +—+ , x---x, ◊---◊ Batycky, Maini, and Fisher (1980); ◊—◊ Spence and Watkins (1980); Δ-----Δ, ∇-----∇, Δ—Δ, ∇--∇, ▷-----▷, ◊-----◊ Yellig and Baker (1980); ◊-----◊ Baker (1977).

A fundamental assumption inherent in the arguments given by Coats and Smith (1964), Stalkup (1970), and Baker (1977) is that the dispersion and mass transfer coefficients remain constant as the scale of the displacements is increased. That assumption is probably not accurate. In real porous media, the dispersion and mass transfer coefficients measured inevitably include averaged effects of local heterogeneities (Heller 1963). For instance, dispersion coefficients measured on field scales are often several orders of magnitude larger than those determined on a laboratory scale, and quantitative estimates of the effects of heterogeneity on dispersion are available in the pioneering analysis of the impact of random variations on apparent dispersion coefficients by Gelhar, Gutjahr and Naff (1979). No such analysis of mass transfer from stagnant pore volume has been attempted, but it appears likely that a similar dependence on scale exists. Hence, it also appears likely that effects of mass transfer similar to those observed on a laboratory scale will occur on a field scale.

Multiphase Displacements

Of particular interest for this study is the effect of high water saturations on the efficiency of CO₂ displacements. Effects of varying wetting phase saturation have been investigated by Raimondi, Torcaso and Henderson (1961); Thomas, Countryman and Fatt (1963); Raimondi and Torcaso (1964); Stalkup (1970); and Shelton and Schneider (1975). In their first paper, Raimondi, Torcaso, and Henderson (1961) reported that while some oil was shielded by high water saturations, it could all be recovered eventually by continued miscible displacement. In their second paper (Raimondi and Torcaso 1964), however, they argued that the experiments reported previously were not conclusive since they had been performed with fluids for which the mobility ratio was adverse. In the second paper, they reported results of displacements of fluids with matched density and viscosity and found that significant fractions of hydrocarbons were permanently trapped. Their displacements were performed in Berea sandstone.

Thomas, Countryman, and Fatt (1963) reported evidence for what they called "dendritic pore volume" in the nonwetting phase caused by high wetting phase saturations, and reported that apparent dispersion coefficients determined for the nonwetting phase increased with increasing water saturation. They performed displacements in which paraffin was the wetting phase in Boise sandstone. The core was saturated with liquid paraffin, and then air was injected to establish a nonwetting phase saturation. The paraffin was solidified, and the pore space previously occupied by air was saturated with brine. Displacements of that brine by brine of a different sodium chloride concentration were used to investigate effects of a truly immobile "wetting" phase (solidified paraffin) on dispersive mixing in the "nonwetting" (water) phase. Thomas, Countryman, and Fatt (1963) argued on the basis of early breakthrough of the displacing fluid that some of the nonwetting phase was located in pores which did not contribute to the flowing stream, dead-end or dendritic pores whose shape was determined by the location of the wetting phase. They hypothesized that slow mass transfer out of the dendritic pores accounted for the broad transition zones they observed at high wetting phase saturations, and concluded that such flows could not be described adequately by a simple convection-dispersion model.

Stalkup (1970) interpreted miscible displacements of the oil phase at varying water saturations using the Coats-Smith model, and found that the model did an adequate job of describing displacement of nonane (C_9) by undecane (C_{11}), but attempts to predict the displacement of C_9 by propane were much less successful. Stalkup argued that in an actual rock, there must be a spectrum of mass transfer coefficients and proposed a model in which two separate stagnant fractions were allowed to have different mass transfer coefficients. The new model did improve the fit to experimental results to some extent, but the agreement was still not as good as for the stable miscible displacements. It seems likely that the principal reason for the lack of agreement was that the displacements of C_9 by propane were unstable and probably dominated by viscous fingering. The Coats-Smith model does not attempt to account for the physics of finger growth so it is not surprising that it does a poor job of predicting results of unstable displacements. Stalkup's results for stable, miscible displacements, however, clearly indicate that as water saturation increases, the flowing fraction decreases and apparent dispersion coefficient increases. Those observations are consistent with the idea that some of the oil present at a given water saturation resides in pores which may have more than one entrance or exit but which are effectively dead-end because water blocks access of the flowing solvent stream to the trapped oil. Both effects indicate that, on a laboratory time scale at least, displacements of oil by CO_2 at high water saturations will be less efficient in rocks similar to the Berea sandstone used, which presumably was strongly water-wet.

Shelton and Schneider (1975) also used Berea cores to investigate effects of high water saturations. They suggested that at any given level of oil relative permeability, the difference in saturation between the primary drainage and imbibition oil relative permeability curves provides a measure of the trapped oil saturation. In addition, they argued that the wetting phase maintains continuous flow paths at all saturations and hence is not trapped and should be completely recoverable by solvent injection. In separate miscible displacements in the oil-water phases, they found that the presence of a second mobile phase slowed recovery of either phase, but the nonwetting phase recovery was much more strongly affected. All of the wetting phase could be recovered by a miscible displacement, but significant amounts of nonwetting phase remained unrecovered at the end of the tests, though oil was still being produced slowly. Those results suggest that oil recovery by solvent injection would be more efficient in oil-wet rocks.

Shelton and Schneider (1975) also compared secondary and tertiary miscible displacements for wetting and nonwetting phases. They found little difference between secondary and tertiary flood results. The floods were conducted, however, with adverse viscosity ratios in the neighborhood of 40:1, so that it is possible that viscous fingering dominated both sets of displacements. Transition zones were much longer than could be attributed to dispersion in both secondary and tertiary displacements, which suggests that effects of the distributions of phases on mixing may have been swamped by viscous fingering. Watkins (1978) successfully correlated residual oil saturations to CO_2 core floods with estimates of the importance of viscous fingering and suggested that the low recoveries observed by Shelton and Yarborough at high displacement rates were a reflection of the effects of

viscous fingering, and hence did not accurately measure the local displacement efficiency in the swept zone.

The extensive displacement results for CO₂ and rich gas systems reported by Shelton and Schneider offer a good example of the difficulty of interpreting displacement experiments from effluent composition data. Viscous fingering, unfavorable phase behavior, and heterogeneity can all cause a broad transition zone, and hence, it can be difficult to sort out which mechanism or mechanisms dominate displacement efficiency. The experimental procedures described below are an attempt to eliminate the effects of viscous instability and the complications of CO₂-crude oil phase behavior, and thereby isolate the effects of core heterogeneity and screening of oil by high water saturations. It is clear, however, that quantitative interpretations of such experiments are still strongly dependent on the assumptions inherent in the model used to describe the flow, whether it be a dispersion model, a capacitance-dispersion model (Coats and Smith 1964) or some other approach. While there is no tractable alternative to describing complex flows in complicated porous media in terms of lumped parameters of some sort, the limitations inherent in that approach must be recognized.

2.2 Results of Displacement Experiments

Figures 2.7 and 2.8 show schematics of the simple displacement equipment used to perform stable miscible displacements in two cores which represent the range of porous media to be studied in this project. The properties of the two cores studied so far are given in Table 2.1. The first is a Berea sandstone core which is reasonably uniform, at least by comparison with the San Andres carbonate core obtained from the Algerita Escarpment in northeastern New Mexico.* The apparatus shown in Figure 2.7 is used to perform miscible displacements in which only one phase is present in the core. The core is saturated with one fluid, ethylbenzene for example, flow at the displacement velocity is established, and then the injected fluid is switched rapidly from ethylbenzene to ethylbutyrate. Fluids produced from the core are collected and their compositions determined by gas chromatography. Amounts produced are determined by weight.

The apparatus shown in Figure 2.8 is used to prepare cores for separate, simultaneous miscible displacements in the oil and water phases. In two-phase displacements, the core is first saturated with brine of a given salt concentration (2 wt. % NaCl). Then, brine and oil (ethylbenzene, for example) are injected simultaneously at fixed volumetric flow rates until steady state saturations of oil and water in the core have been established. Saturations are determined by material balance on injected and produced fluids and relative permeability to each phase is determined from the pressure drop. High injection rates are used during this portion of the experiment to reduce capillary end effects. Once steady state saturations have been established,

*We are grateful to Shell Development Co. for providing us with this core material.

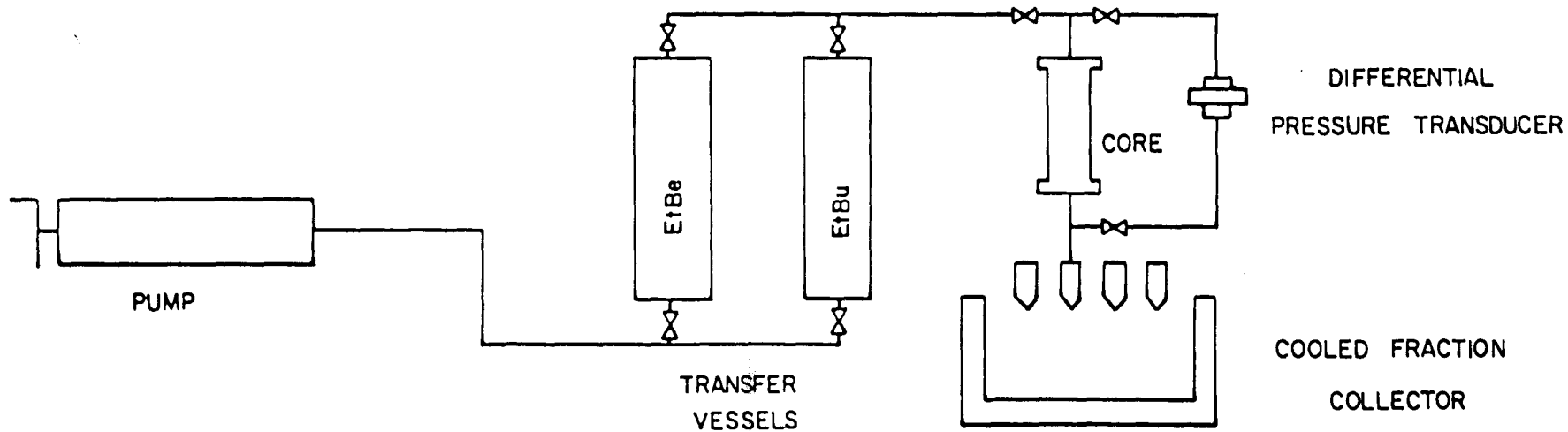


Figure 2.7 Schematic of equipment used to perform miscible core floods.

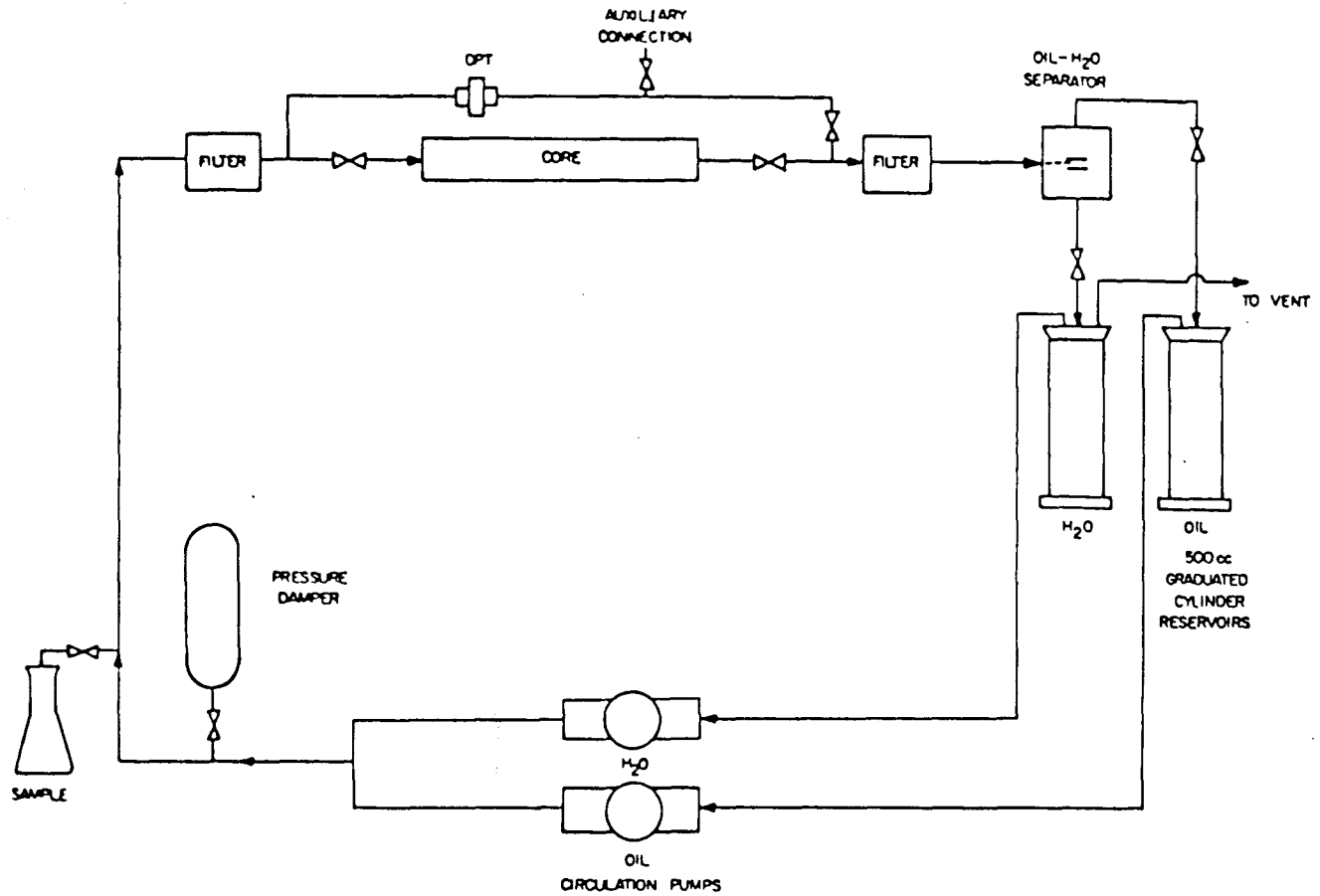


Figure 2.8 Schematic of equipment used to prepare cores for simultaneous miscible displacements in two flowing phases.

Table 2.1 Properties of Core Materials

<u>Symbol</u>	<u>Core</u>	<u>Length (cm)</u>	<u>Diameter (cm)</u>	<u>Permeability (md)</u>	<u>Porosity (%)</u>	<u>Pore Volume (cm³)</u>
SS	Berea Sandstone	15.05	3.82	177	18.4	31.7
C	San Andres Outcrop	66.7	5.08	29.5	17.4	235.2

Table 2.2 Properties of Fluids Used in Miscible Displacements at 25°C

<u>Component</u>	<u>Abbreviation</u>	<u>Density (g/cm³)</u>	<u>Viscosity (mPa·s)</u>
Ethylbenzene	EtBe	0.8600	0.619
Ethylbutyrate	EtBu	0.8728	0.619
Isopropanol	IPA	0.7815	2.12

the core is transferred to an apparatus similar to that shown in Figure 2.7 in which the miscible displacements are performed. In that portion of the experiment, the injection rate of each phase is reduced proportionately to produce a flow velocity more representative of reservoir flow rates. The fractional flow of oil and water is maintained constant, however. Then, injection of oil is switched from ethylbenzene to ethylbutyrate and that of 2 wt. % NaCl brine to 1 wt. % NaCl brine. Effluent oil-water mixtures are separated continuously by a membrane separator. Oil samples are collected, weighed and analyzed by gas chromatography. Brine samples are analyzed on-line with a conductivity meter with amounts measured by weight of samples collected.

The sequence of experiments planned for each reservoir core is:

- (1) Miscible displacements in the absence of water with fluids of matched density and viscosity.
- (2) Simultaneous, steady-state miscible displacements in oil and water phases at various flowing fractions of oil and water, again performed with fluids of matched density and viscosity.
- (3) Displacements of oil by CO₂ at various flowing fractions of CO₂ and water.

Properties of fluids used for the miscible displacements under (1) and (2) are given in Table 2.2. The displacements to be performed in part (1) of the characterization of a given reservoir core are intended to assess the effects of rock pore structure efficiency of the simplest possible displacement process, a stable, single phase displacement. Spence and Watkins (1980) found that the efficiency of such displacements correlated well with results of continuous secondary and tertiary CO₂ floods in the same cores, though they did not attempt to measure the effects of high mobile water saturations. As discussed above, effects of pore structure alone can be difficult to interpret even without the complications of the distributions of phases, phase behavior, viscous fingering and so on.

The experiments in part (2) are designed to provide information concerning the effects of mobile water saturations on dispersive mixing, transfer of components from dead-end pores or droplets, and screening of trapped oil from contact with flowing solvent. While such measurements have been reported for Berea sandstone cores, no results have been published for reservoir cores typical of fields which are likely to be flooded with CO₂. Since the use of mobile water saturations to reduce mobility of CO₂ is planned for many CO₂ floods, some assessment of the impact of high water saturations on the process by which CO₂ contacts and displaces trapped oil appears essential. Again, elimination of the effects of viscous instability and phase behavior by performing the displacements with first contact miscible fluids of matched density and viscosity is designed to isolate the effects to be studied and to provide a base for interpreting more complex floods with CO₂ and crude oil.

The displacements in part (3) will parallel those in part (2) with the exceptions that the viscosities and densities will no longer be matched and the complex phase behavior of CO₂-crude oil mixtures will be a factor. In the absence of a detailed theory of the development of viscous fingers, interpretation of the displacement experiments will require that the floods be stabilized by gravity segregation in vertical displacements (Saffman and Taylor 1958; Dumore 1964) or by the injection of a transition zone between CO₂ and oil in which concentration, and hence fluid property, gradients are small enough that a stable displacement occurs. In practice, the maximum rates at which gravity stabilized displacements can be performed may be very low because the difference in viscosities is large and the difference in densities small. Furthermore, because the viscosity of one of the injected phases will change when injected oil is switched to injected CO₂, the fractional flow of water, and hence the water saturation in the core, will change, unless the injection rate for CO₂ is altered appropriately at the time of the switch. If a transition zone between oil and CO₂ is injected, the problem of maintaining constant water saturation in the core becomes more complex. Details of the experimental procedures to be used to perform the CO₂-oil-water displacements are still under consideration, therefore. Results of fluid property measurements for ethylbenzene and ethylbutyrate are given in Figures 2.9-2.12. Figure 2.9 indicates that the viscosities of ethylbenzene and ethylbutyrate are very closely matched in the neighborhood of room temperature. Figure 2.10 shows that the densities of the two oils differ by only about 1% at room temperature. Figures 2.11 and 2.12 report viscosities and densities of mixtures of the two oils measured at 25°C. The results presented in Figures 2.11 and 2.12 indicate that mixtures which occur in the transition zone of a miscible displacement will have fluid properties differing only slightly from those of the pure components.

Table 2.3 summarizes displacements completed to date. The first series of displacements were performed to test the assumption that effects of differences in viscosity and density were insignificant. For instance, in runs S1A and S1B and runs S3A and S3B, ethylbenzene was displaced by ethylbutyrate, and then the ethylbutyrate was displaced by ethylbenzene. In both pairs of runs the flow velocity was held approximately constant. Effluent composition data for runs S1A and S1B are given in Figure 2.13. The two effluent composition profiles are almost identical, evidence that the small difference in density does not measurably alter apparent dispersion levels. Runs S3A and S3B were a similar test. Effluent composition data for those runs are given in Figure 2.14. Again, the agreement between the runs is within the level of experimental error typical for this type of experiment.

Dispersion coefficients were determined for the six displacements in sandstones by performing least squares fits of the effluent composition data to a straight line in arithmetic probability coordinates. That procedure is equivalent to fitting effluent compositions to equation (2.6) (Brigham, Reed, and Dew 1961; Perkins and Johnston 1963). A typical plot is shown in Figure 2.15 for run S1A. The straight line shown resulted from the least squares fit to the effluent compositions in the leading edge of the transition zone. Use of that data avoids distortion from tailing of the trailing edge or from small errors in the analysis of samples containing very small concentrations of one component.

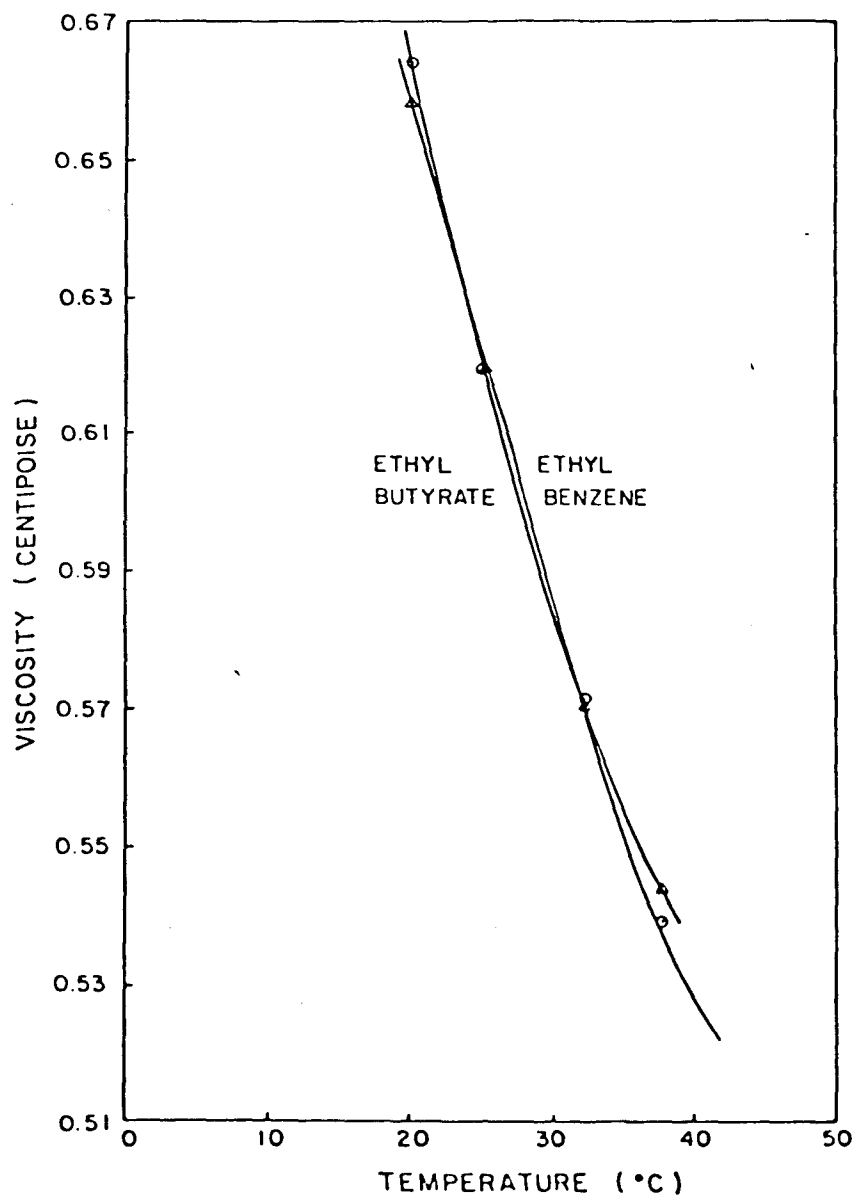


Figure 2.9 Viscosities of ethylbenzene and ethylbutyrate at various temperatures.

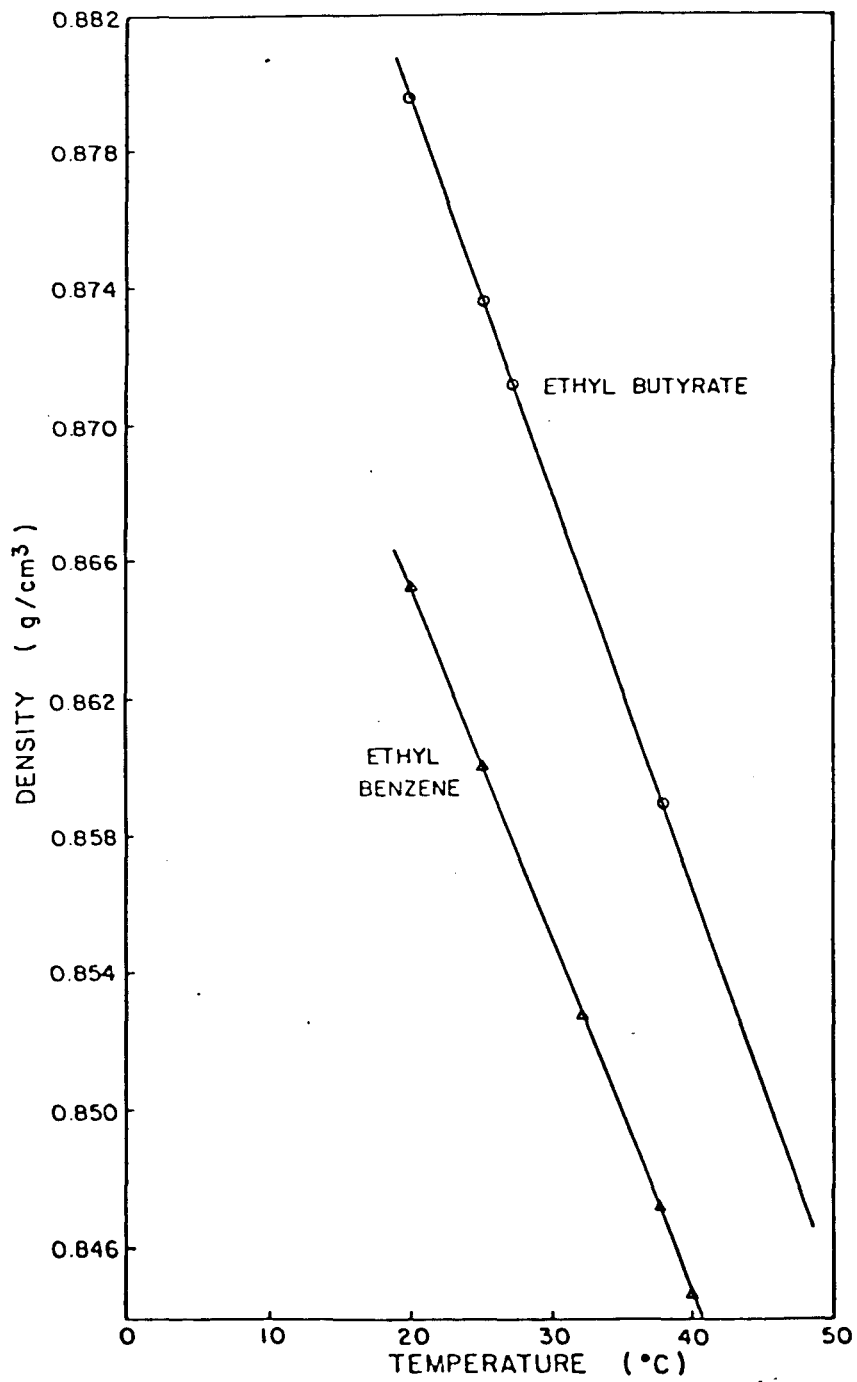


Figure 2.10 Densities of ethylbenzene and ethylbutyrate at various temperatures.

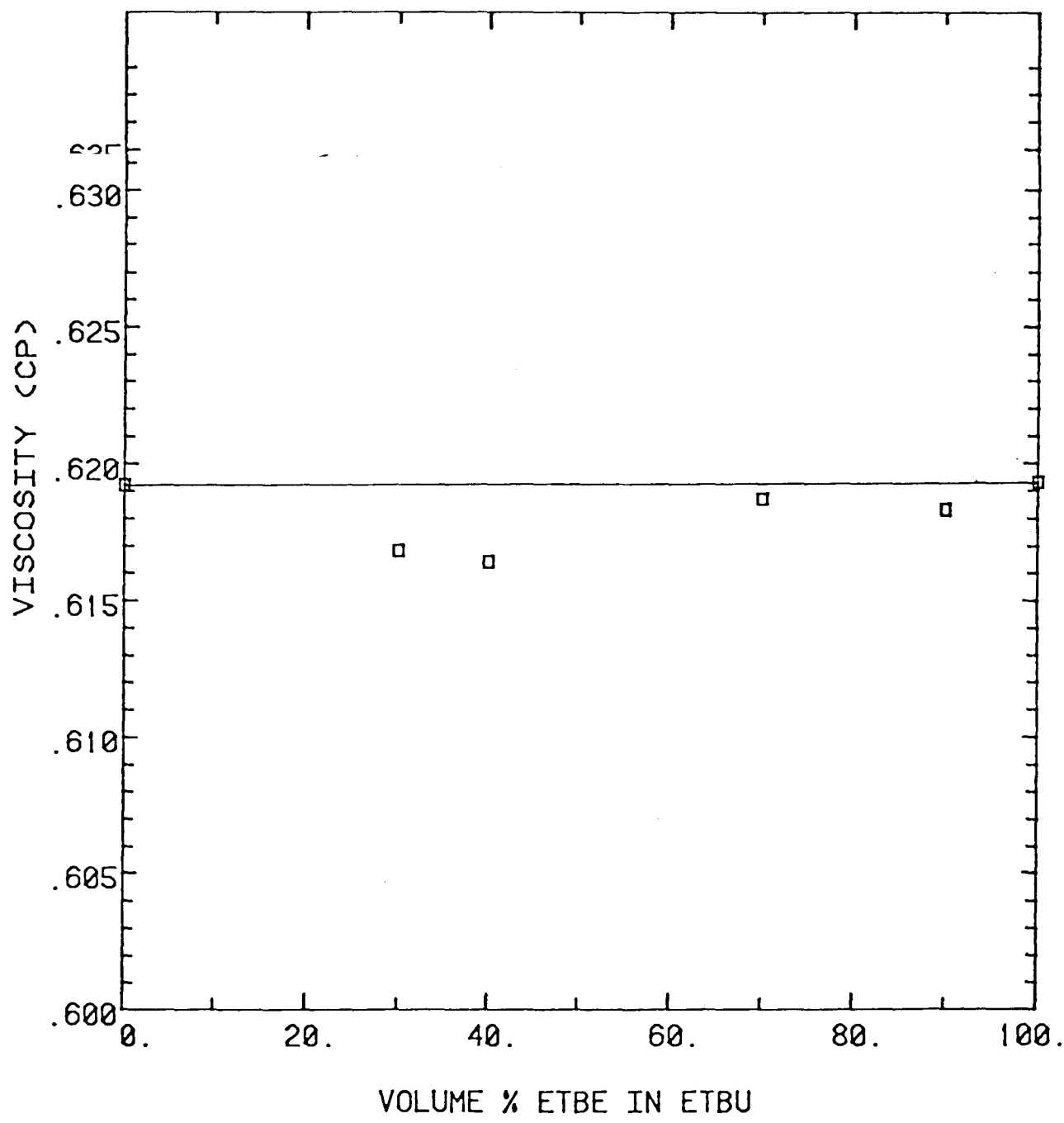


Figure 2.11 Viscosity of mixtures of ethylbenzene and ethylbutyrate at 25°C.

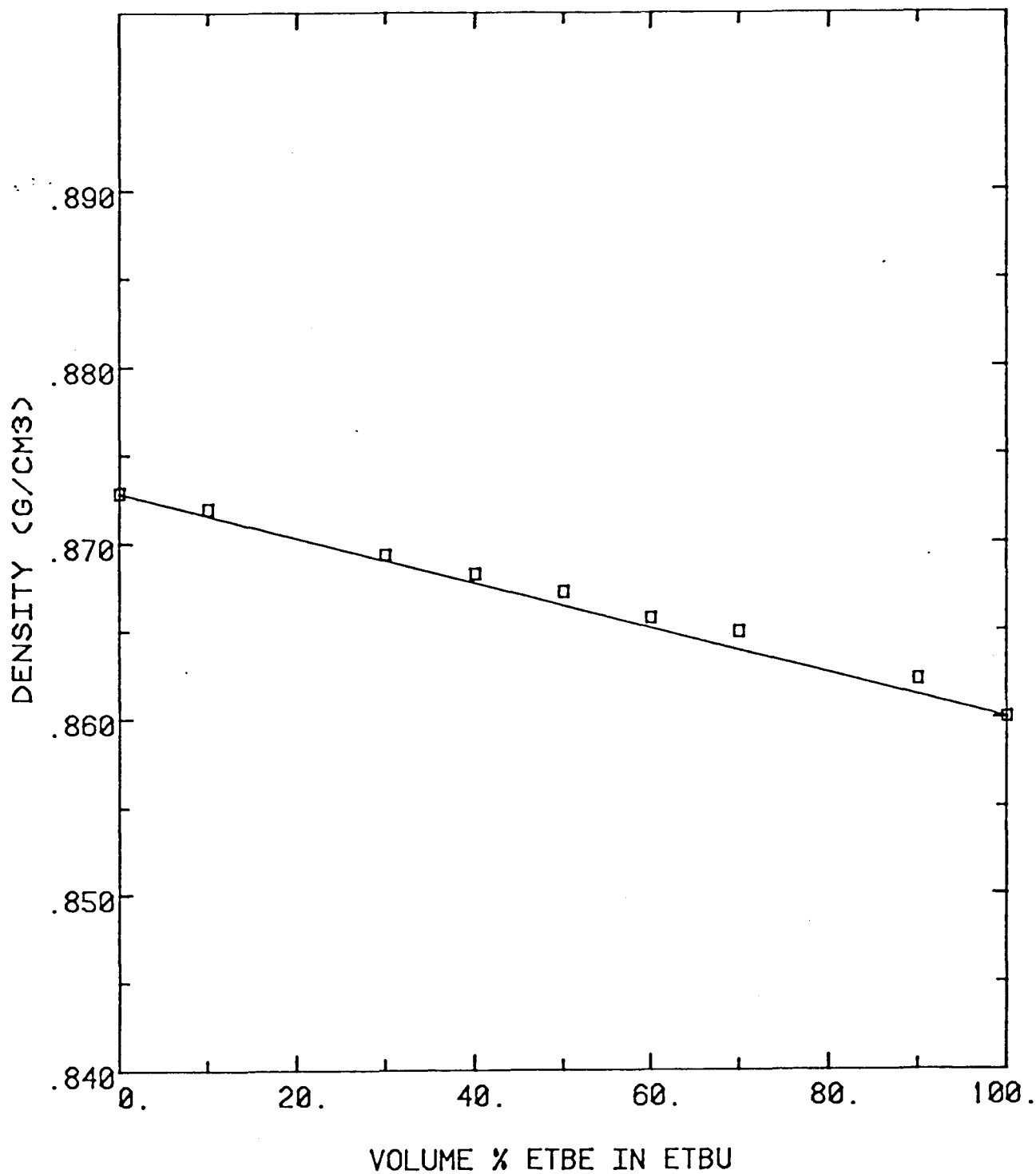


Figure 2.12 Densities of mixtures of ethylbenzene and ethylbutyrate at 25°C.

Table 2.3 Summary of Miscible Displacements

<u>Run</u>	<u>Core</u>	<u>Flow Velocity (cm/sec) x 10³</u>	<u>Displacing Fluid</u>	<u>Displaced Fluid</u>	<u>Direction</u>	<u>Dispersion Coefficient (cm²/sec) x 10⁴</u>	<u>PV Injected at 50% Conc.</u>
S1A	SS	3.61	EtBu	EtBe	Downward	3.40	1.007
S1B	SS	3.84	EtBe	EtBu	Downward	3.85	.986
S2A	SS	8.66	EtBu	EtBe	Downward	7.86	.991
S2B	SS	4.81	EtBe	EtBu	Upward	6.39	.954
S3A	SS	1.97	EtBu	EtBe	Downward	1.49	.980
S3B	SS	1.27	EtBe	EtBu	Downward	1.14	.976
C1A	C	1.50	EtBu	EtBe	Downward	74.1	.826
C2A	C	2.34	EtBu	EtBe	Downward	104	.800
C3A	C	6.41	EtBu	EtBe	Downward	331	.799
C3B	C	6.26	EtBe	EtBu	Downward	425	.802
S4	SS	1.05	EtBu	IPA	Downward	--	1.118
S5	SS	1.05	IPA	EtBu	Upward	--	.987
C4	C	3.15	EtBe	IPA	Upward	--	.693

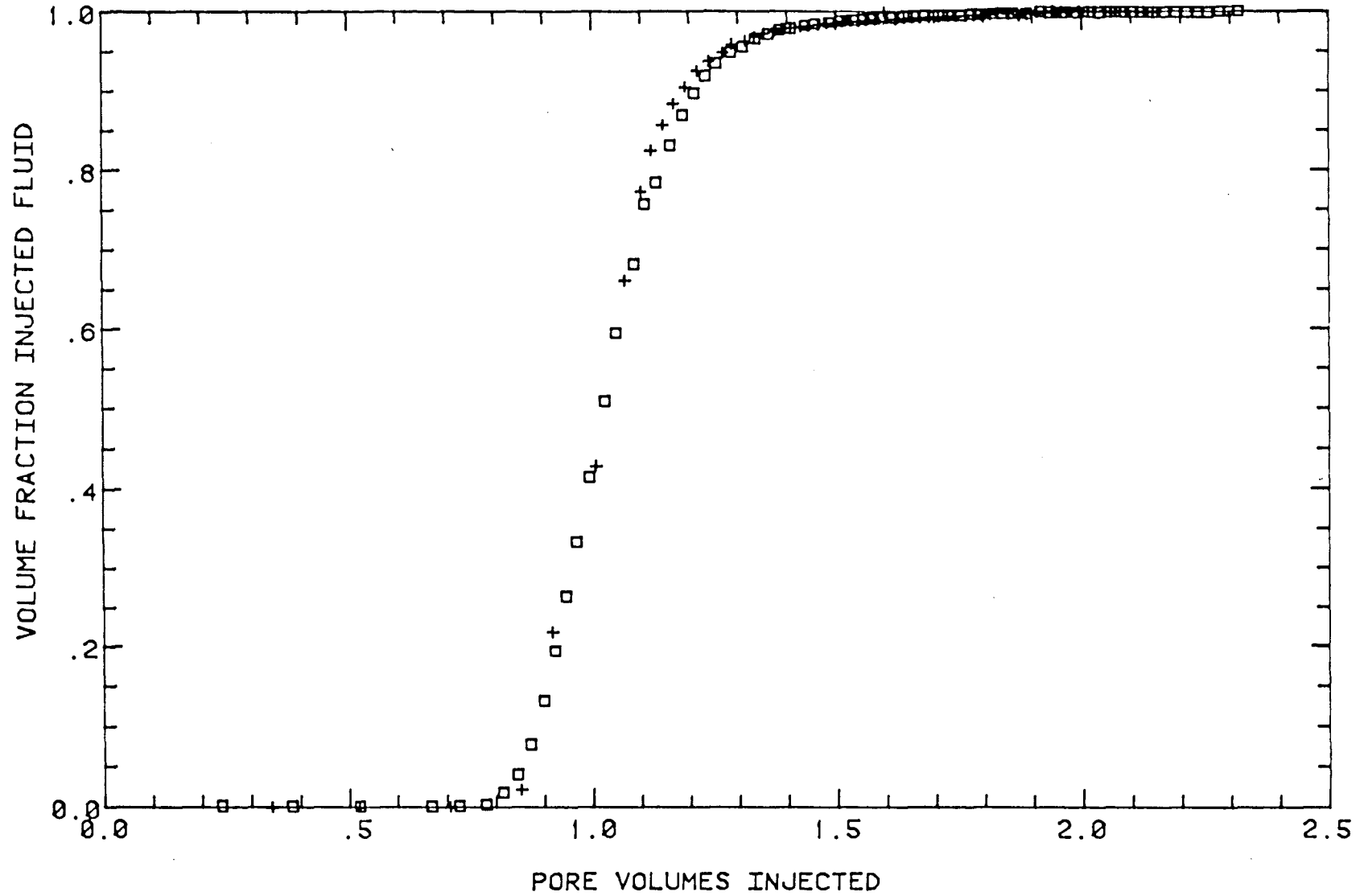


Figure 2.13 Compositions of fluids produced during miscible displacements of ethylbenzene and ethylbutyrate in Berea sandstone, runs S1A (\square) and S1B (+).

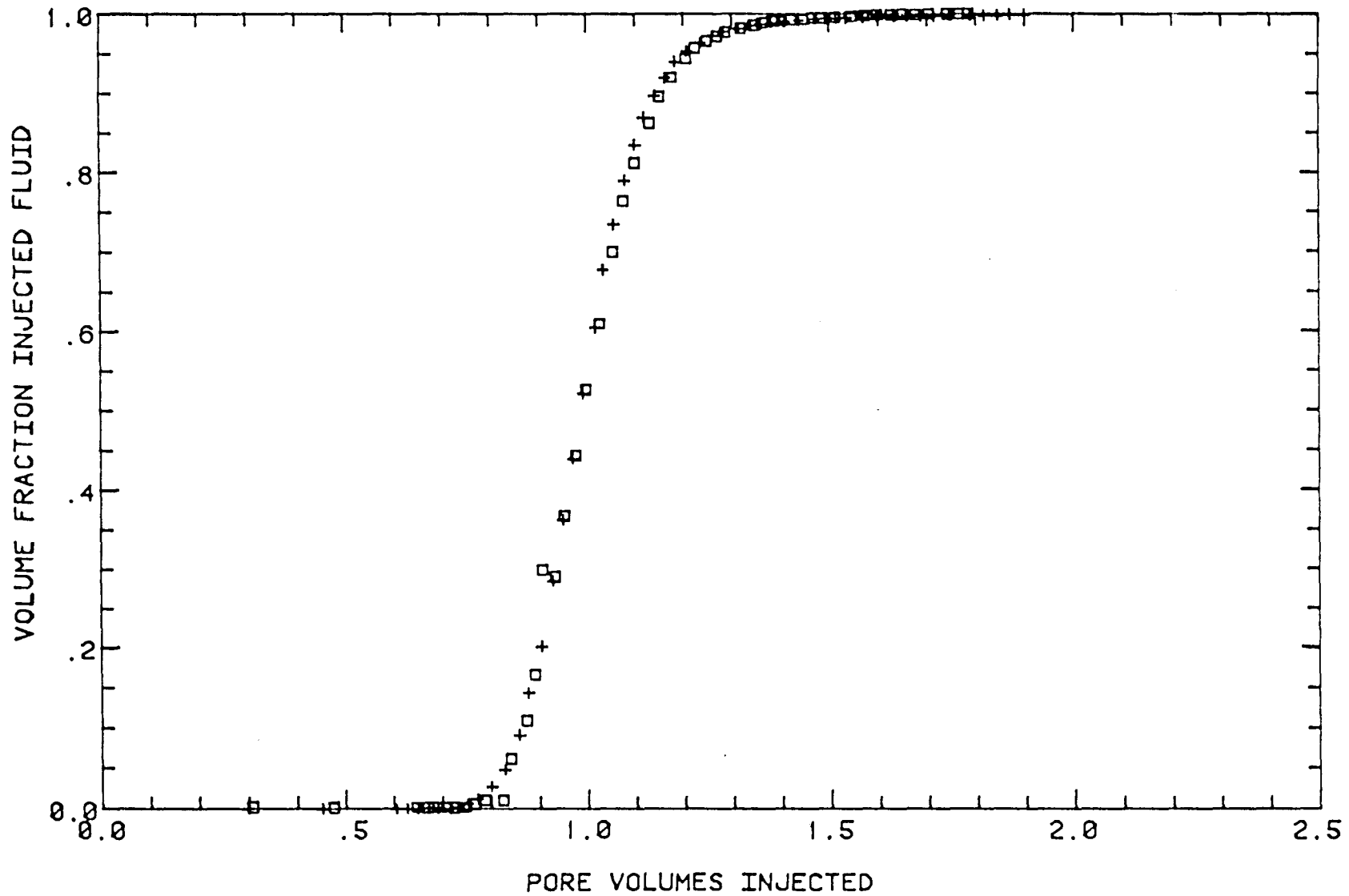


Figure 2.14 Compositions of fluids produced during miscible displacements of ethylbenzene and ethylbutyrate in Berea sandstone, runs S3A (\square) and S3B (+).

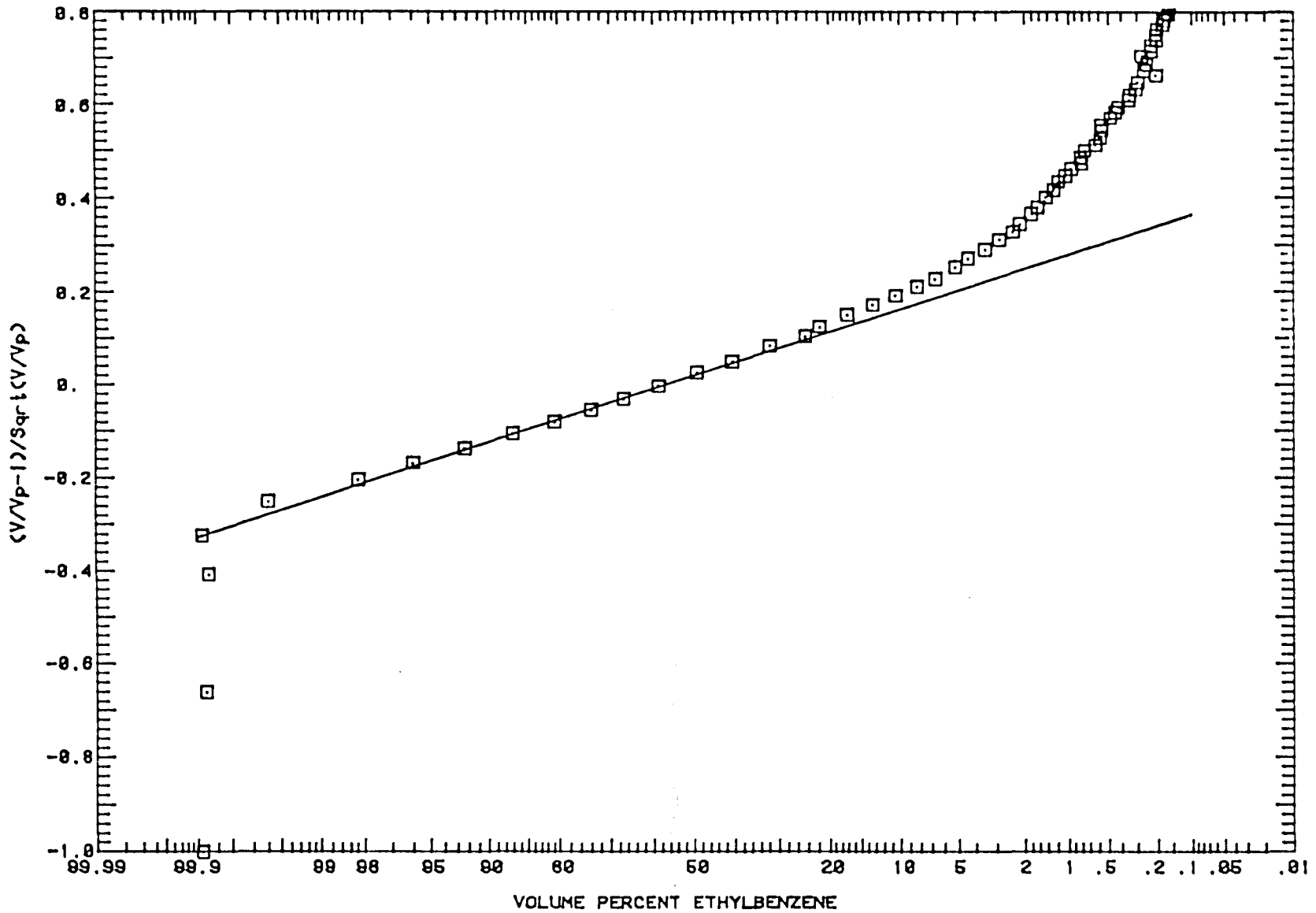


Figure 2.15 Comparison of least squares fit (—) and effluent compositions (□) for run S1A.

Dispersion coefficients so determined are plotted against average interstitial flow velocity in Figure 2.16. The solid curve shown is that suggested by Spence and Watkins (1980) for Berea sandstone.

$$D = 0.0718 \times 10^{-4} + 0.3565 v^{1.26} \quad (2.8)$$

where D is the dispersion coefficient (cm^2/sec) and v the average interstitial velocity (cm/sec). The agreement is good, especially given the relatively low sensitivity of calculated effluent composition profiles to scatter in the dispersion coefficient.

History matches to determine mass transfer coefficients and the flowing fraction for the Coats-Smith model have not yet been completed, but it is apparent from the effluent compositions that the flowing fractions will be very close to one for the Berea core. The last column of Table 2.3 reports the time (in pore volumes injected) at which the 50 vol % concentration of injected fluid appeared at the outlet. While the value is not identical to that which would be obtained from a fit to the capacitance-dispersion model, it is a reasonable initial guess. It is apparent from the values obtained that flowing fractions will be close to one for the sandstone core. The range of values shown in Table 2.3 is consistent with ranges reported by Spence and Watkins (1980); and Batycky, Maini, and Fisher (1980) for sandstones.

Four displacements were performed in the carbonate core to test repeatability of displacements in less homogeneous porous media. Figure 2.17 reports effluent compositions for the two low velocity displacements (runs C1A and C2A), and Figure 2.18 gives similar data for the two displacements at higher velocities (runs C3A and C3B). While the results of the displacements show somewhat more scatter than those in the Berea core, the results generally indicate acceptable repeatability.

Effluent composition histories from the four displacements in the carbonate core show clear evidence of a much more heterogeneous porous medium than the sandstone. Production of the injected fluid occurred before 0.5 PV injected in contrast with a value of about 0.8 PV for the sandstone, and a long tail of production of the fluid originally present was observed in all displacements. While displacements were essentially complete at 1.5 PV injected in the sandstone core, small amounts of original fluid were still being recovered at 3.0 PV injected in the carbonate core. Dispersion coefficients estimated from effluent compositions at the leading edge of the transition zone were one to two orders of magnitude larger than those in the sandstone (Table 2.3). It is apparent, as discussed above, that measurement of a dispersion coefficient is open to question when the flow is nonuniform. The values reported should be treated, therefore, as qualitative measures of the heterogeneity of the flow system rather than as results to be used to predict effluent composition profiles. Times at which the 50% concentration of injected fluid appeared at the outlet also reflect the heterogeneous nature of the carbonate core. It is clear from the results given here, that even ideal miscible displacements are much less efficient in a heterogeneous porous medium such as the carbonate core than in a more uniform rock such as Berea

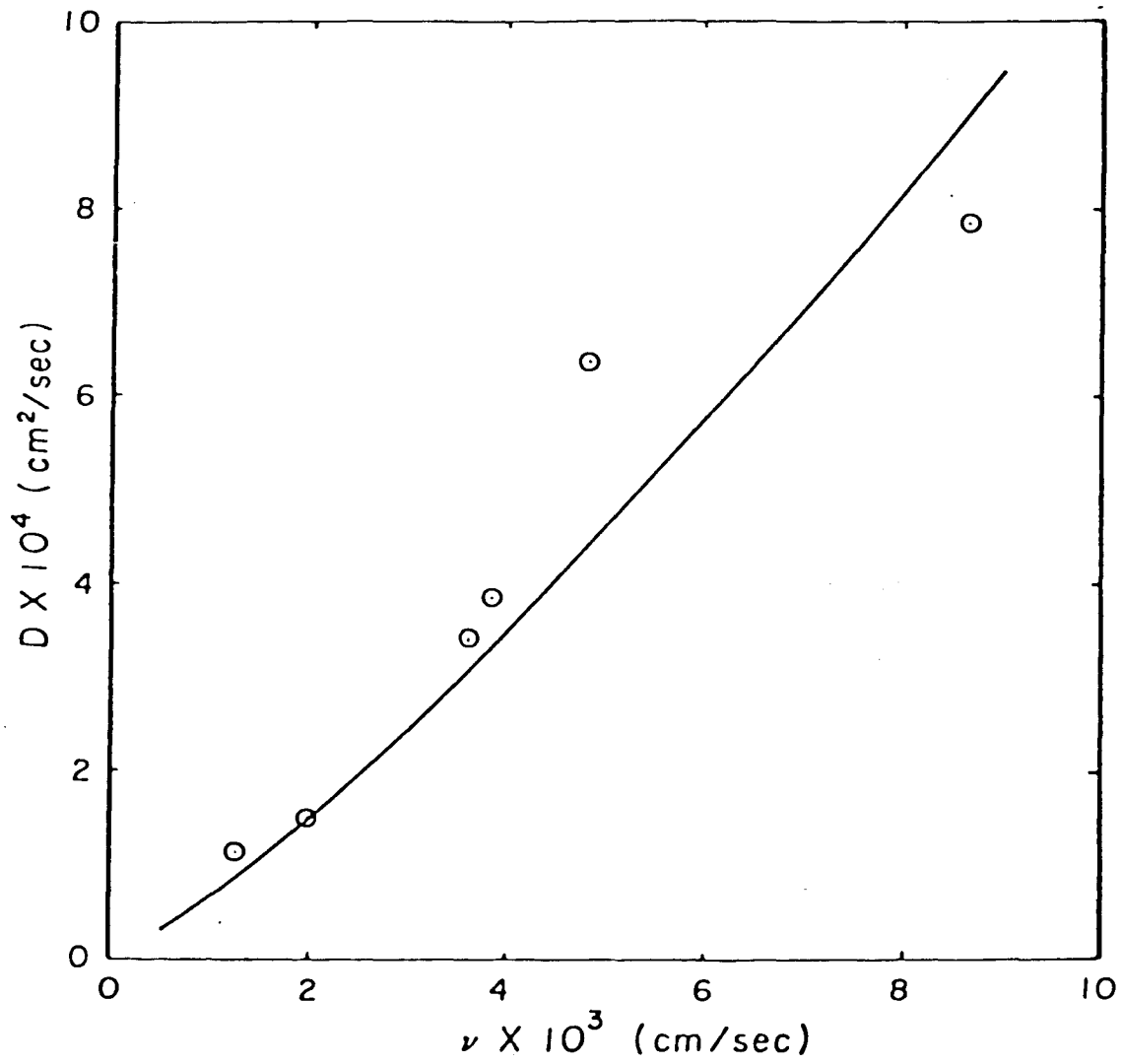


Figure 2.16 Dependence of the dispersion coefficient on flow velocity for a Berea sandstone core.

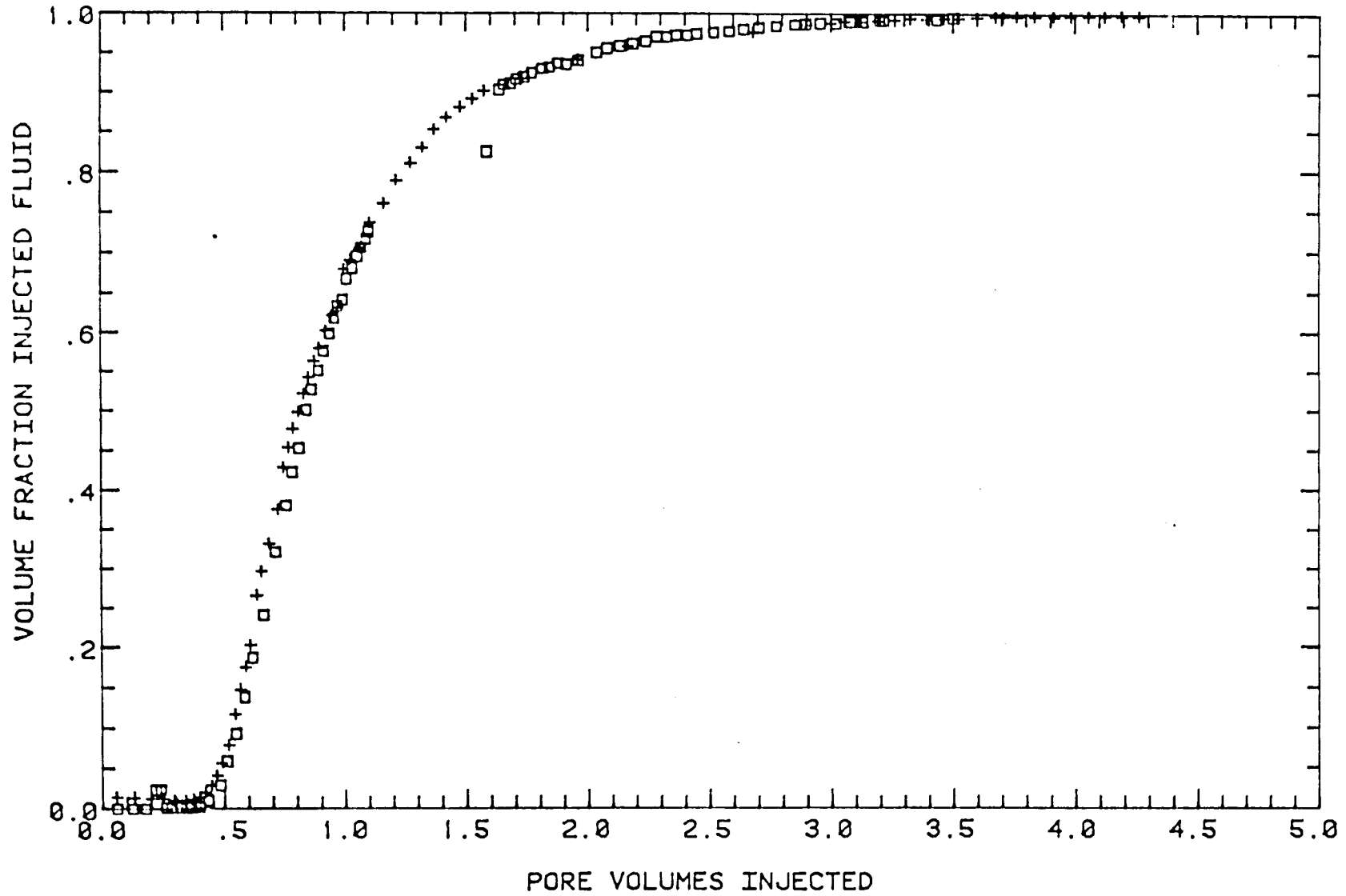


Figure 2.17 Compositions of fluids produced during miscible displacements of ethylbenzene and ethylbutyrate in a San Andres carbonate core, runs C1A (\square) and C2A (+).

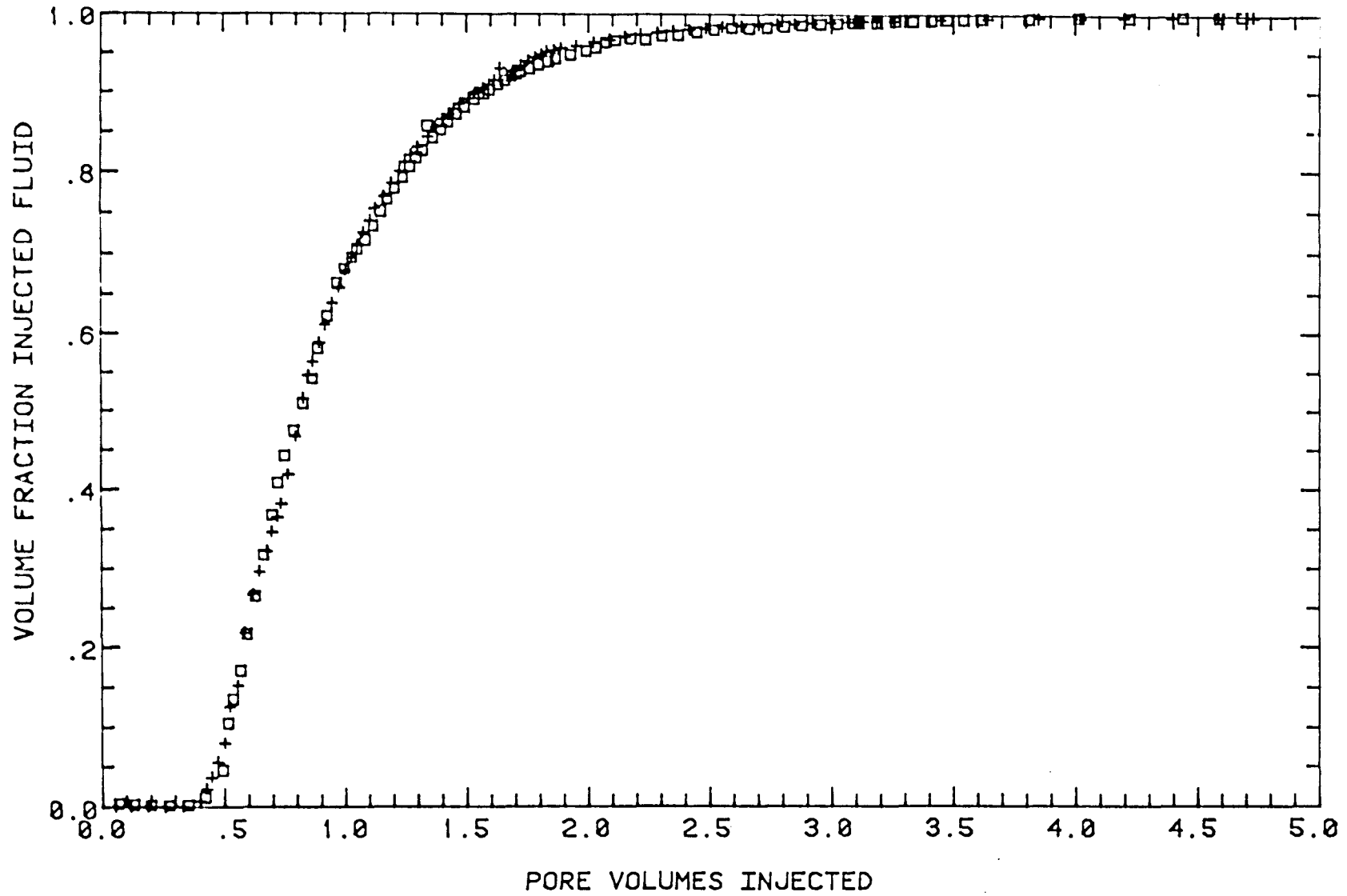


Figure 2.18 Compositions of fluids produced during miscible displacements of ethylbenzene and ethylbutyrate in a San Andres carbonate core, runs C3A (\square) and C3B (+).

sandstone. For CO₂ flooding applications, however, the behavior of heterogeneous carbonates is of greatest interest.

Three additional displacements were performed to obtain effluent composition profiles for floods in which nonuniform fluid properties were deliberately introduced. In run S4, isopropanol (IPA) was displaced downward by more dense, less viscous ethylbutyrate (EtBu) in the sandstone core. The effluent composition profile which resulted is shown in Figure 2.19, along with the profile for run S5, in which low density, high viscosity IPA displaced EtBu upward. Run S4 was clearly unstable. Breakthrough occurred at about 0.5 PV injected. Run S5, however, was stable because at the relatively high displacement velocity, viscous pressure drop dominated the adverse density difference between phases. In the unstable displacement (run S4), viscous fingering broadened the transition zone enough that the 50% concentration did not appear at the outlet until about 1.1 PV had been injected. In the stable displacement (run S5), it appeared at approximately the same time (0.987 PV) as in displacements with fluids of matched density and viscosity.

Results of run C4 are shown in Figure 2.20. In that run, low viscosity, high density ethylbenzene (EtBe) displaced high viscosity, low density IPA upward in the carbonate core. That displacement was also unstable. The effluent composition profile shows clearly that the effect of viscous fingering is to exaggerate the effects of heterogeneity in the carbonate core. Breakthrough occurs very early, and a very broad transition zone occurs.

The results presented here are consistent with those presented by Lacey, Draper, and Binder (1958) who showed conclusively that viscous fingering can significantly alter displacement efficiency even in small diameter laboratory cores. It should be noted that the viscosity ratio used in this displacement is substantially less adverse than values typical in actual CO₂ floods. Thus, it is apparent that unless some measure, such as gravity stabilization, is taken to eliminate instability, viscous fingering will have an important effect in short laboratory core floods. Given the potential complexity of interactions of phase behavior, heterogeneity, and viscous fingering, interpretation of the relative importance of competing mechanisms in such displacements may be very difficult.

2.3 Conclusions

Displacement results available to date establish that:

- (1) Ethylbenzene and ethylbutyrate have densities and viscosities sufficiently closely matched that effects of gravitational and viscous instability are eliminated from vertical displacements in short cores.
- (2) Repeatable effluent compositions can be obtained for both uniform and heterogeneous cores in the absence of water.

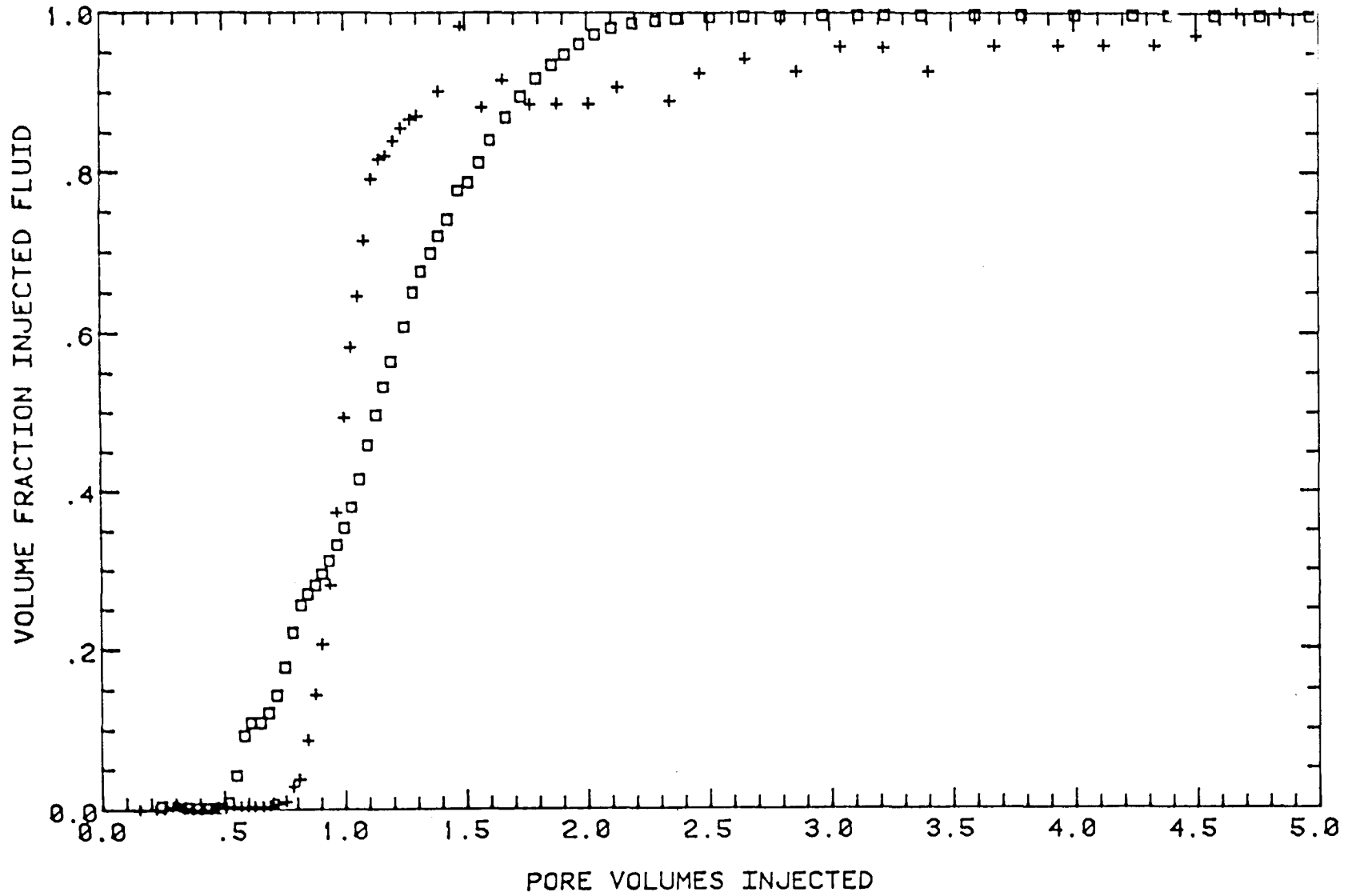


Figure 2.19 Comparison of compositions of fluids produced during stable and unstable miscible displacements of ethylbutyrate and isopropanol, runs S4 (□) and S5 (+).

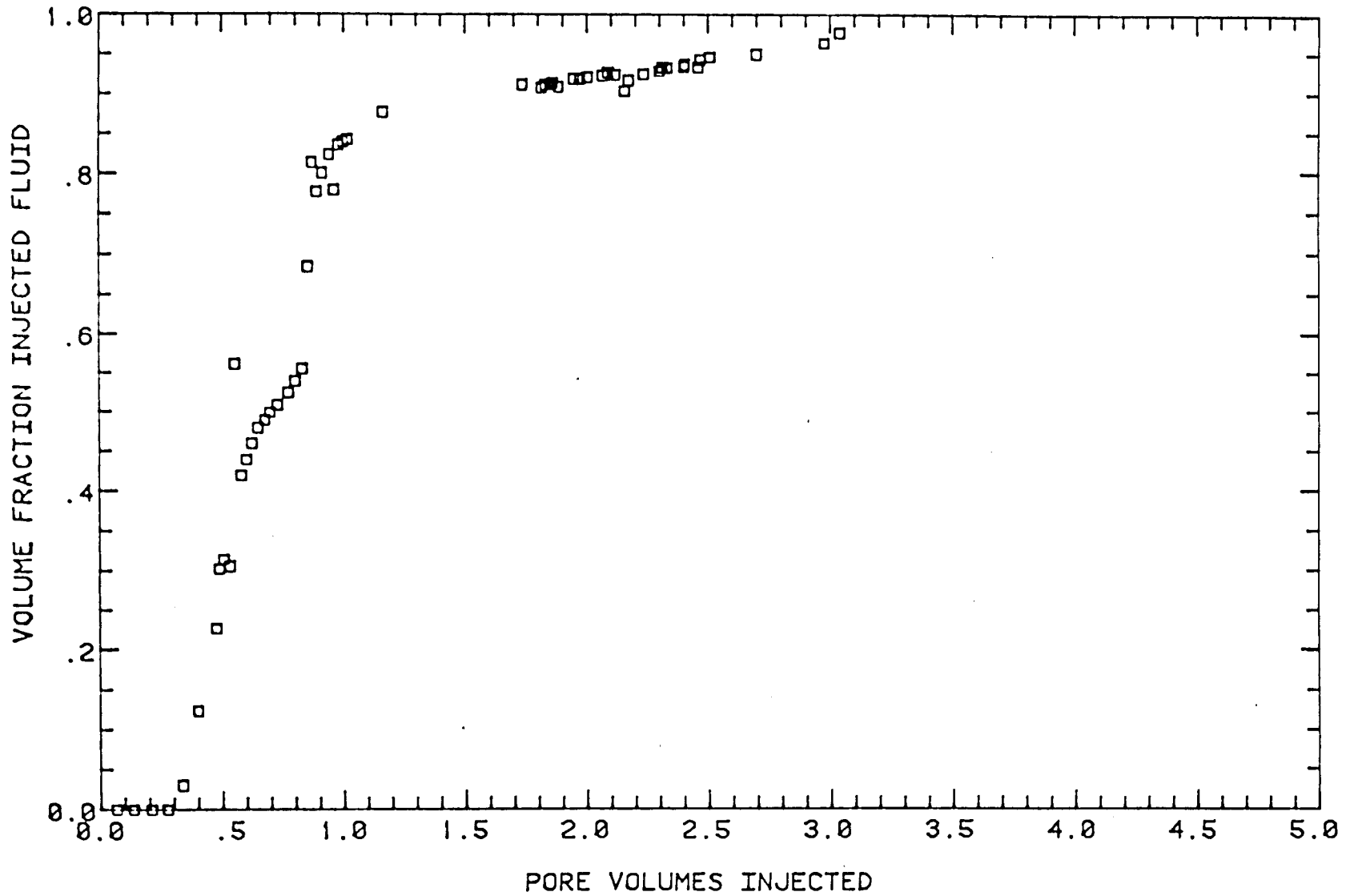


Figure 2.20 Compositions of fluids produced during an unstable displacement of isopropanol by ethylbenzene in a San Andres carbonate core, run C4.

- (3) Effects of core heterogeneity on miscible displacement efficiency can be detected easily with the experimental technique used. Single phase miscible displacements provide a relatively convenient way to characterize rock properties.
- (4) Effects of viscous or gravitational instability must be eliminated if first contact or multiple contact miscible displacements are to be interpreted with reasonable certainty.

3. SUPPORTING MEASUREMENTS: PHASE BEHAVIOR AND FLUID PROPERTIES OF CO₂-CRUDE OIL MIXTURES

Detailed interpretation of flow experiments in which CO₂ displaces crude oil requires independent measurements of the compositions, densities and viscosities of phases which develop as CO₂ mixes with and displaces the oil and water present in the core. In this section, we report results of single contact PVT experiments for two systems: recombined Maljamar reservoir fluid at 90°F and Wasson stock tank oil at 105°F. Results of the experiments for the recombined Maljamar sample shed some light on the effects of solution gas on phase behavior and displacement performance. Results of the study of the Wasson stock tank oil are similar to those reported previously for Maljamar separator oil (Orr and Taber 1981; Orr, Yu, and Lien 1981). Also reported in this section are details of the continued development of the continuous multiple contact (CMC) experiment for measurement of phase compositions and fluid properties. Work to improve the experiment by adding continuous measurement of phase viscosities and densities is reviewed. An analysis of the behavior of the experiment for binary systems is given and tested experimentally for the CO₂-decane system. In addition, results of measurements of phase compositions and densities are reported for mixtures of CO₂ with Maljamar separator oil at several pressures. Results of one experiment in which solution gas was present are also given.

3.1 Volumetric Behavior of CO₂-Crude Oil Mixtures

Maljamar Recombined Reservoir Fluid

The volumetric behavior of ten mixtures of CO₂ with a recombined reservoir fluid (RRF) was made by adding 672 SCF/BBL of solution gas to separator oil from the Maljamar Field, Lea County, New Mexico. Compositions of the solution gas, separator oil and RRF are given in Table 3.1. The bubble point of the RRF was 1450 psia (10000 kPa) at 90°F. Phase volumes were measured as a function of pressure for each mixture in a visual cell described previously (Orr, Yu, and Lien 1981; Orr and Taber 1981).

Figure 3.1 summarizes volumetric behavior and saturation pressures for the CO₂-RRF mixtures. For comparison, results of similar measurements for mixtures of CO₂ with the separator oil alone are reproduced in Figure 3.2. Details of those experiments have been reported previously (Orr, Yu, and Lien 1981; Orr and Taber 1981). In the CO₂-RRF system, mixtures containing less than about 60 mol % CO₂ formed liquid and vapor phases at low pressures and a single liquid phase at high pressures. At CO₂ mole fractions above 0.6, liquid and vapor phases were present at low pressure, two liquids formed at high pressure, and two liquids and a vapor coexisted at intermediate pressures. In the CO₂-separator oil system (Figure 3.2), mixtures containing less than about 74 mol % CO₂ separated into liquid and vapor at low pressures

Table 3.1 Composition of Maljamar Solution Gas, Separator Oil and Recombined Reservoir Fluid

Carbon Number	Solution Gas (Mol %)	Separator Oil (Mol %)	Recombined Reservoir Fluid* (Mol %)
1	56.55	-	29.39
2	19.61	-	10.19
3	16.06	-	8.35
4	6.37	-	3.31
5	1.41	3.90	2.61
6	-	9.37	4.50
7	-	10.27	4.93
8	-	13.54	6.50
9	-	11.91	5.72
10	-	7.50	3.60
11	-	5.59	2.68
12	-	4.32	2.07
13	-	3.93	1.89
14	-	3.29	1.58
15	-	2.73	1.31
16	-	2.26	1.09
17	-	2.23	1.07
18	-	1.34	0.63
19	-	1.07	0.51
20	-	1.36	0.65
21	-	1.10	0.53
22	-	0.77	0.37
23	-	0.96	0.46
24	-	0.88	0.42
25	-	0.68	0.33
26	-	0.38	0.18
27	-	0.59	0.28
28	-	0.38	0.18
29	-	0.40	0.19
30	-	0.40	0.19
31	-	0.40	0.19
32	-	0.40	0.19
33	-	0.13	0.06
34	-	0.14	0.07
35	-	0.14	0.07
36	-	0.13	0.06
37+**	-	7.50	3.60

* Calculated for a GOR of 650 SCF/BBL

** Assumed molecular weight 563

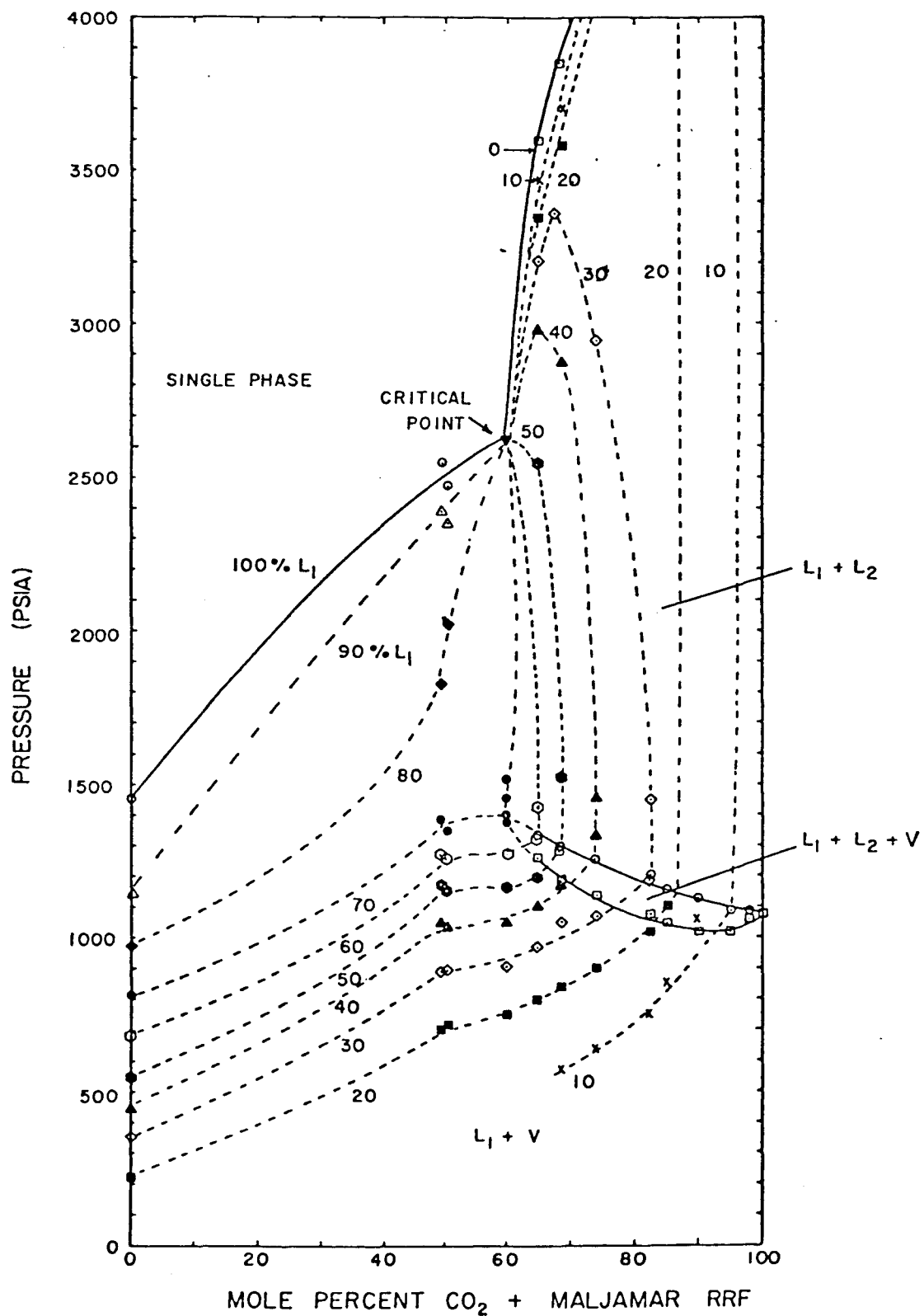


Figure 3.1 Phase behavior of binary mixtures of CO_2 with Maljamar recombined reservoir fluid at 90°F . Solid curves indicate boundaries of two- or three-phase regions. Dashed lines indicate constant volume fraction of the lower liquid (L_1) phase.

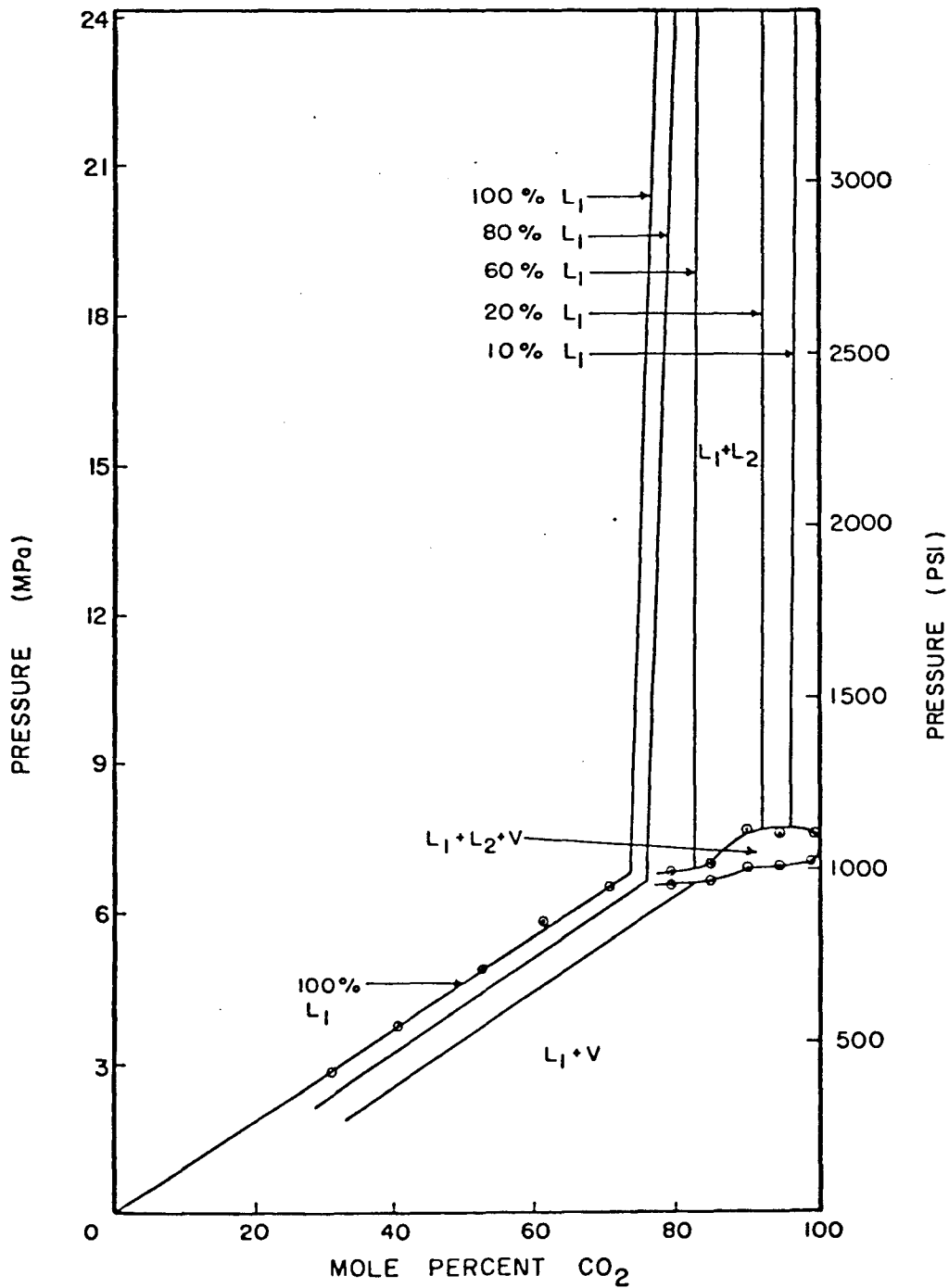


Figure 3.2 Phase behavior of binary mixtures of CO₂ with Maljamar separator oil at 90°F. Curves labeled as a constant percentage lower liquid phase (L₁) report the fraction of the total volume of the mixture occupied by the L₁ phase.

and formed a single liquid phase at high pressure. Bubble point pressures of those mixtures increased with increasing CO₂ concentration. Mixtures containing more than 74 mol % CO₂ formed liquid and vapor (L₁-V) at pressures below about 1000 psi (6890 kPa). With a small increase in pressure (but a large volume change) the vapor phase was liquefied into a CO₂-rich liquid (L₂) phase. For pressures above about 1100 psi (7580 kPa) two liquid phases were present in the cell. Phase volumes in the liquid-liquid (L₁-L₂) region varied slowly with changing pressure.

Comparison of Figures 3.1 and 3.2 yields the following observations. Two or more phases existed over a much wider range of compositions and pressures when solution gas was present. Bubble point pressures at low CO₂ concentrations were, of course, much higher. The three-phase (L₁-L₂-V) region appeared at much lower CO₂ concentrations in the CO₂-RRF system, and the pressures at which three phases coexisted declined as the mole fraction of CO₂ was increased. In contrast, pressures at which three phases were present increased slightly with CO₂ concentration in the CO₂-separator oil system. At CO₂ mole fractions approaching unity, both systems showed three phases near 1075 psia (7410 kPa) which is close to the extrapolated vapor pressure of CO₂ at 90°F (Newitt et al 1956; Orr, Lien, and Pelletier 1981). Reasons for the differences in the shape of the three-phase regions have been discussed by Orr, Yu, and Lien (1981).

For CO₂-RRF mixtures containing between 50 and 60 mol % CO₂, the distinction between L₁-L₂ and L₁-V behavior was not clear. Figure 3.3 shows volumetric behavior of a mixture containing 60 mol % CO₂. At low pressures (below about 1450 psia, 10000 kPa) the mixture appeared to behave as a liquid-vapor system. That is, the overall compressibility of the mixture was high, as it would be in a liquid-vapor system. For pressures between about 1450 and 2620 psia (10000 to 18060 kPa) the overall compressibility was low, as would be the case in a liquid-liquid system. At no time, however, were three distinct phases present in the cell. The two phases present at pressures just below 2620 psia, however, were dark, and separated slowly, so that it was difficult to measure the volumes of the phases. At pressures above 2620 psia, the mixture appeared to form a single phase. The similar appearance of the phases, the small difference in densities, and the abrupt disappearance of the upper phase all suggest that the composition of the mixture was close to that of a critical mixture.

Figure 3.4 shows the behavior of a mixture containing slightly more CO₂ (65 mol %). That mixture did form three coexisting phases, and exhibited a liquid-liquid dew point at about 3600 psia (24820 kPa). Figure 3.5 shows volumetric behavior typical of mixtures containing more than 80 mol % CO₂. At the highest pressure investigated, two liquid phases were present. The volume fractions of the two liquid phases changed little with large decreases in pressure until a vapor phase appeared at the top of the cell. Then, over a narrow pressure range, the CO₂-rich upper liquid (L₂) phase vaporized, though little change in the L₁ phase was observed. Behavior similar to that shown in Figure 3.3 was observed for mixtures containing more than 80 mol % CO₂.

Finally, Figure 3.6 illustrates the behavior typical of the oil containing only solution gas or a mixture containing a low concentration of

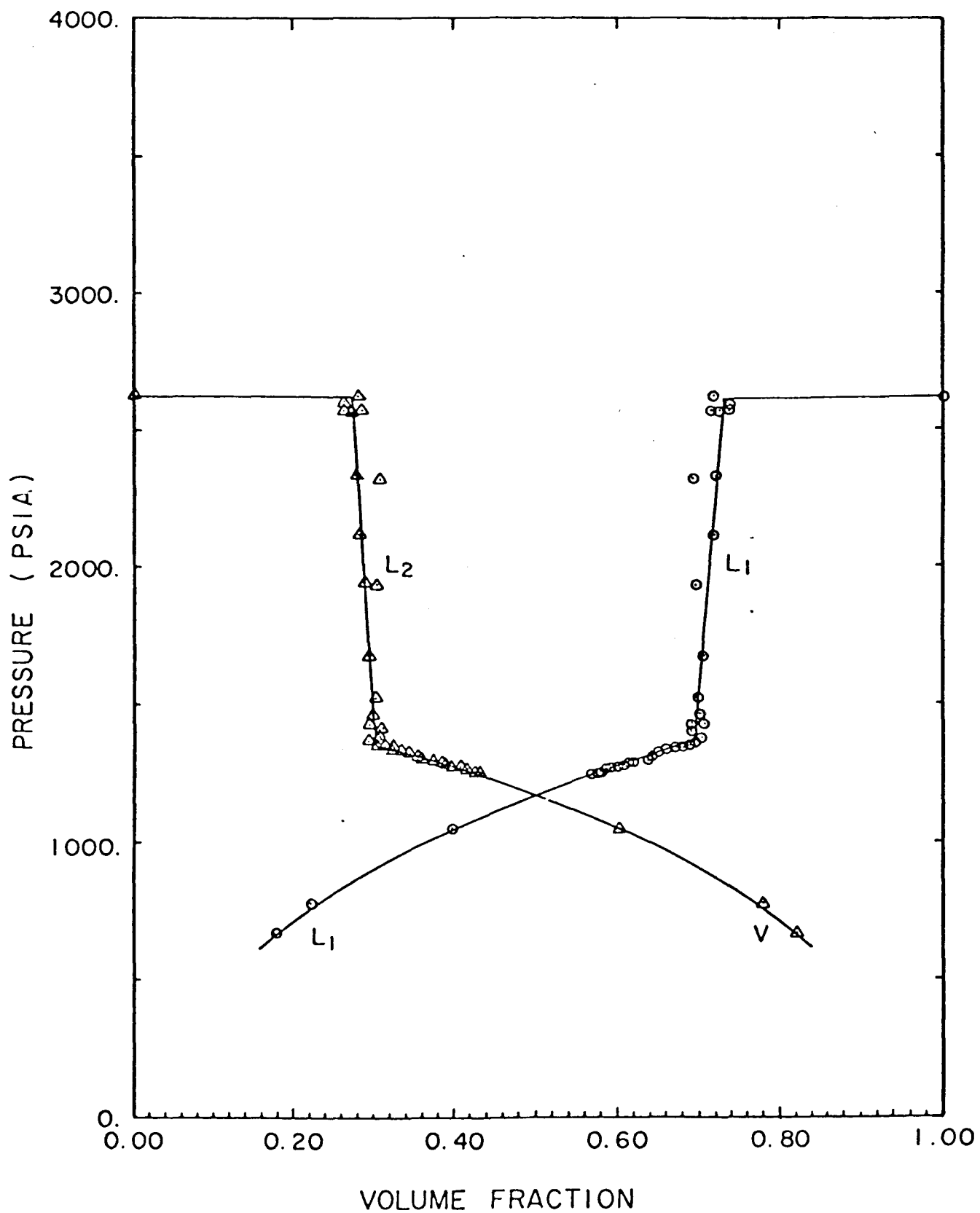


Figure 3.3 Volumetric behavior at 90°F of a mixture containing 60.0 mol % CO₂-40.0 mol % Maljamar recombinated reservoir fluid.

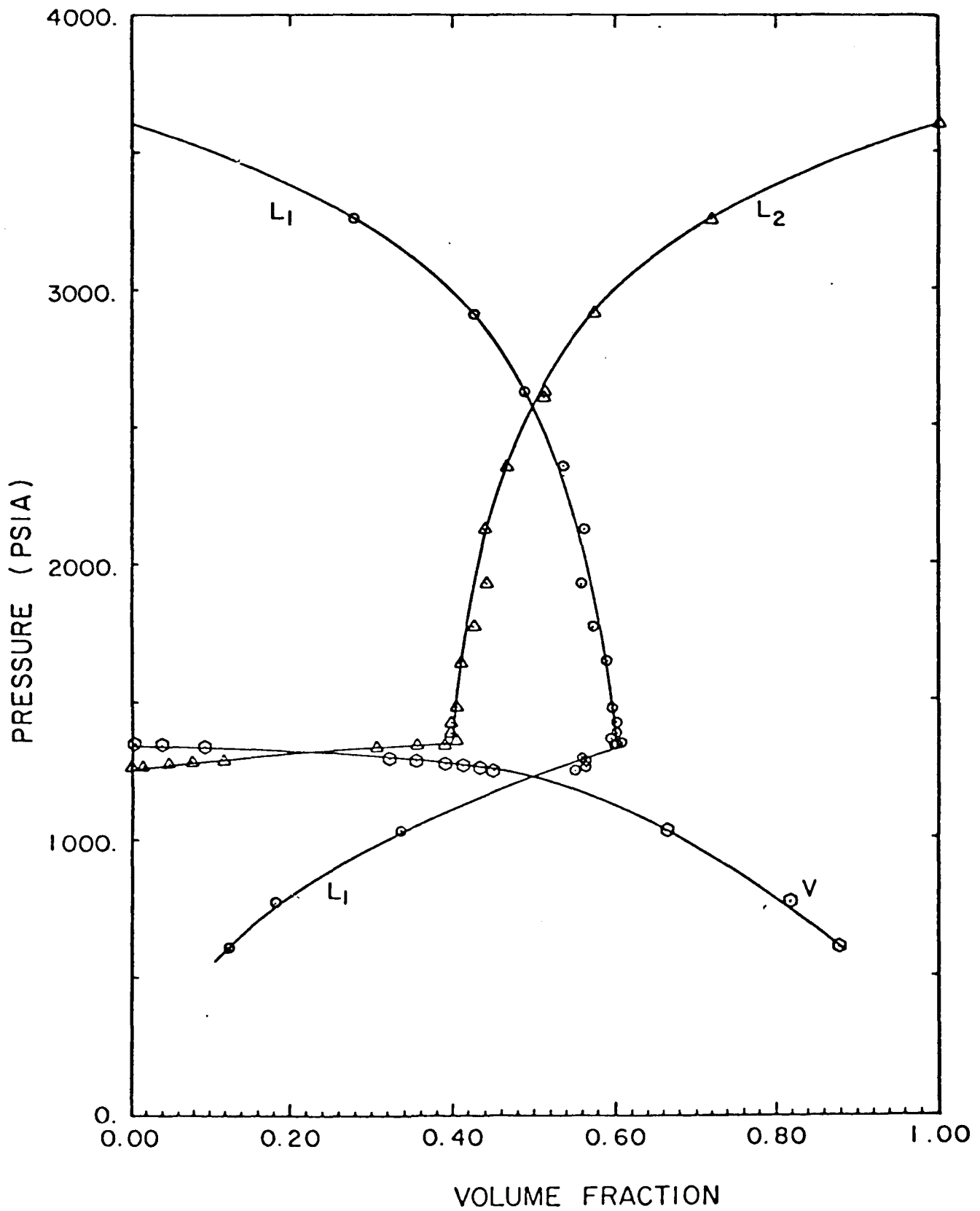


Figure 3.4 Volumetric behavior at 90°F of a mixture containing 65.0 mol % CO₂-35.0 mol % Maljamar recombined reservoir fluid.

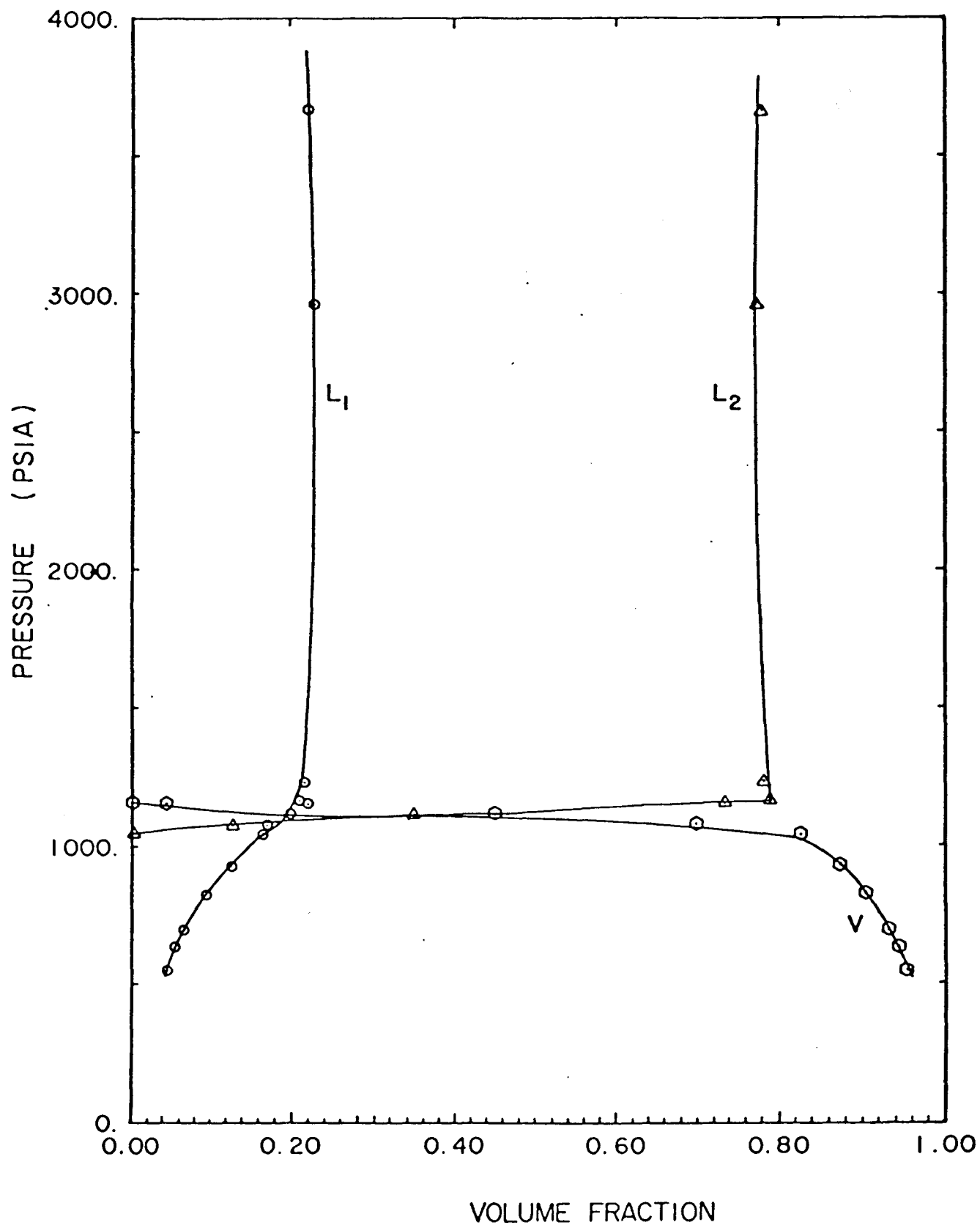


Figure 3.5 Volumetric behavior at 90°F of a mixture containing 85.0 mol % CO₂-15.0 mol % Maljamar recombined reservoir fluid.

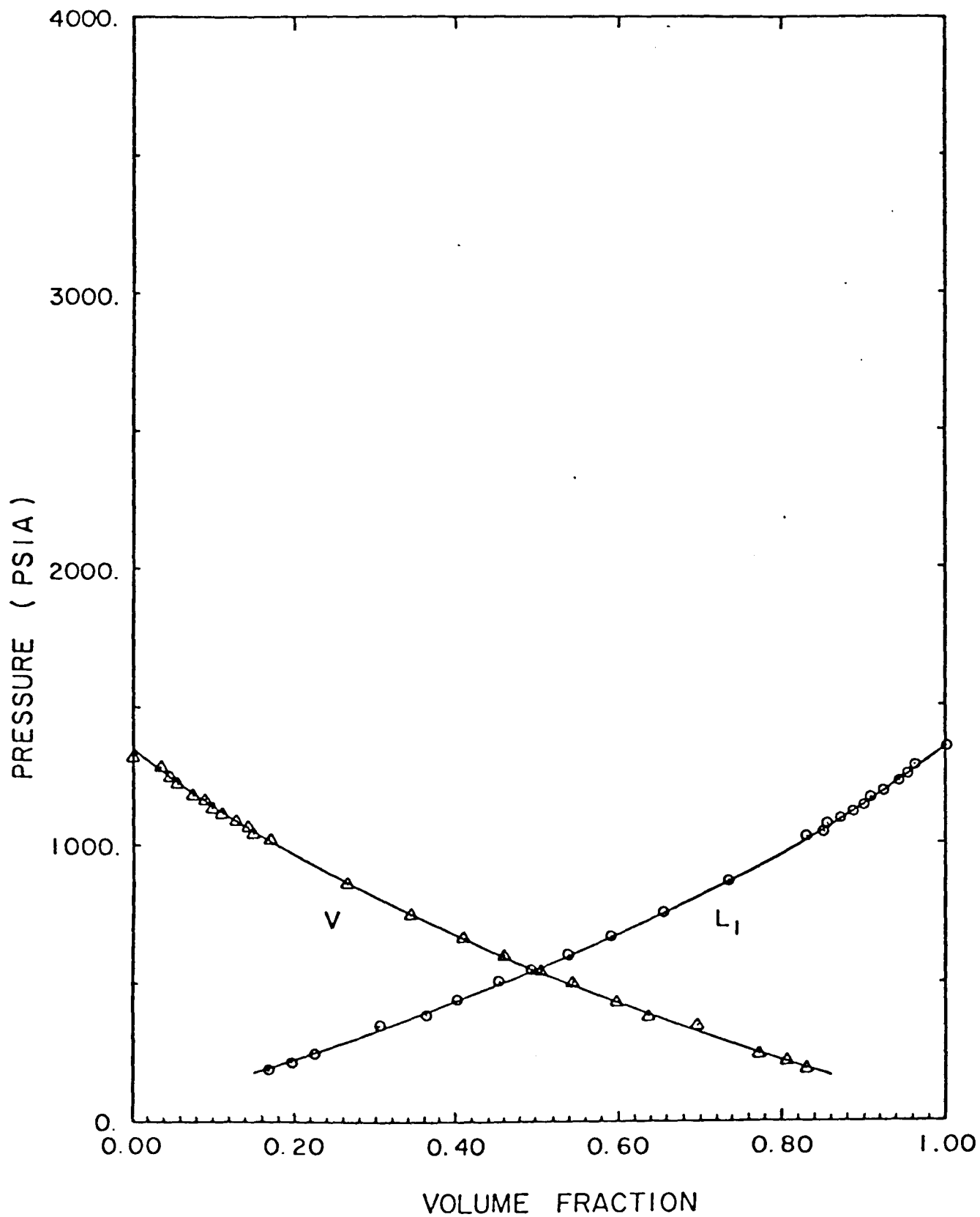


Figure 3.6 Volumetric behavior of Maljamar recombined reservoir fluid at 90°F.

CO₂ (less than about 40 mol % CO₂). At pressures above the bubble point pressure, only a single liquid phase was present in the cell. As the pressure was reduced below the bubble point pressure, a vapor phase appeared at the top of the cell. Its volume grew rapidly with further reductions in pressure, while the volume of the liquid (L₁) phase decreased slowly, so that the volume fraction of the L₁ phase decreased rapidly.

A more direct comparison of the behavior of mixtures with and without solution gas is given in Figure 3.7, reproduced from Orr and Taber (1981). Figure 3.7a illustrates the volumetric behavior of a CO₂-separator oil mixture containing 79.7 mol % CO₂. As the pressure was increased from 950 psi (6550 kPa) to 1000 psi (6890 kPa), the vapor phase changed to a liquid with little apparent change in the L₁ phase. Large additional pressure increases reduced the volume of the L₂ phase as additional CO₂ was compressed into the L₁ phase. Apparently, additional pressure increases would lead to the disappearance of the L₂ phase at a liquid-liquid bubble point. Figure 3.7b illustrates the behavior of a CO₂-RRF mixture containing 74.4 mol % CO₂. The low pressure behavior was qualitatively similar to that observed when solution gas was absent except that the pressure required to liquefy the vapor phase was several hundred psi higher, presumably because the methane concentration in the vapor phase was appreciable. With pressure increases above about 1300 psia, the L₁ phase volume began to decrease as the hydrocarbons in the L₁ phase were extracted into the L₂ phase. Apparently, the L₁ phase would have disappeared at a liquid-liquid dew point had the pressure been increased above 4000 psia (27580 kPa).

The results shown in Figure 3.7 clearly indicate that the addition of solution gas to the separator oil substantially altered the distributions of hydrocarbon components between phases at the higher pressures. Comparison of phase volumes at 2000, 3000 and 4000 psia (13780, 20680 and 27580 kPa) shows that larger volumes of hydrocarbons were extracted into the L₂ phase when solution gas was present even though the overall mole fraction of CO₂ was slightly lower.

Interpretation of the single contact PVT results presented here in terms of pseudo-ternary diagrams is discussed and compared with results of CMC phase composition measurements (given below) in §4.

Wasson Stock Tank Oil

Volumetric behavior of seven mixtures of oil from the Willard Unit of the Wasson Field (Gaines County, Texas) was studied at 105°F. Figure 3.8 summarizes results of those measurements. The phase diagram shown in Figure 3.8 is remarkably similar to that shown in Figure 3.2 for Maljamar separator oil at 90°F. The principal features of the two-phase diagrams, the locations of the L-V, L₁-L₂, and L₁-L₂-V regions, are nearly the same. The bubble point pressure curve climbed slightly more rapidly with increasing CO₂ concentration for Wasson because the temperature was higher. The L₁-L₂-V region also occurred at slightly higher pressures, again because the temperature was higher. At the highest CO₂ concentration for which a three-phase region was observed (95.0 mol % CO₂), the L₁-L₂-V region appeared very near the

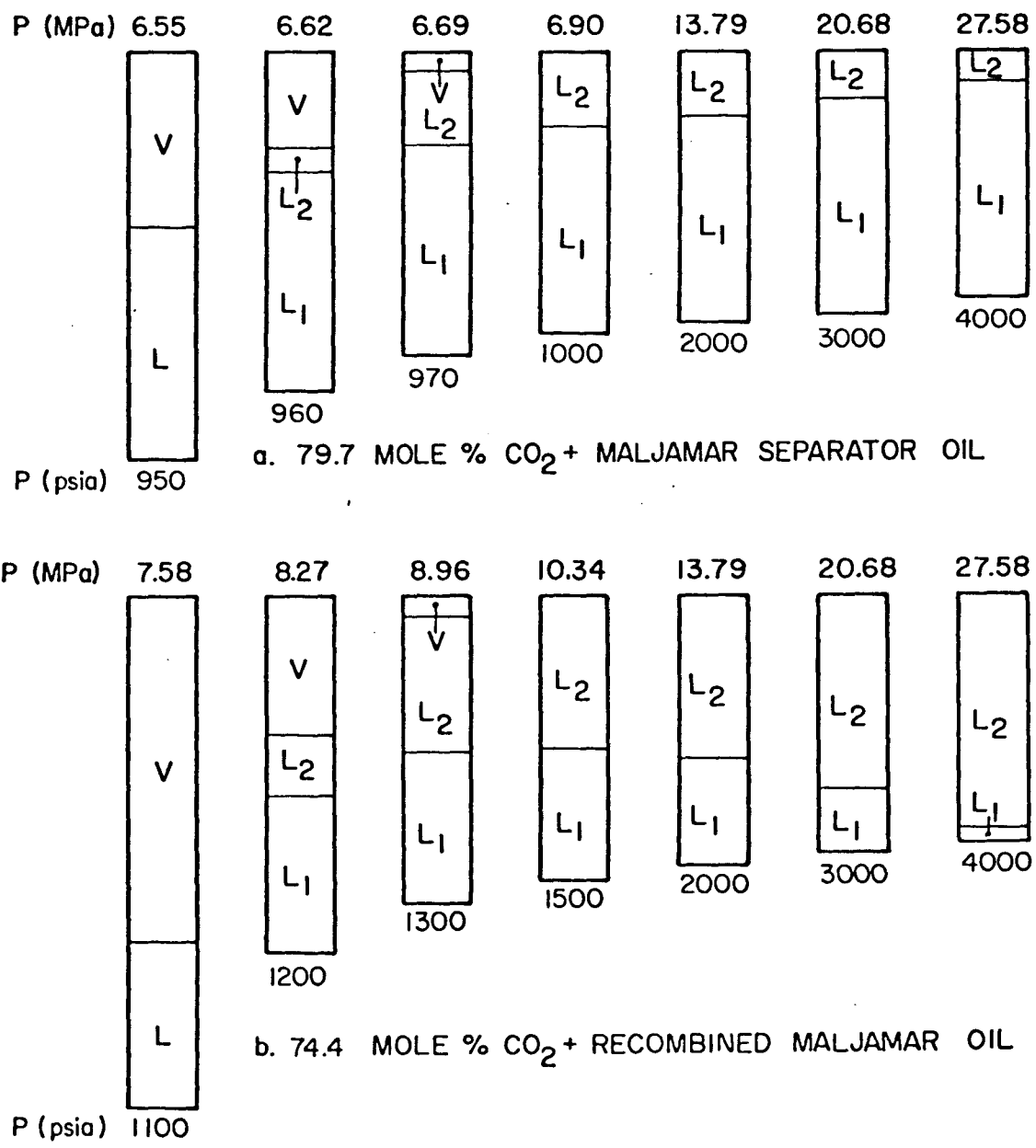


Figure 3.7 Volumetric behavior at 90°F of CO₂-crude oil mixtures with and without solution gas.

extrapolated vapor pressure of CO_2 , as Orr, Lien, and Pelletier (1981) argued it should. Figure 3.9 compares approximate carbon number distributions for Wasson and Maljamar oils. It is not surprising that the behavior of the two oils is similar, since their compositions are also similar.

Figures 3.10-3.16 report the volumetric behavior of each of the mixtures studied. Vapor-liquid bubble point pressures were observed for mixtures containing 60.36 mol % CO_2 or less. The volumetric behavior shown in Figures 3.10, 3.11, and 3.12 simply reflects the fact that an increase in the CO_2 concentration increases the pressure required to dissolve all the CO_2 in the oil. As the amount of CO_2 dissolved in the oil increases, so does the volume of the saturated mixture. Figure 3.13 compares the swelling of Maljamar and Wasson dead crudes. In Figure 3.13, the swelling factor is defined as the ratio of the volume of the mixture containing oil and CO_2 at its bubble point pressure to the volume of the original oil at atmospheric pressure. There was essentially no difference in swelling for the two oils.

Figures 3.14, 3.15, and 3.16 report behavior observed for mixtures containing enough CO_2 that two or more phases were present over very large pressure ranges. At low pressures, only a black oil phase and a clear vapor were present. At pressures slightly below the extrapolated vapor pressure of CO_2 at 105°F (1308 psia, 9020 kPa), a middle liquid (L_2) phase appeared, and with a small increase in pressure, grew rapidly in volume at the expense of the vapor phase. In the L_1 - L_2 region phase volumes were much less dependent on pressure. As in the Maljamar system, saturation pressures in the L_1 - L_2 region could only be estimated because both phases were so black and separated so slowly that it was nearly impossible to tell whether more than one phase was actually present in the cell.

3.2 Phase Compositions and Fluid Properties: Measurement by the Continuous Multiple Contact Experiment

Experimental Apparatus

Details of the continuous multiple contact (CMC) experiment have been described previously (Orr et al 1980; Orr and Taber 1981). In this section, we review briefly the experimental procedure and describe improvements to the design reported previously. A schematic of the apparatus currently in use is given in Figure 3.17. In a typical experiment, a high pressure cell (a 1.27 cm ID stainless steel tube with a volume of 134 cm^3) is filled with crude oil. A Ruska pump injects mercury into a thermostatted vessel containing CO_2 at the test temperature, which displaces CO_2 into the mixing vessel at a fixed rate, usually 12 cm^3/hr . The temperature of the mixing cell is controlled to within $\pm 0.2^\circ\text{F}$ of the test temperature. An Eldex liquid chromatography pump removes fluid from the bottom of the cell and circulates it to the top of the cell to mix the fluids within the cell. The circulation rate of 450 cm^3/hr is large compared to the injection rate.

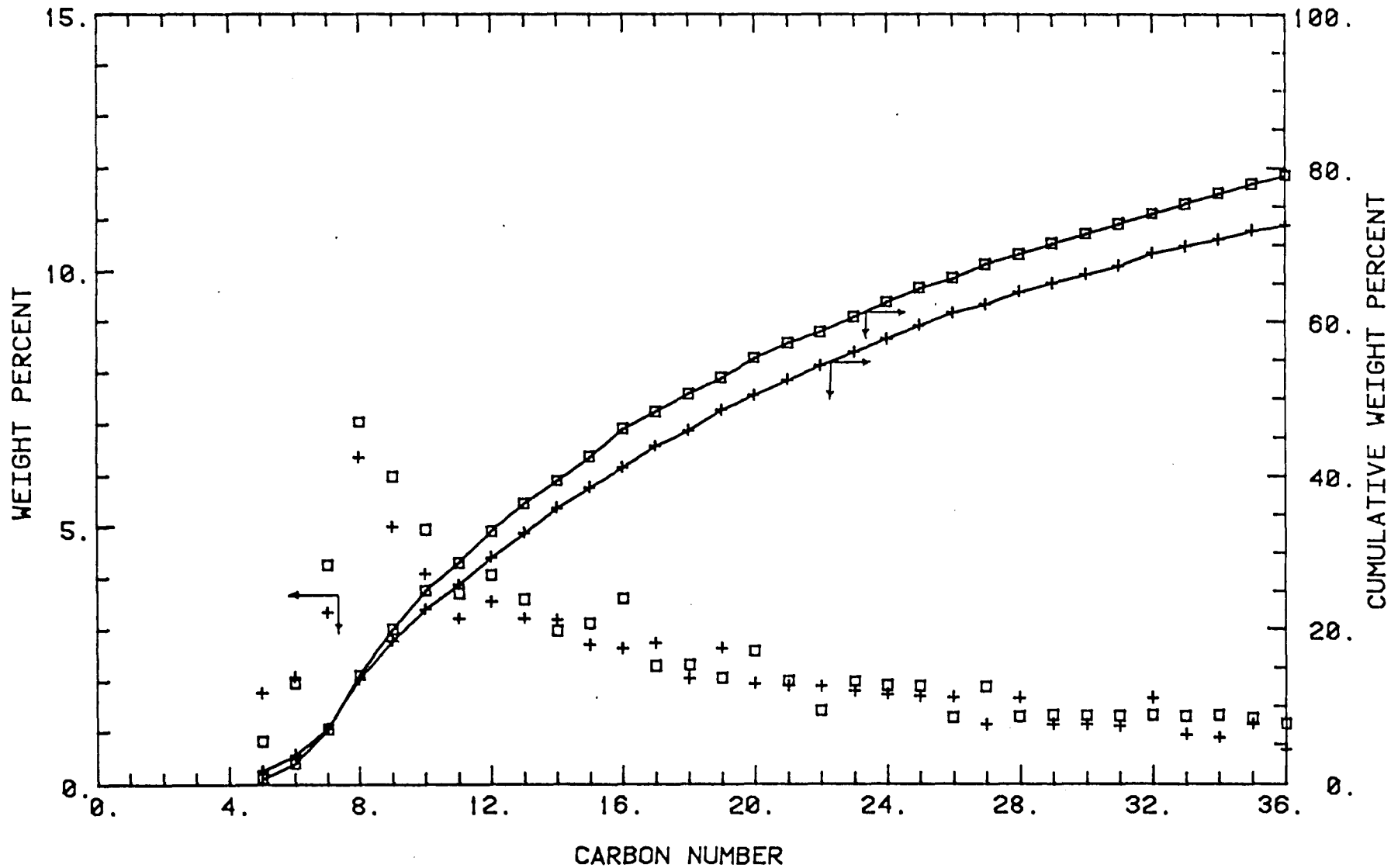


Figure 3.9 Comparison of the compositions of Maljamar (□) and Wasson (+) crude oils.

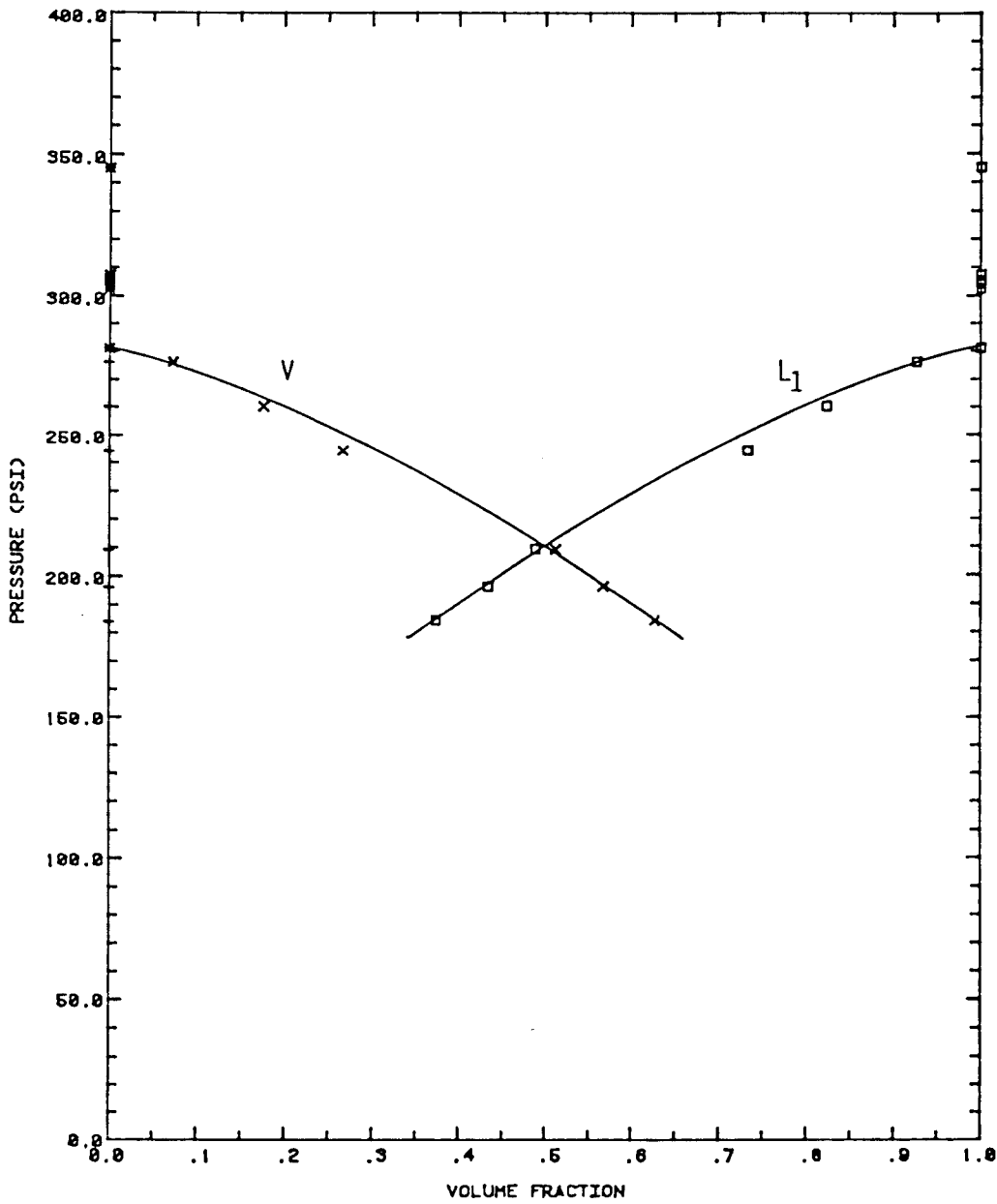


Figure 3.10 Volumetric behavior at 105°F of a mixture containing 14.2 mol % CO₂ in Wasson stock tank oil.

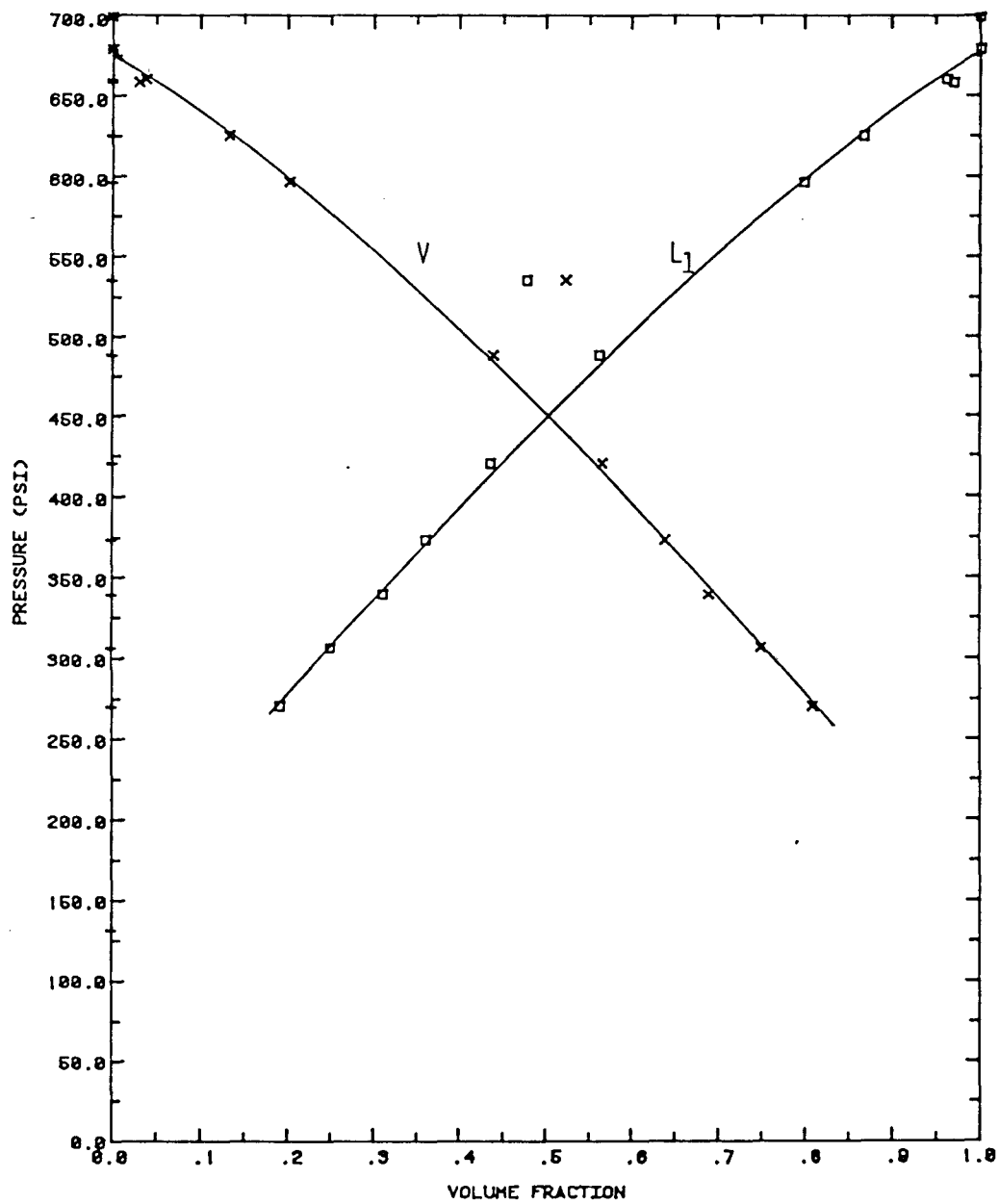


Figure 3.11 Volumetric behavior at 105°F of a mixture containing 34.8 mol % CO₂ in Wasson stock tank oil.

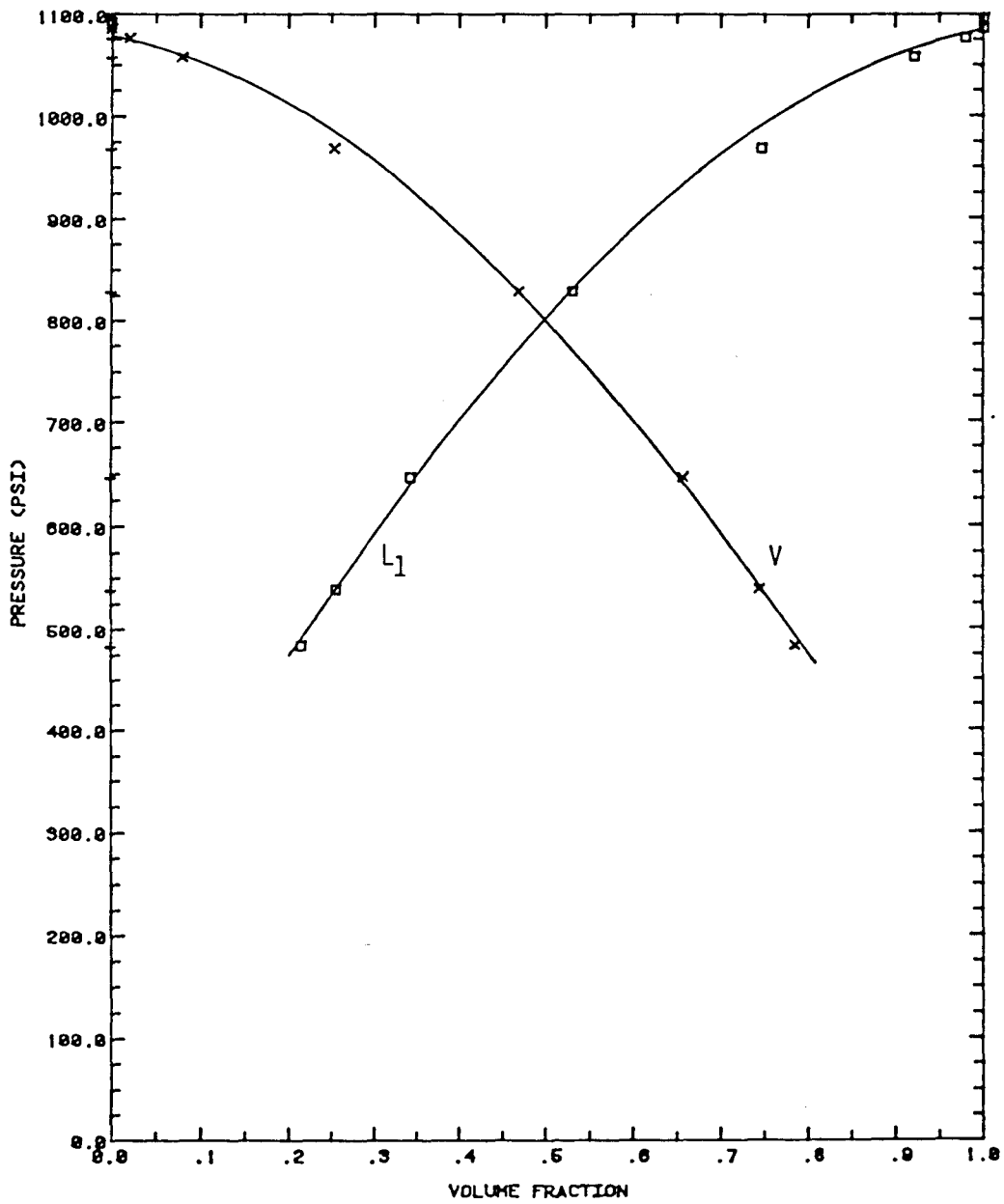


Figure 3.12 Volumetric behavior at 105°F of a mixture containing 60.4 mol % CO₂ in Wasson stock tank oil.

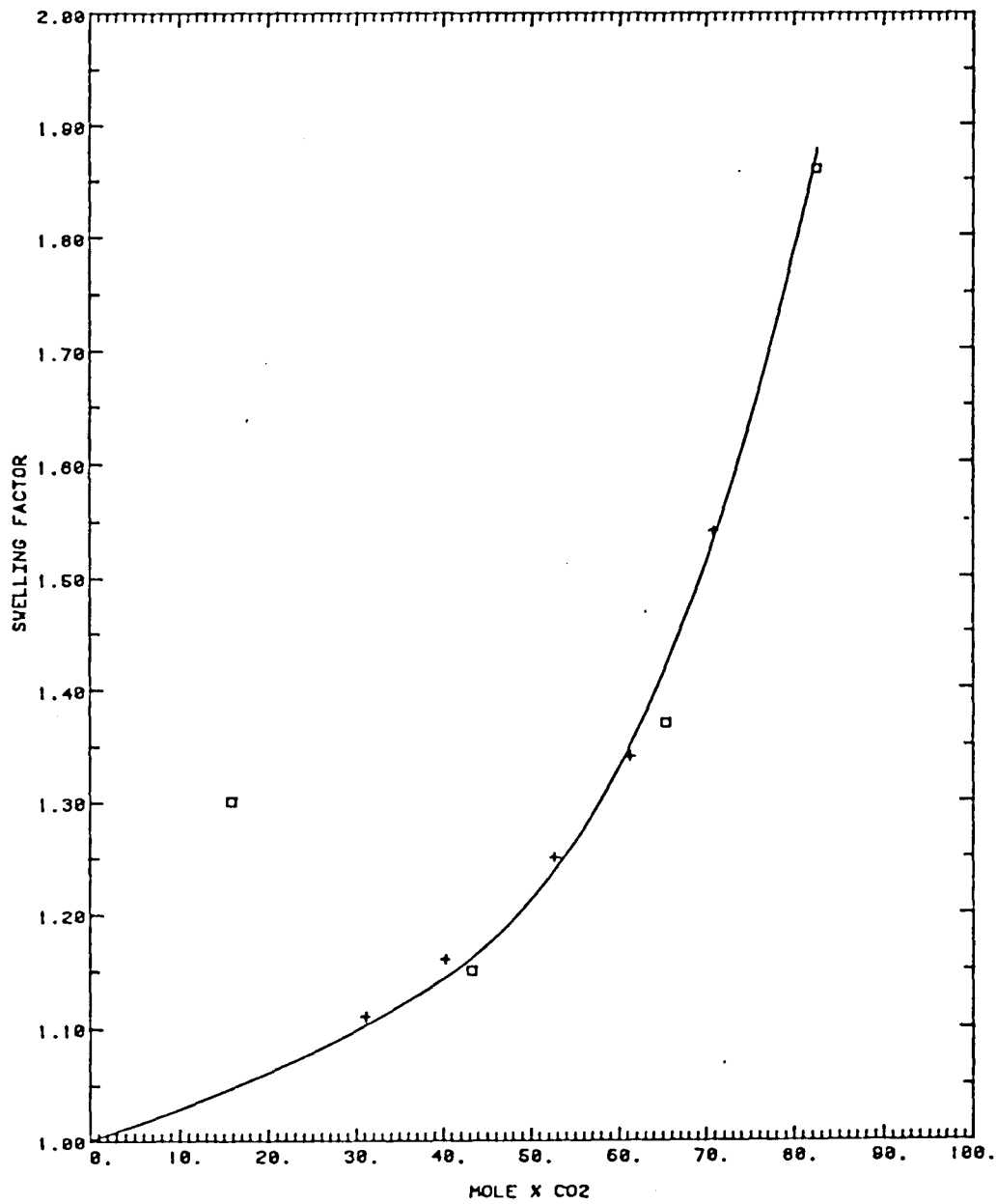


Figure 3.13 Swelling of Maljamar and Wasson crude oils by dissolved CO₂.

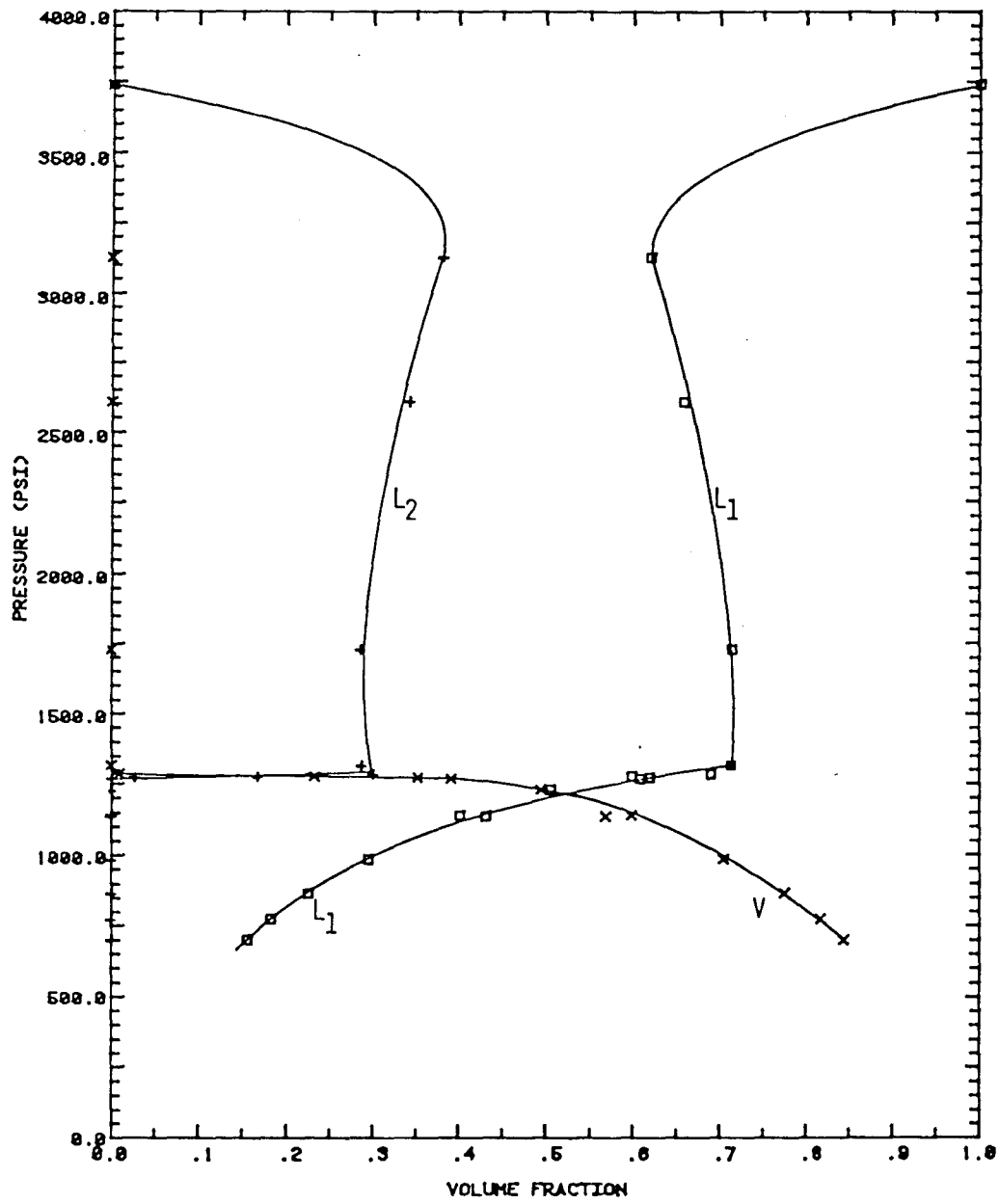


Figure 3.14 Volumetric behavior at 105°F of a mixture containing 80.0 mol % CO₂ in Wesson stock tank oil.

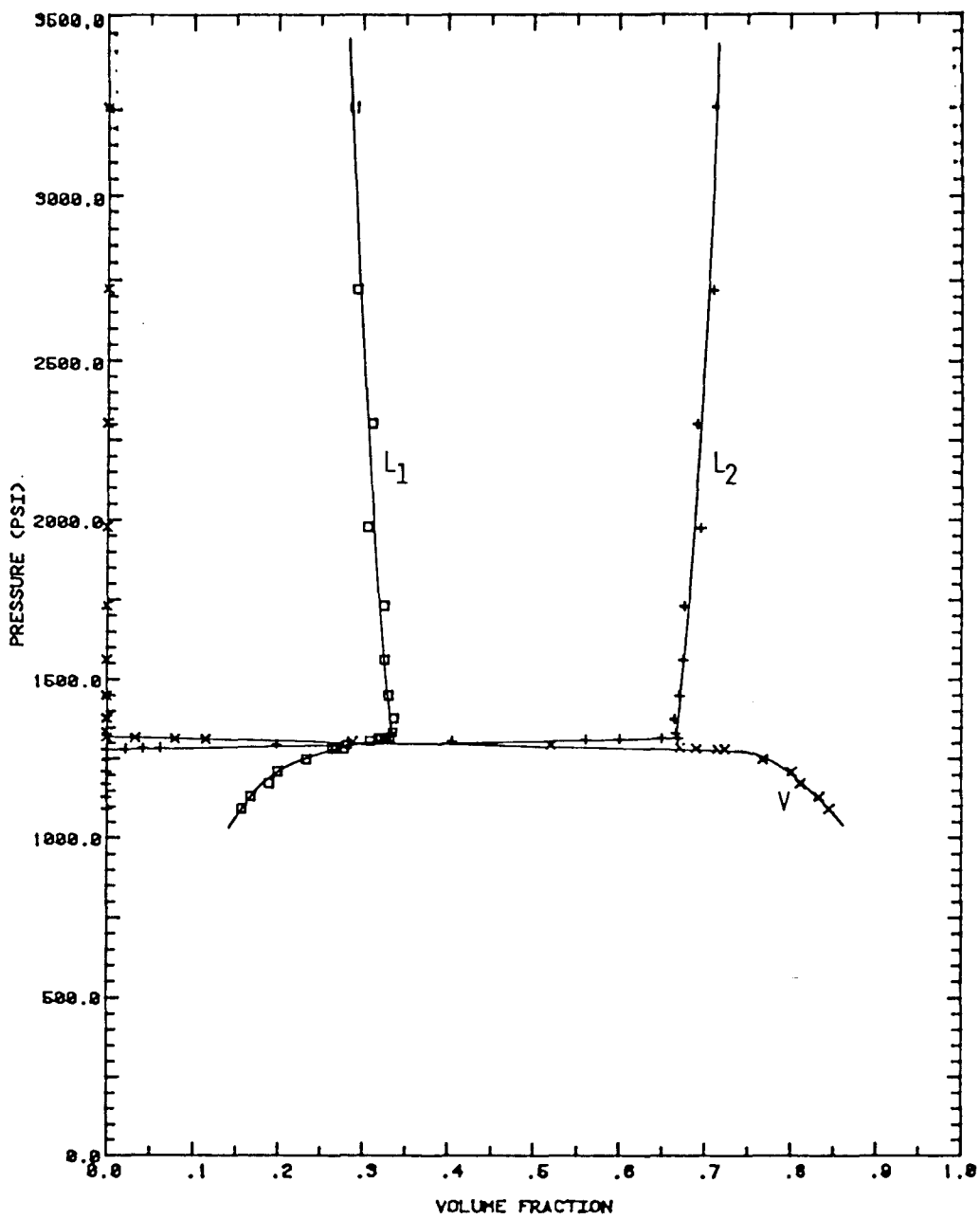


Figure 3.15 Volumetric behavior at 105°F of a mixture containing 90.0 mol % CO₂ in Wasson stock tank oil.

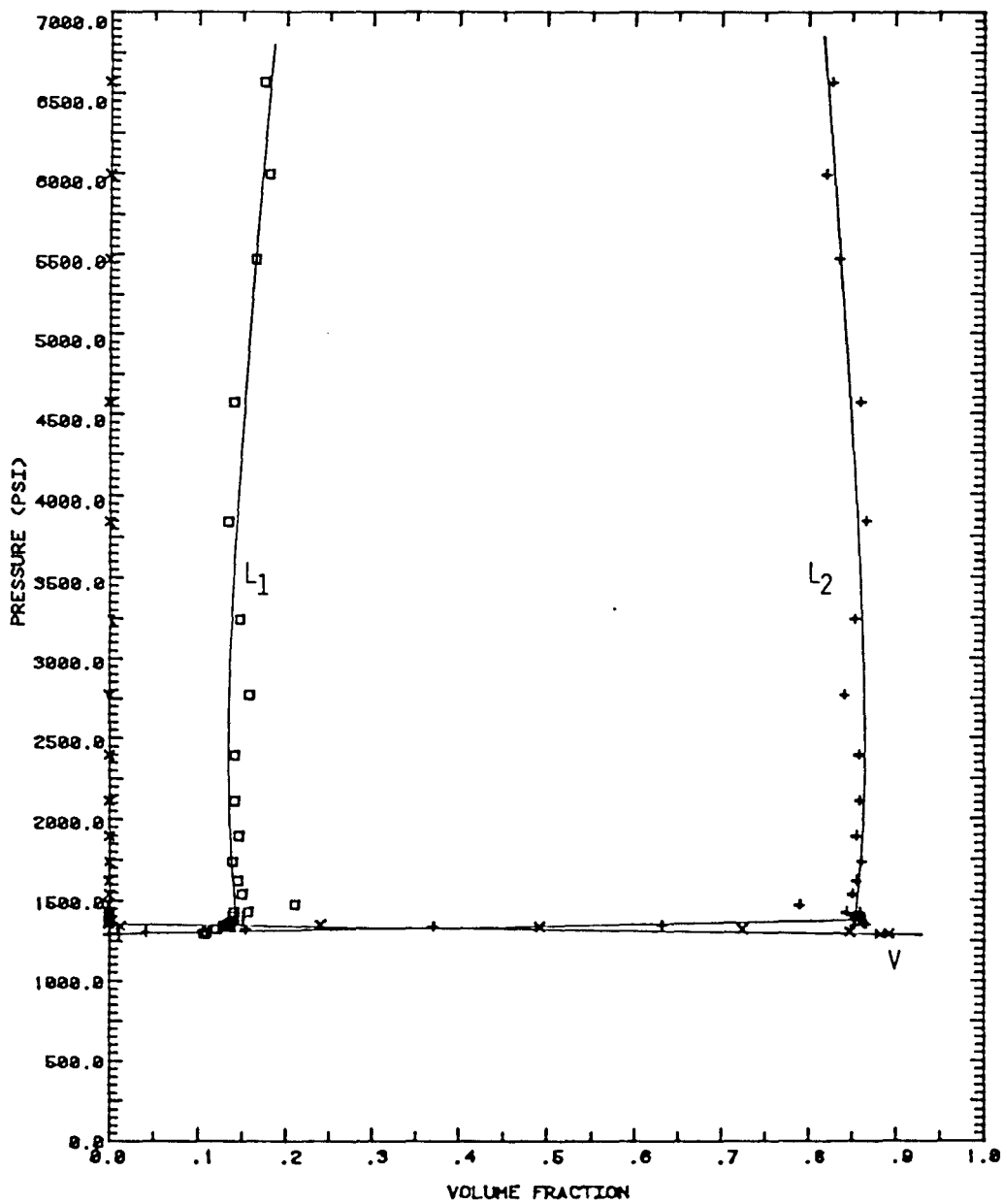


Figure 3.16 Volumetric behavior at 105°F of a mixture containing 95.0 mol % CO₂ in Wasson stock tank oil.

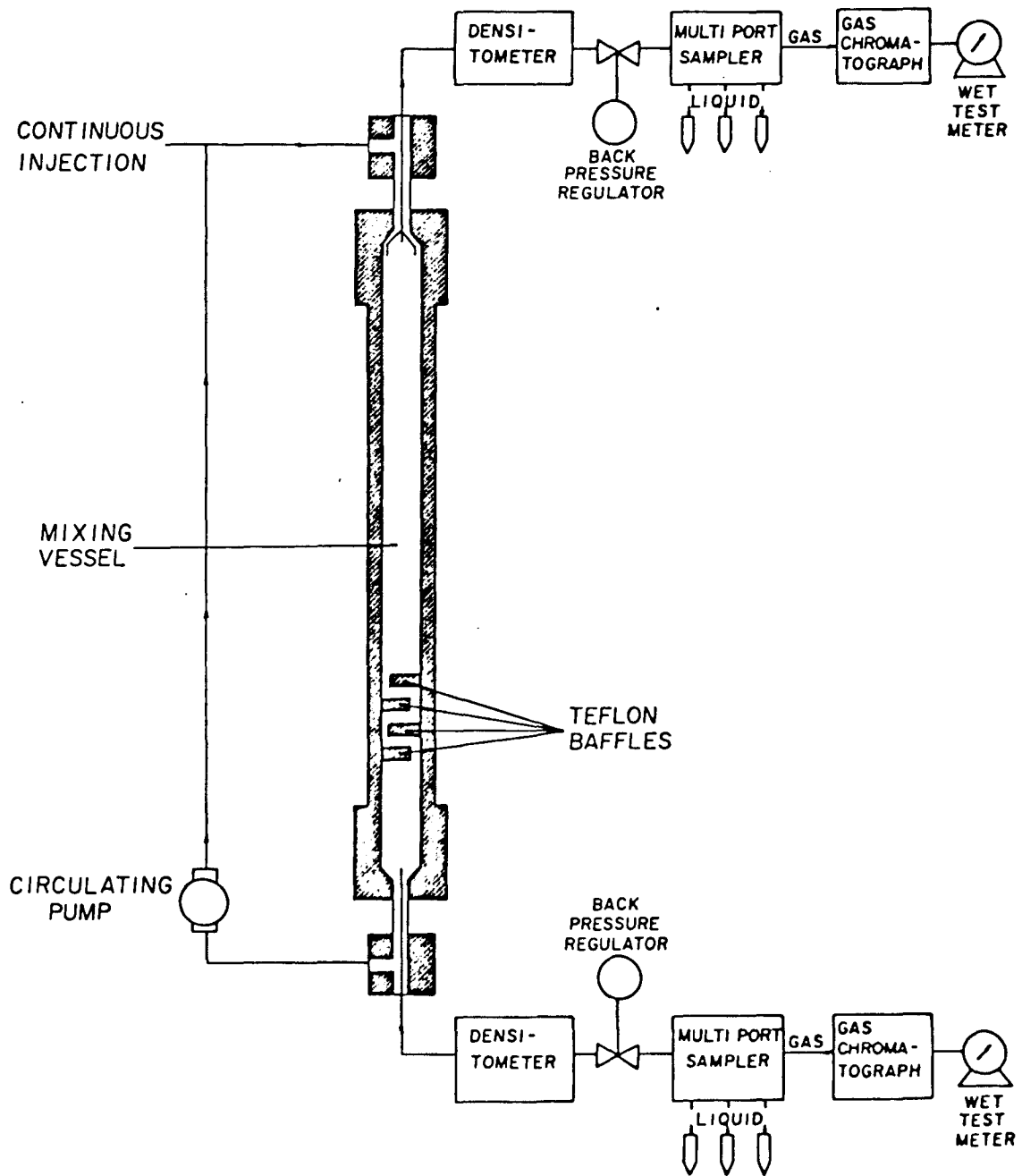


Figure 3.17 Schematic of the apparatus for measurement of phase compositions by continuous multiple contacts.

Several versions of the sample collection and circulation inlet and outlet ports were tested to find a combination which provides rapid mass transfer between phases but which also allows withdrawal of samples of each phase uncontaminated by the other phase. The design currently in use is also shown in Figure 3.18. Lower phase samples are drawn from the base of the cell through a 1/16 in. OD tube, and lower phase to be circulated is withdrawn from

Upper and lower phase samples leaving the cell pass through separate Mettler/Paar DMA512 high pressure density measuring cells. Separate temperature controllers maintain the temperature in each densitometer cell to within $\pm 0.1^\circ\text{F}$. The densitometers must be calibrated with two fluids of known density at the test temperature and pressure. Calibrations for the experiments reported below were performed with pure CO_2 or methane (C_1) as the low density fluid, and decane (C_{10}) as the high density fluid. Density data of Newitt et al (1956) were interpolated for CO_2 at 160°F and those of Michels, Botzen, and Schurrman (1957) were used for CO_2 at 90°F . Densities for methane were interpolated from data given by Harrison, Moore, and Douslin (1973). Density data for decane were obtained from Reamer and Sage (1963). The resolution of the density measurement is $\pm 0.0003 \text{ g/cm}^3$. Uncertainties in the densities of calibration fluids probably reduce the accuracy of the measurement about $\pm 0.001 \text{ g/cm}^3$.

Constant pressure is maintained in the cell by controlling the rate at which samples are produced. A separate back pressure control valve regulates production from each sample stream. Each control valve is a low dead volume Nupro SS-2SG fine metering valve. Its position is adjusted continuously by a DC motor driven by the difference between a set-point pressure and the output of a Setra 204 transducer. To prevent conflict between the regulators, an automatic switching circuit selects one to control the flow. During this period (approximately five minutes), an air actuated shutoff valve is closed downstream of the other control valve.

Downstream of the back pressure regulators, upper and lower phase samples flow to separate multiport sampling valves which direct the two-phase mixtures to one of a series of centrifuge tubes in which liquids are caught. Gas samples flow out of the centrifuge tubes to an automatic gas sampling valve installed in and controlled by a Hewlett-Packard 5840A gas chromatograph. A second valve switches between gas sample streams. Gas samples are analyzed on-line with a cycle time of about ten minutes. Liquid samples are analyzed after completion of a displacement experiment because the analysis time (about one hour per sample) is too long to allow on-line analysis. Amounts of heavy components not eluted at the highest temperature were estimated using the technique outlined in a proposed ASTM test method (American Society for Testing and Materials, 1976) for analysis of crude oils. Amounts of liquids produced are determined by weight. Produced gas volumes are measured with a separate wet test meter for each sample stream. Samples are collected for one hour to ensure that quantities of liquid and vapor are sufficient for accurate measurements of amounts and compositions. The overall average composition of each sample is calculated from the quantity and composition of the liquid and vapor sample for each sample stream.

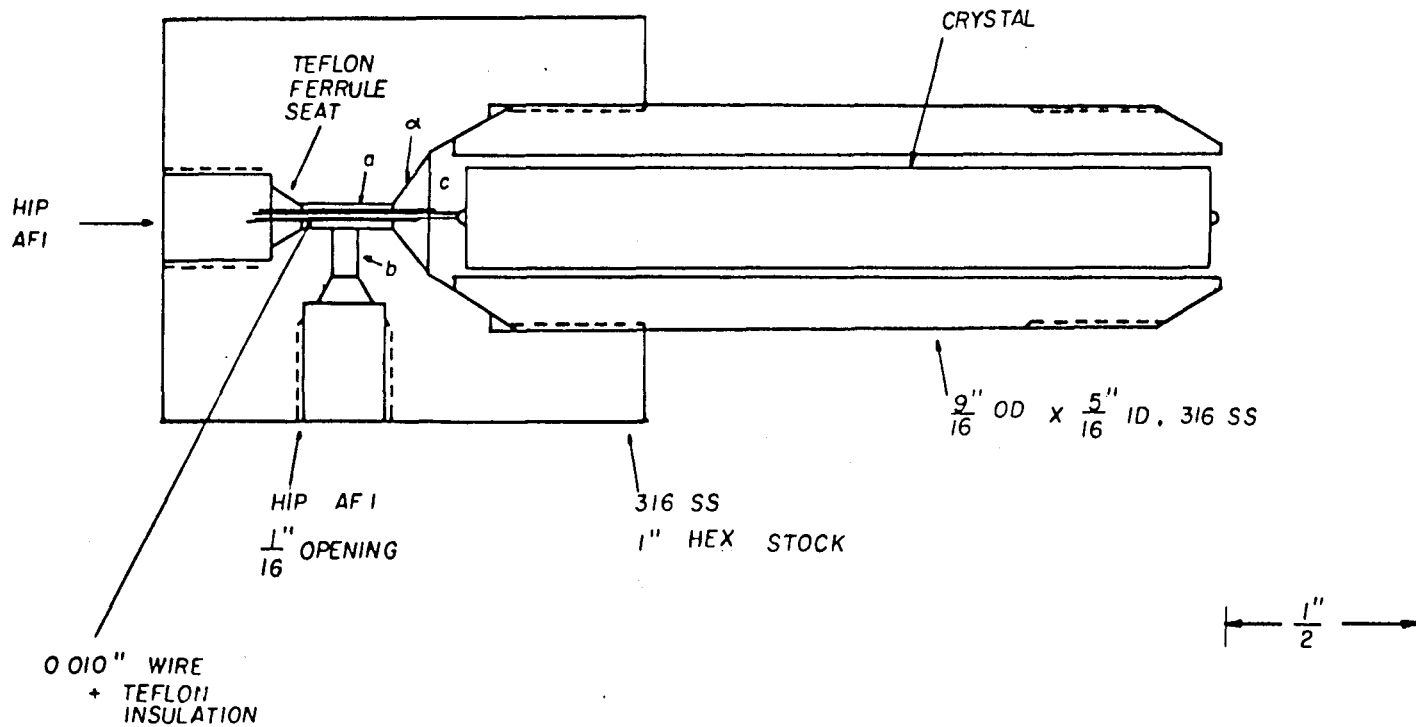


Figure 3.18 High pressure cell for a vibrating quartz crystal viscometer.

The apparatus currently in use differs from that described previously in the following ways:

- (1) High pressure densitometers have been installed.
- (2) Separate back pressure regulators control each sample stream to provide more precise control of the volume of each phase removed from the cell.
- (3) The volume of the mixing cell has been doubled.
- (4) The direction of circulation has been reversed; the circulation intake and outlet, and sampling ports have been redesigned.
- (5) Sample production lines were rerouted to minimize dead volume.

The volume of the cell was doubled to reduce the effects of averaging during a sampling period (see below), so that large enough samples could be taken to ensure complete displacement of the dead volume associated with the densitometers (1.3 cm^3 each) and with the high pressure cells for measurement of phase viscosities to be added later. The direction of circulation was reversed to avoid attempts at pumping a highly compressible vapor phase in experiments at low pressure.

Measurement of Phase Viscosities

The goal of the research effort to improve the core experiment is to develop a technique with which simultaneous measurements of phase compositions, densities, and viscosities can be obtained at reasonable cost. Phase compositions and densities can now be measured reliably, and an attempt to add equipment for phase viscosity measurements is well underway. Standard techniques for measurement of viscosities at high pressures, such as measurement of pressure drop across a capillary tube, were eliminated from consideration, because flow rates in the sample production lines are not known accurately and because the flow rates are so low that the pressure drop across a capillary would be small compared to the pressure oscillations caused by the circulation pump and by the operation of the back pressure regulators. One method which appears to be well-suited to the flow setting of the CMC experiment relies on the measurement of the damping of the torsional vibration of a cylindrical quartz crystal by a viscous fluid surrounding it. The technique was first applied to viscometry of liquids at room temperature by Mason (1947), and has since been used to study the viscosity of compressed gases and liquids by a number of investigators (Welber 1960; Webeler 1961; De Bock, Grevendonk, and Herreman 1967; De Bock, Grevendonk, and Awouters 1967; Collings and McLaughlin 1971; Haynes 1973; Diller 1980). The technique has been used to measure viscosities of pure components over wide ranges of temperature, pressure and viscosities, but it has apparently not been applied to the complex mixtures of interest here. The method appears to have several advantages for the experimental application planned:

- (1) Quartz is inert to the components present in CO₂-crude oil mixtures (though the possibility that heavy asphaltic components may adsorb at the crystal surface will have to be investigated).
- (2) The boundary layer in which the sample fluid is sheared near the vibrating crystal is very thin, so the measurement can be made with small sample volumes.
- (3) A low dead-volume crystal holder can be easily installed in the sample flow lines of the CMC apparatus.

A high pressure crystal holder has been designed, built, and pressure tested. A schematic of the holder is shown in Figure 3.18. The cell is designed to withstand pressures in excess of 5000 psia. It is a modification of an MS-11 Micro Series Reactor Vessel made by the High Pressure Equipment Company. The cell will have a fluid volume of about 1.2 cm³, nearly all of which is in the annulus between the crystal and the cell wall. Crystal electrical leads will be sealed by teflon ferrules; otherwise, all seals will be metal to metal. Thus, there will be no o-rings to be damaged by CO₂ or solvents used to clean the cell. Preparation of several crystals is underway. Testing of the new apparatus will begin upon receipt of the crystals.

The crystal will be supported at the nodes at either end by wires bonded to the crystal surface. Electrodes will be plated directly onto the crystal surface. A simple experiment to evaluate effects of CO₂-crude oil mixtures on electrode coatings was performed in the apparatus shown in Figure 3.19. Glass slides coated with platinum and gold were placed on a perforated teflon support to isolate them electrically from the steel walls of the high pressure sight glass. The samples were not in contact with each other to avoid inducing galvanic corrosion.

After purging the system with carbon dioxide gas, 200 cm³ of crude oil and 40 cm³ of 3% calcium chloride brine were injected. Liquid carbon dioxide was then injected until the pressure reached 2500 psi. The interface between the CO₂-rich and oil-rich phases was positioned so that the samples were located at the interface. The calculated system composition was 19 mole % brine, 8% oil, and 73% CO₂. The vessel was maintained at 2500 psi and 50°C for 500 hours.

At the end of the 500 hour period, the system was decompressed, and the samples were removed and prepared for viewing with a scanning electron microscope (SEM). SEM photographs taken after the test were compared with similar photographs taken before the test. Qualitative elemental analysis were run at the same time using an energy dispersive x-ray analysis system attached to the SEM. This analytical method is sensitive to small amounts of heavy metals and less sensitive to lighter elements. It is unable to analyze elements lighter than sodium.

The SEM photographs (Pelletier 1981) indicated that the platinum coating was not affected by the test except near the edges of the sample. Apparently,

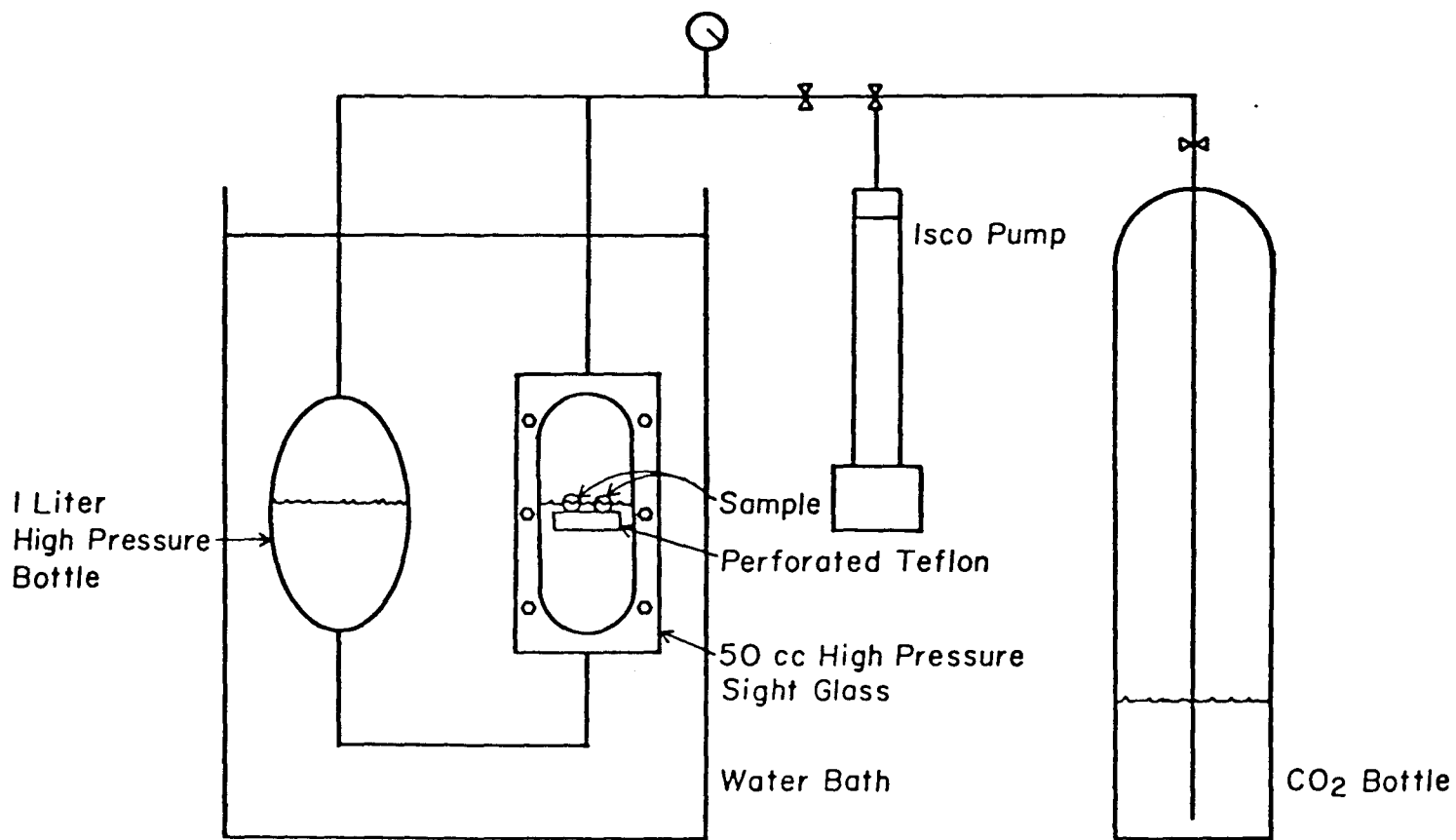


Figure 3.19 Schematic of the apparatus for evaluation of electrode coatings.

the high pressure CO₂ penetrated between the coating and the substrate near the edge of the coating. Upon decompression, the CO₂ expanded by about 700 times damaging the film. Energy dispersive x-ray analysis of the platinum surface showed no evidence of contamination.

The gold coating, however, showed substantial damage. The surface was badly wrinkled. The x-ray analyses of the surface after the test showed that the gold surface had been contaminated by mercury. Evidently, small amounts of mercury present in the high pressure apparatus amalgamated with the gold surface. The volume change which accompanies amalgamation caused the film to buckle and blister.

Of the two films, gold is clearly unsuitable for use in standard high pressure petroleum fluid laboratories since mercury is commonly used as an incompressible pumping fluid. Some contamination of equipment which had previously contained mercury is apparently very likely. The test apparatus had components that had been used in a mercury system although the apparatus itself had not. These components were cleaned with solvents and a chelating agent before they were installed in the test apparatus. It appears, therefore, that trace contamination by mercury is a greater problem than anticipated.

The platinum film retained its surface characteristics very well. The only possible problem is the flaking along the edge. It is not clear whether the flaking was caused by the presence of the sharp edge of the glass slide or whether it would occur at a smooth transition from the platinum coating to a cylindrical crystal surface. To eliminate this problem, the platinum surface should be free of cracks and crevices, or procedures which produce rapid decompression in gas systems should be avoided. Another possible solution would be to coat the platinum surface with some material which would prevent penetration of high pressure CO₂ under the surface. It seems likely that problems will be minimal if the platinum surface is firmly bonded to the crystal surface at the edges of the coatings.

CMC Displacements in Binary Systems

Binary systems offer simple tests to evaluate the operation of the apparatus. It is important to establish that fluids within the cell are well-mixed and that representative samples of each phase present can be obtained. If the cell contains a pure hydrocarbon in which CO₂ is soluble, then CO₂ injected initially will dissolve completely in the hydrocarbon, and the mixture will form a single phase. If the contents of the cell are well-mixed, then the composition of the fluids produced from the upper and lower sample ports will be the same. If the mole fraction of CO₂ in the liquid phase is z_1 , then a material balance on CO₂ yields

$$v \frac{d}{dt} (\rho_L z_1) = \rho_1 q_1 - \rho_L q_p z_1 \quad (3.1)$$

where v is the volume of the cell, ρ_2 the molar density of the liquid phase, ρ_1 the molar density of pure CO_2 , q_i the volumetric injection rate, and q_p the sum of the production rates from upper and lower sample ports. If there is no volume change on mixing, then $q_i = q_p$. Otherwise, q_p will be less than q_i . In what follows, we assume that the molar density of CO_2 dissolved in the liquid phase has a constant value, ρ_{1L} , and that the molar density of the hydrocarbon in the liquid phase remains that of the pure component. The production rate is then

$$q_p = \frac{\rho_1 q_i}{\rho_{1L}} \quad (3.2)$$

and the molar density of the liquid phase is

$$\rho_L = \frac{\rho_{1L} \rho_2}{\rho_{1L} + z_1 (\rho_2 - \rho_{1L})} \quad (3.3)$$

where ρ_2 is the molar density of the hydrocarbon. That this assumption is reasonable can be seen from Figure 3.20, which reports densities of liquid phase mixtures of CO_2 and decane (C_{10}) measured in the CMC apparatus at 1250 psia and 160°F. Linear interpolation between the density of pure C_{10} and on apparent density of CO_2 slightly higher than that of C_{10} fits the data well. The solution to equation (3.1) with the assumptions included in equations (3.2) and (3.3) is

$$z_1 = \frac{\alpha \{1 - \exp(-\beta t)\}}{1 + (\alpha - 1) \{1 - \exp(-\beta t)\}} \quad (3.4)$$

where $\alpha = \rho_{1L}/\rho_2$, and $\beta = (\rho_1 q_i)/(\rho_{1L} v)$. This solution is valid as long as z_1 is less than the solubility of CO_2 at the operating pressure and temperature.

In a typical CMC experiment, samples are collected for a fixed period, usually one hour. For samples taken while the overall composition lies in the single phase region, the rate at which CO_2 is produced is

$$q_{\text{CO}_2} = q_p \rho_L z_1 = \frac{q_i \rho_1 \rho_L z_1}{\rho_{1L}} \quad (3.5)$$

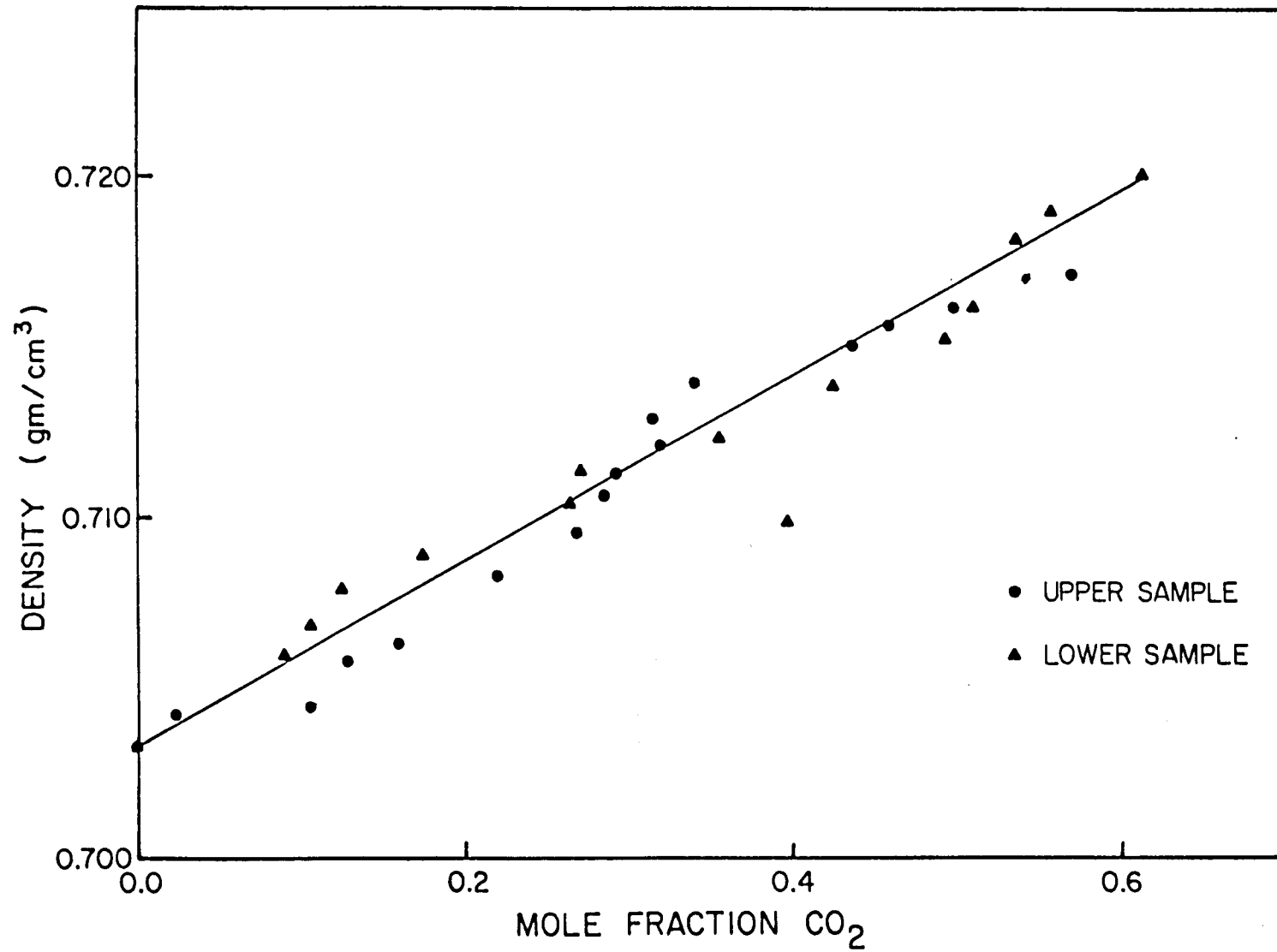


Figure 3.20 Density of CO₂-C₁₀ mixtures at 1250 psia and 160°F.

and the production rate of C_{10} is

$$q_{C_{10}} = q_p \rho_L (1 - z_1) = \frac{q_i \rho_i (1 - z_1)}{\rho_{1L}} \quad (3.6)$$

The total production of CO_2 and C_{10} during a sampling period is, then

$$Q_{CO_2} = \int_{t_j}^{t_{j+1}} q_{CO_2} dt = q_i \rho_i (t_{j+1} - t_j) - \rho_{1L} V \left\{ \exp(-\beta t_j) - \exp(-\beta t_{j+1}) \right\} \quad (3.7)$$

$$Q_{C_{10}} = \int_{t_j}^{t_{j+1}} q_{C_{10}} dt = \rho_2 V \left\{ \exp(-\beta t_j) - \exp(-\beta t_{i+1}) \right\}$$

Figure 3.21 shows a comparison of predicted and experimental values of the amounts of CO_2 and C_{10} for a CMC displacement at 1250 psia and 160°F. The results show considerable scatter due to variations in the production rate caused by problems with the operation of one of the back pressure regulators. If the effects of rate variations are removed by plotting cumulative CO_2 production against cumulative decane production, as in Figure 3.22, experimental results match closely the prediction made with equation (3.7). The agreement shown in Figure 3.22 is convincing evidence that the assumption that fluids within the cell are well-mixed is reasonable, and that the performance of the apparatus, in the single phase region at least, is not too different from the simple model used to describe it.

The second fundamental assumption inherent in the CMC technique is that representative samples can be obtained for phases which are being mixed vigorously by the circulation system. Figures 3.23 and 3.24 report results of CMC experiments for the CO_2 - C_{10} system which provide evidence that the phases present are well-mixed enough to establish equilibrium phase compositions and densities, and that clean samples of each phase can be obtained. Figure 3.23 compares binary phase compositions measured in the CMC apparatus with those reported by Reamer and Sage (1963). Run conditions for the CMC experiments at 1250, 1500, and 1750 psia are summarized in Table 3.2. Agreement between the CMC results and those of Reamer and Sage is excellent. Densities measured for the liquid and vapor phases also agreed well with those reported by Reamer and Sage (Figure 3.24). The density measurement is a sensitive indicator of the effectiveness of the sampling procedure. In early experiments, small amounts of contamination of one phase by the other caused rapid fluctuations in the measured density. Sample collection and circulation ports were redesigned as a result. The densities reported in Figure 3.24 were steady values within a

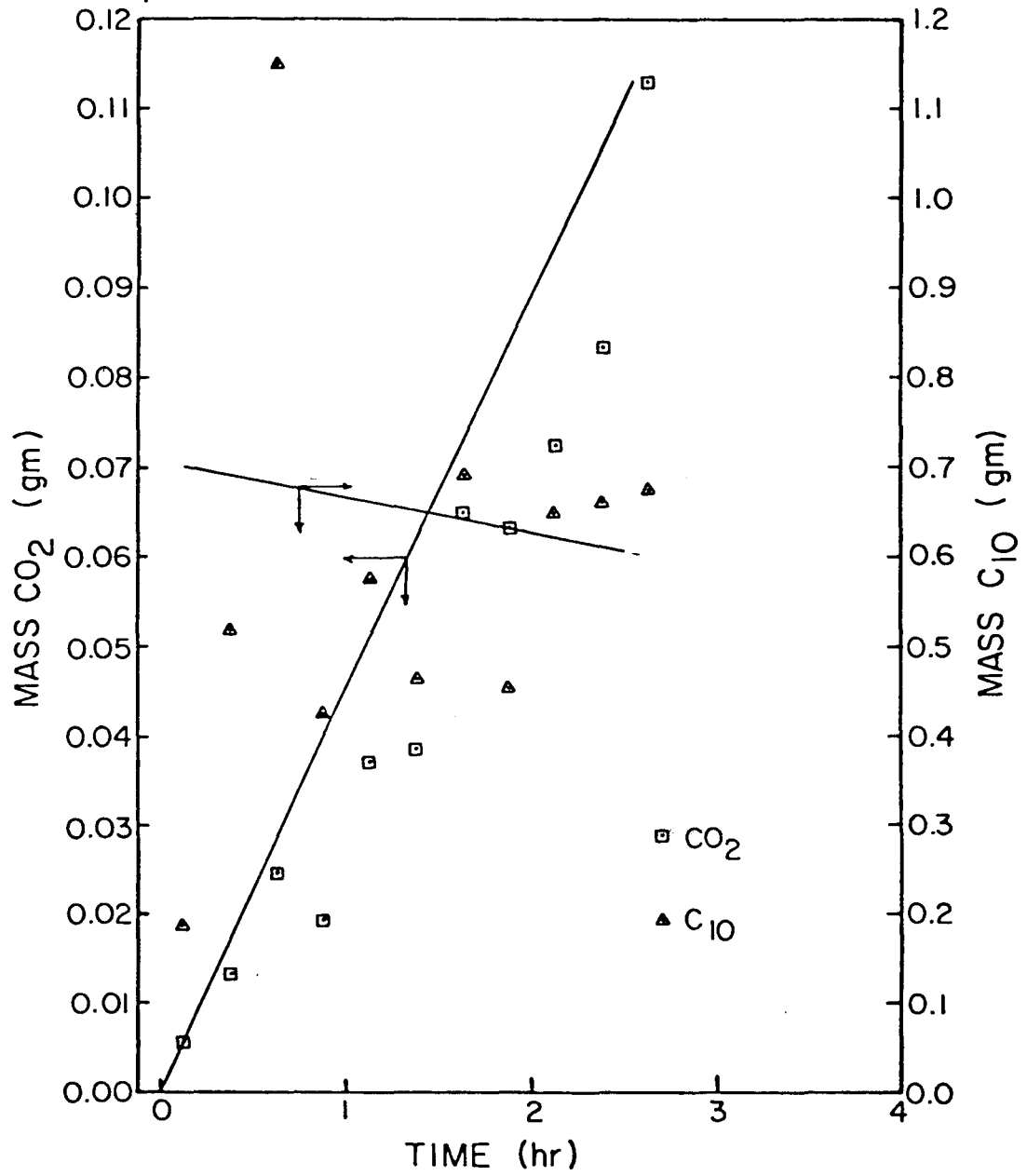


Figure 3.21 Comparison of predicted and experimental rates of production of CO₂ and C₁₀ during a CMC displacement at 1250 psia and 160°F.

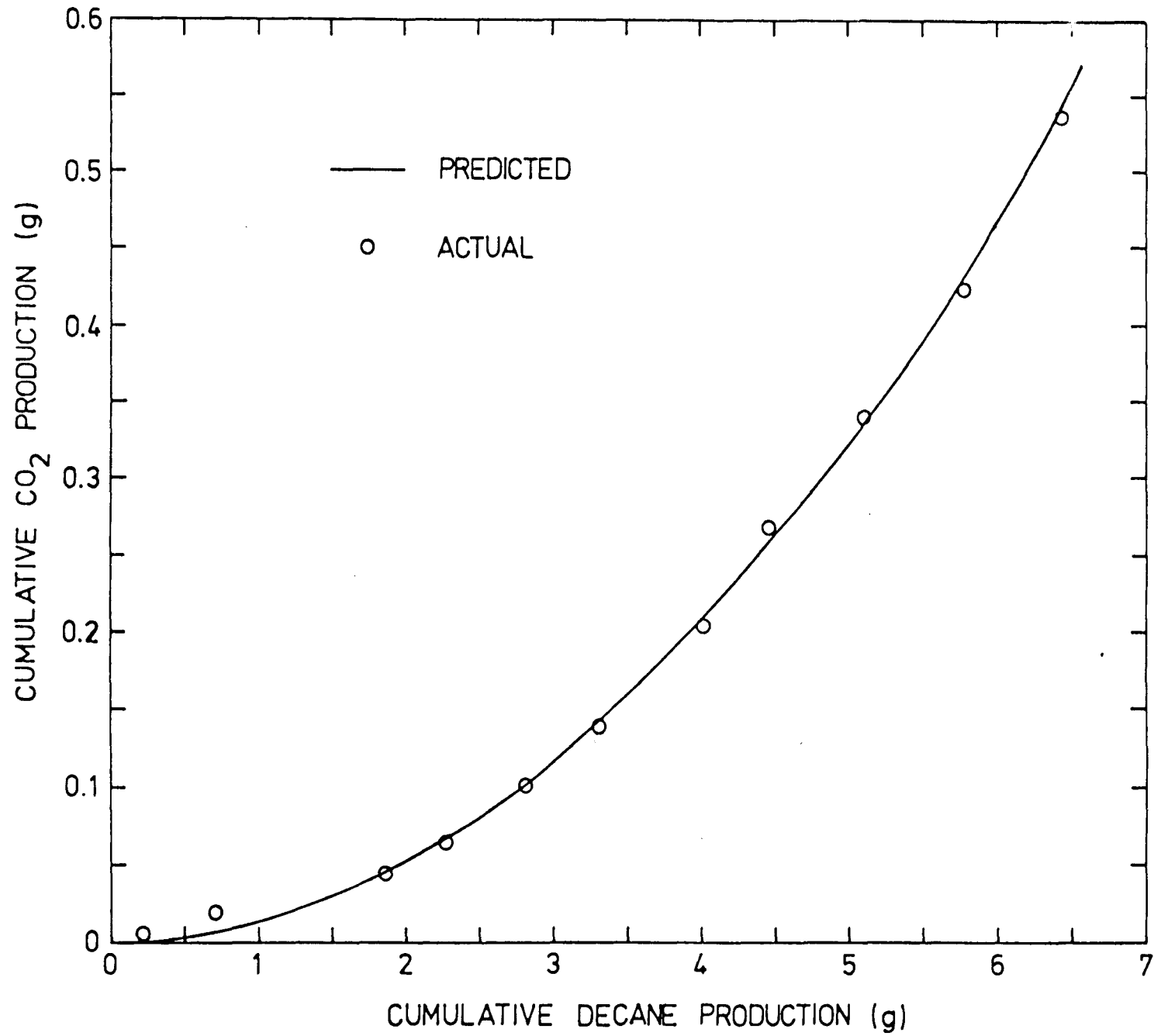


Figure 3.22 Comparison of predicted and experimental cumulative production of CO₂ and C₁₀ during a CMC displacement at 1250 psia and 160°F.

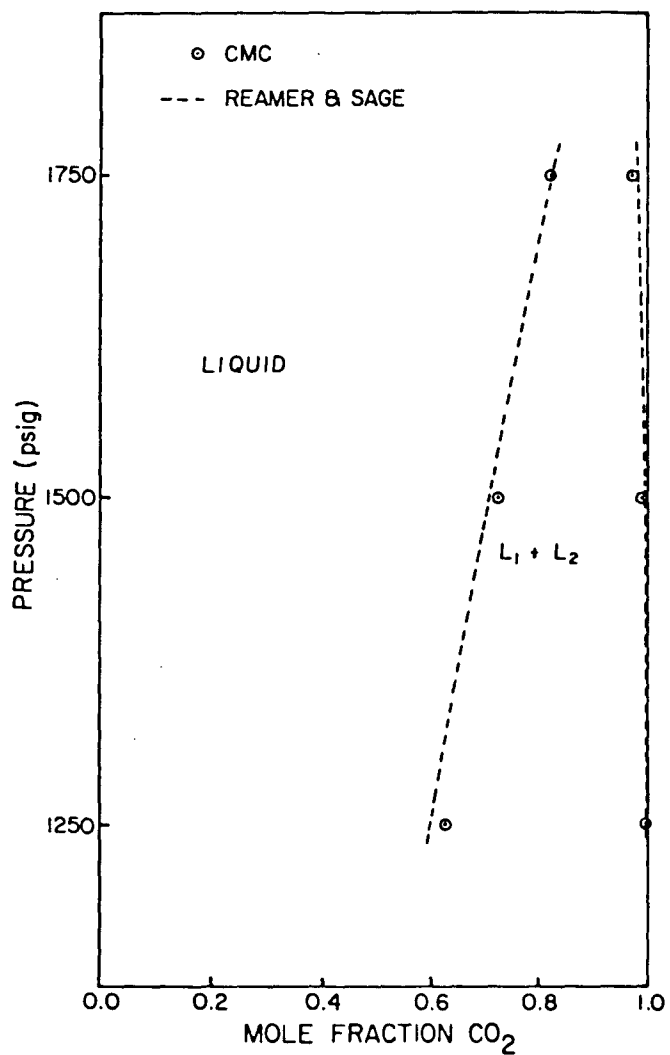


Fig. 3.23 Phase composition for the CO₂-C₁₀ system in two-phase region.

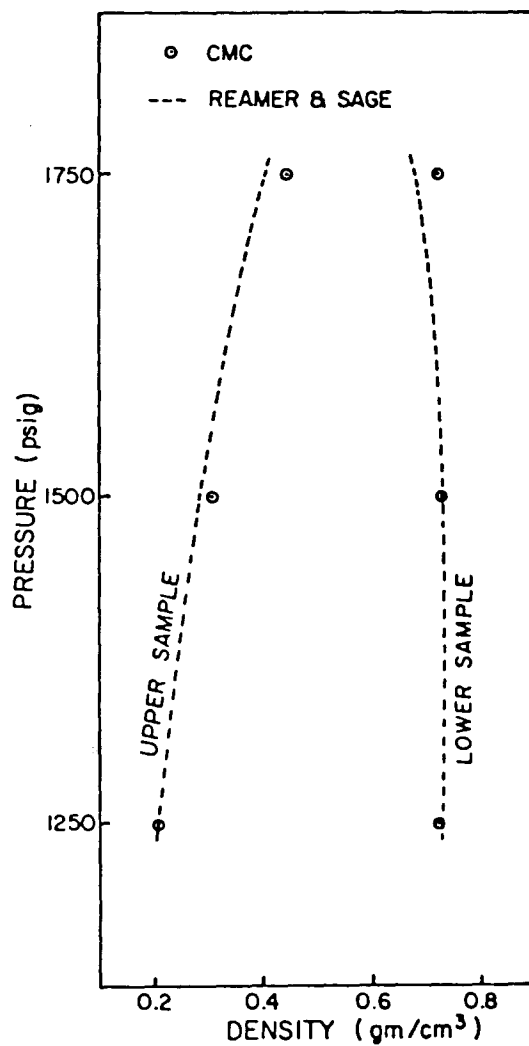


Fig. 3.24 Density vs. pressure of a CO₂-C₁₀ mixture in two-phase region.

Table 3.2 Operating Conditions and Fluid Properties for Continuous Multiple Contact Displacements of Decane by CO₂ at 160°F

	Pressure (psia)		
	<u>1250</u>	<u>1500</u>	<u>1750</u>
Injection Rate, q_i (cm ³ /hr)	16	16	16
Upper Phase Sample Production Rate, q_u (cm ³ /hr)	8.8	8.8	8.8
Lower Phase Sample Production Rate, q_l (cm ³ /hr)	7.2	7.2	7.2
CO ₂ Density (g-mol/cm ³)	0.0045	0.0063	0.0079
C ₁₀ Density (g-mol/cm ³)	0.0049	0.0049	0.0050
Apparent Density of Dissolved CO ₂ (g-mol/cm ³)	0.0179	0.0170	0.0148
Saturated Liquid Phase Density (g-mol/cm ³)	0.0087	0.0100	0.0111
Saturated Vapor Phase Density (g-mol/cm ³)	0.0046	0.0063	0.0087
Mole Fraction CO ₂ in Vapor	0.9972	0.9942	0.9822
Mole Fraction CO ₂ in Liquid	0.6000	0.7132	0.8295

short time after the appearance of upper phase. Thus, density data can be used to detect sampling problems if they occur. The results presented in Figures 3.23 and 3.24 clearly indicate that phase composition and density measurements of acceptable accuracy can be obtained.

When enough CO₂ has been injected and the overall composition exceeds the solubility of CO₂ in the hydrocarbon, a CO₂-rich phase appears. For a binary system at fixed temperature and pressure, the compositions of the two phases present are fixed for any overall composition in the two-phase region. Hence, only the volumes of the phases change with continued injection. Because the lower phase is then saturated with CO₂ and because the upper phase density is close to that of pure CO₂, the effect of volume change on mixing is much smaller after the second phase appears. Hence, we assume that the effect of volume change on mixing is negligible when two phases are present. This assumption is also reasonable for the CO₂-C₁₀ binary system, as can be seen from the pure component and phase densities given in Table 3.2 (Newitt et al 1956; Reamer and Sage 1963). Table 3.3 reports the ratio of the volume of one mole of liquid or vapor mixture to the sum of the volumes of the individual components at their pure component densities. While the liquid phases show substantial volume change, the vapor phase ratios are close to one, as assumed.

A material balance on CO₂ yields

$$v \frac{d}{dt} \left\{ S_U \rho_U x_{1U} + (1 - S_U) \rho_L x_{1L} \right\} = \rho_i q_i - \rho_U q_U x_{1U} - \rho_L q_L x_{1L} \quad (3.8)$$

where S_U is the volume fraction of the upper phase, x_{1U} and x_{1L} the mole fractions of CO₂ in the upper and lower phases, q_U and q_L the volumetric production rates of upper and lower phase samples, and ρ_U and ρ_L the molar densities of the upper and lower phases. Since the phase compositions and densities are fixed, and the injection and production rates assumed to be constant, then

$$S_U = a (t - t_1) \quad (3.9)$$

where t_1 is the time at which the liquid phase is saturated with CO₂ and the constant, a , is given by

$$a = \frac{\rho_i q_i - \rho_U q_U x_{1U} - \rho_L q_L x_{1L}}{v (\rho_U x_{1U} - \rho_L x_{1L})} \quad (3.10)$$

Table 3.3 Volume Change on Mixing* of
CO₂ with Decane at 160°F

<u>Pressure (psia)</u>	<u>Liquid Phase</u>	<u>Vapor Phase</u>
1250	0.536	0.983
1500	0.584	0.994
1750	0.645	0.889

* Defined as the volume of the mixture divided by the sum

of the volumes of the pure components $\frac{x_{1j}}{p_1} + \frac{\frac{1/p_j}{(1 - x_{1j})}}{p_2}$

The overall mole fraction of CO₂ can be calculated easily from the upper phase saturation as

$$z_1 = \frac{S_U (\rho_U x_{1U} - \rho_L x_{1L}) + \rho_L x_L}{S_U (\rho_U - \rho_L) + \rho_L} \quad (3.11)$$

The solutions given as equations (3.4) and (3.11) are useful in several ways. Equation (3.4) can be used to estimate the time required to reach the two-phase region for a CO₂-crude oil displacement if an estimate of the solubility of CO₂ in the oil is available, since the CO₂-crude oil mixture can be treated as a binary mixture as long as only one phase is present in the cell. The solution for the two-phase region, equations (3.6) - (3.8), may be used to estimate the time required to traverse the two-phase region in multicomponent systems, though the estimate will be a rough one since the phase densities and compositions are no longer constant. The solutions are probably most useful for calculating the effects of averaging of phase compositions since samples are collected for a finite period during which the overall composition changes in the cell. Table 3.4 compares phase compositions calculated for a sampling period of one hour for the CO₂-C₁₀ displacement at 1250 psia (see Table 3.2) with the exact solution, equation (3.4), at the midpoint of the sampling period. The difference between the two is negligible except in the very early part of the run when the CO₂ concentration is changing most rapidly. Thus, in the single phase region, the effects of averaging are minimal.

In a binary mixture, there is no averaging at all for overall compositions in the two-phase region because phase compositions are fixed. If a multicomponent hydrocarbon mixture is displaced, however, the phase compositions change as the overall composition changes. Figure 3.25 illustrates the effect of an overall composition in a ternary system. As the overall composition changes from point a to point b during a sampling period, the liquid phase samples vary in composition from c to d and the vapor phase samples from e to f. The average compositions that would be measured for the sampling period are shown as the triangles connected by a dashed tie line. The composition variation during the sampling period causes some error in the phase compositions, particularly for the upper phase, which in this example exhibits larger composition changes than the lower phase. In phase diagrams where tie lines lie more nearly parallel to the overall composition path of the displacement, the effect of averaging is smaller because some of the variation in overall composition is along a tie line which causes no change in phase compositions.

It is clear from the solutions for binary displacements given as equations (3.4) and (3.7) that the effect of sample averaging can be made arbitrarily small by reducing the change in overall composition during a sampling period, either by decreasing the sampling period or by increasing the volume of the cell, which has the effect of expanding the time scale. The minimum sampling period is determined by the requirements that dead volume downstream of the sampling port be swept adequately and that sufficient

Table 3.4 Comparison of Instantaneous and Averaged Compositions for CO₂ and C₁₀ at 1250 psia, 160°F

One Hour Sampling Period		Exact Solution		Difference
Sampling Period (hr)	Average Mole Fraction CO ₂	Time (hr)	Mole Fraction CO ₂	%
0 - 1	0.1007	.5	.0994	1.31
1 - 2	0.2554	1.5	.2545	0.35
2 - 3	0.3704	2.5	.3698	0.16
3 - 4	0.4591	3.5	.4587	0.09
4 - 5	0.5294	4.5	.5292	0.04

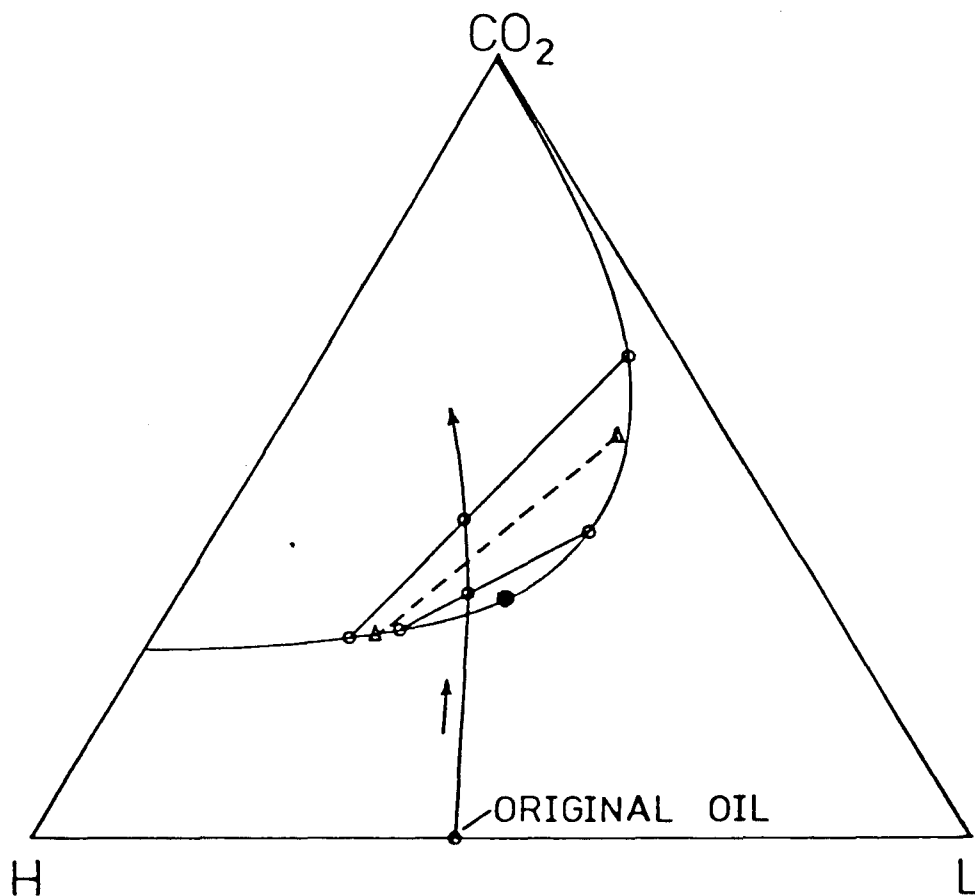


Figure 3.25 Effect of changing compositions during a sampling period on apparent compositions of the samples.

quantities of samples be collected to allow acceptably accurate measurements of the amounts and compositions of oil and gas samples. Equations (3.4) and (3.7) can be used to estimate the cell volume required to produce sufficiently low averaging. Figure 3.26, for instance, shows calculated compositions for the binary CO₂-C₁₀ systems described in Table 3.2. The compositions shown in Figure 3.26 were calculated for a cell volume of 67 cm³ and an injection rate of 16 cm³/hr. If samples are collected for a period of one hour, the overall CO₂ concentration changes by 2 to 4 mol % during sampling periods in the first few hours after the appearance of the vapor phase. After completion of the validation experiments, the volume of the cell was increased to 134 cm³, and, in crude oil experiments, discussed below, the injection rate was set at 12 cm³/hr. Both changes reduce the rate of composition change.

In a particular run, the rate of composition change is determined by the compositions and relative rates of withdrawal of the two phases. For instance, compositions change rapidly during the early part of the run in all three cases shown in Figure 3.26 because the produced samples are mostly C₁₀. The rate of increase declines as the CO₂ concentration rises, however, because more CO₂ is removed in samples and because more moles of CO₂ must be added to increase the mole fraction if it is already at a high level. When the vapor phase appears, the rate at which z₁ increases declines further because the rate of withdrawal of CO₂ in the new phase, which is much richer in CO₂, is higher than that of the single phase with the saturated liquid composition. In principle, at least, the composition path of a displacement can be controlled by adjusting the rates at which individual phases are produced. In practice, however, knowledge of phase compositions and densities are needed to do so accurately, and furthermore, the freedom to adjust rates may be limited by the need to displace the dead volume in the sample lines. In the crude oil displacements reported below, upper and lower phases were produced at approximately equal rates.

The results presented in this section establish that phase compositions and densities can be measured with reasonable accuracy in the CMC apparatus. Because the experiment operates continuously, it can be performed much more rapidly than conventional static phase equilibrium experiments. It is probable that slightly greater accuracy could be obtained in static experiments, but the cost in experimental time would be much greater. For CO₂-crude oil systems, the CMC experiment makes possible phase composition measurements which have been attempted only rarely in the past.

CMC Displacement Results: CO₂-Separator Oil Systems

CMC displacements were performed at 90°F and pressures of 800, 1200, and 1400 psia for separator oil from the Maljamar Field, Lea County, New Mexico. Results of single contact phase behavior experiments and slim tube displacements for the same oil have been reported previously (Orr, Yu, and Lien 1981; Orr and Taber 1981). Results of a CMC displacement at 1200 psia but without phase density data have also been reported (Orr et al 1980; Orr and Taber 1981). Figure 3.27 summarizes the primary data collected in each run - the amounts of liquid and gas collected for each sample. The results are reported as the weight fraction of liquid for each sample, defined as

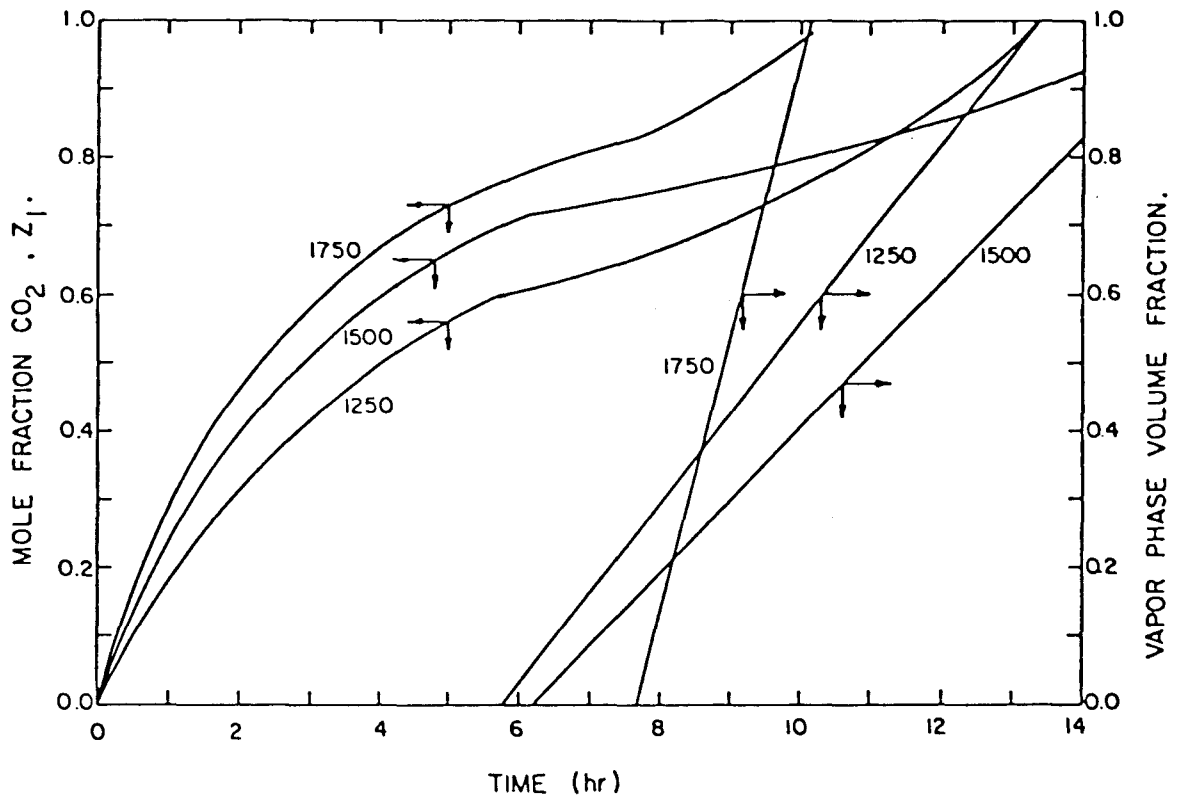


Figure 3.26 Predicted overall compositions and vapor phase volume fractions for a CMC displacement of C₁₀ by CO₂ at 160°F.

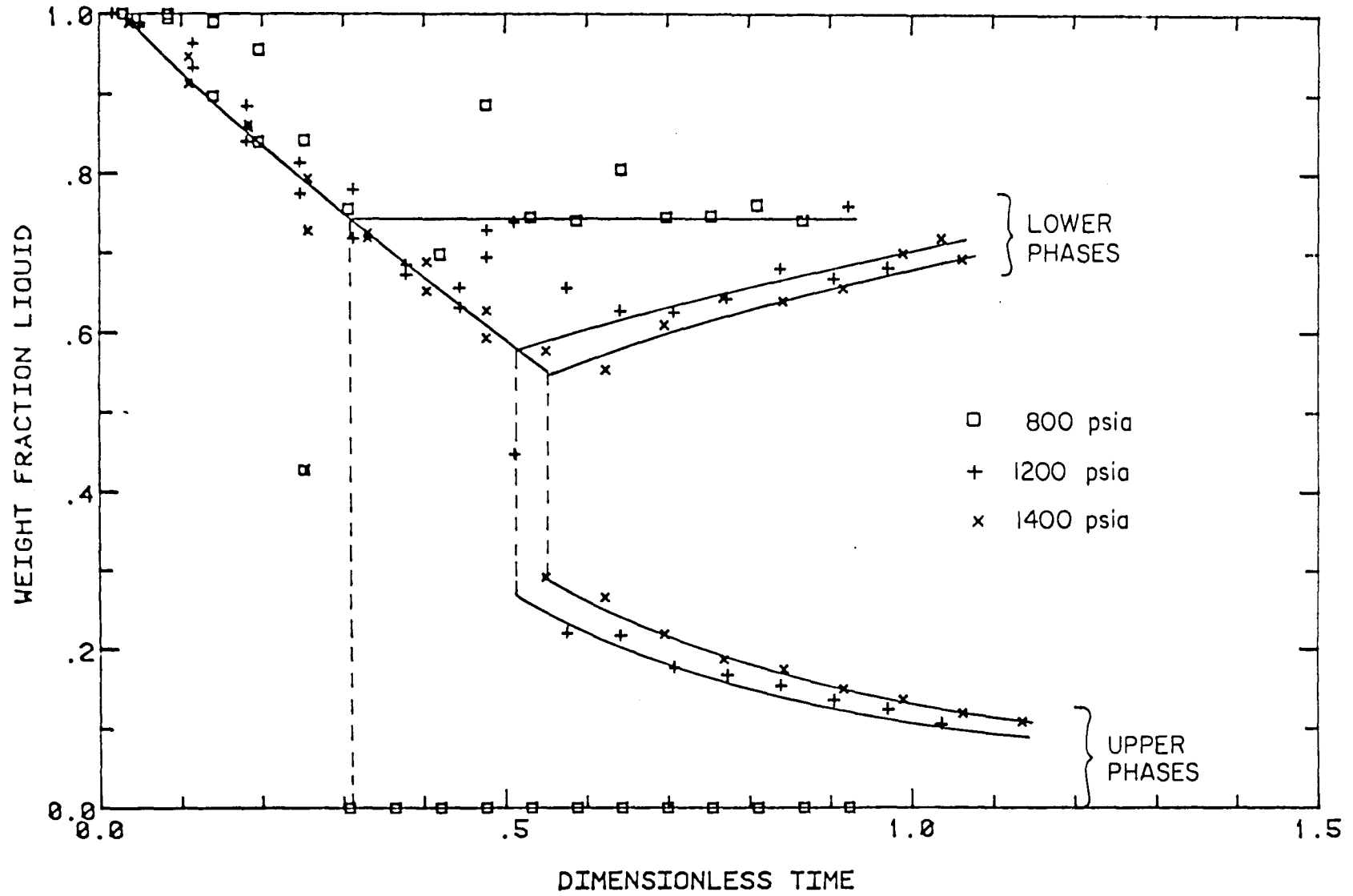


Figure 3.27 Comparison of weight fractions of liquids in upper and lower samples taken in CMC displacements of Maljamar separator oil at 800, 1200, and 1400 psia and 90°F.

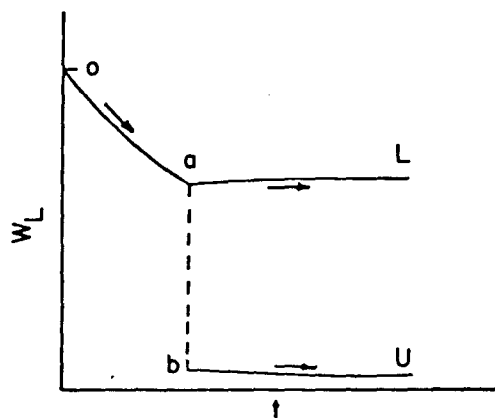
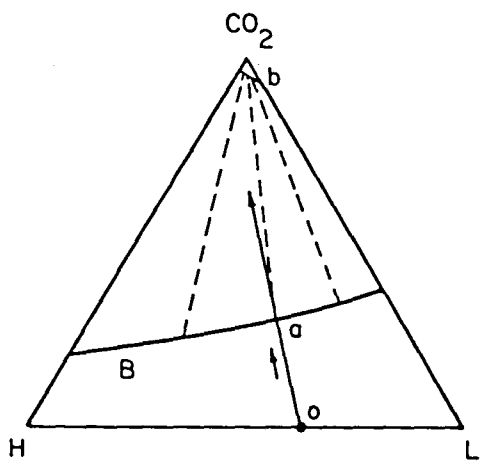
$$W_L = \frac{W_L}{W_G + W_L} \quad (3.12)$$

where W_L is the weight of liquid collected at low pressure for a sample, and W_G the weight of gas for the same sample. No solution gas was present in the separator oil displacements, so low pressure gas samples contained only small amounts of hydrocarbons in addition to CO_2 . Hence, the liquid weight fractions reported in Figure 3.27 were only slightly less than the weight fraction of hydrocarbons present in each phase at high pressure. Early in each run, liquid weight fractions for upper and lower phases were the same within experimental error, as they should be if a single phase is present in the cell. Eventually, however, the solubility of CO_2 in the oil was reached, and the W_L for the upper phase dropped sharply.

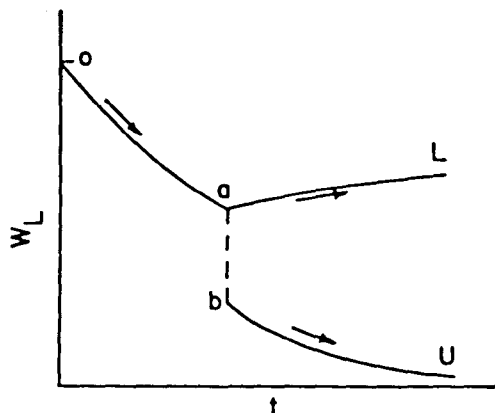
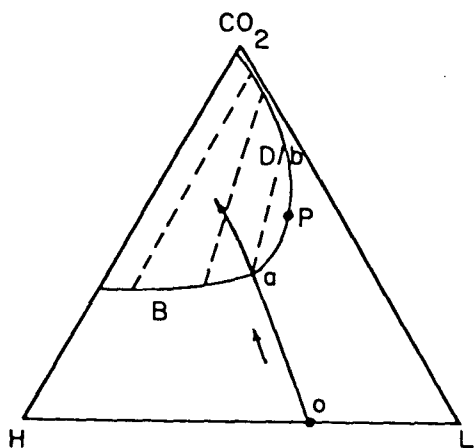
The reason for the step change is illustrated in Figure 3.28, in which the crude oil is represented qualitatively as a mixture of light (L) and heavy (H) pseudo-components. As CO_2 is injected into oil of composition, o, at some relatively low pressure P_1 , single phase mixtures of the CO_2 lie on the straight line o-a in the pseudo-ternary phase diagram. As the amount of CO_2 dissolved in the oil climbs, the liquid weight fraction declines. There is no difference between upper and lower samples because only one phase is present. When the bubble point composition, a, is reached, a new phase of composition b appears. Since it contains much smaller amounts of hydrocarbons than the phase of composition a, W_L drops sharply. At a higher pressure, P_2 (Figure 3.28), the behavior is similar, though in this case, the value of W_L at which the phase split occurs is lower because the solubility of CO_2 is higher at the higher pressure. In addition, the magnitude of the step change is smaller because the new phase contains more hydrocarbons. Clearly, the size of the step change indicates directly the difference in composition between upper and lower phases at the phase split.

If the pressure is high enough that the composition path of the displacement crosses the dew point portion of the binodal curve (labeled D) rather than the bubble point portion, as in Figure 3.28c, then the step change occurs in W_L for the lower phase, because the new phase appears at the bottom of the cell. Thus, a plot of W_L versus time (or dimensionless time $\tau = (q_1 \rho_1 t) / (\rho_{1L} v)$) can indicate whether the new phase appears through a dew or bubble point and furthermore, it provides direct evidence of the efficiency with which hydrocarbons are extracted into the CO_2 -rich phase even in the absence of detailed composition measurements for gas and liquid samples.

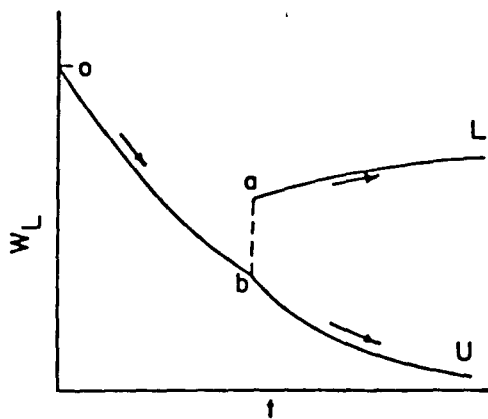
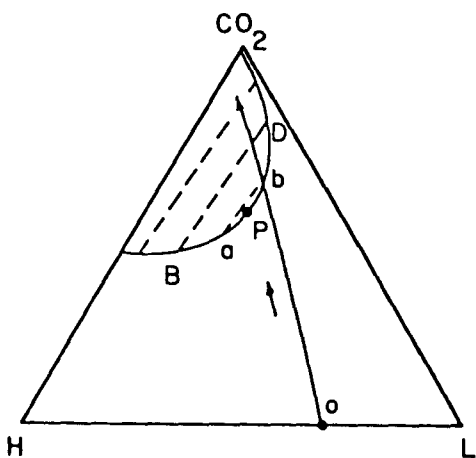
The results shown in Figure 3.27 indicate clearly that CO_2 extracts hydrocarbons more efficiently at higher pressures. Additional compositional data are required to establish which hydrocarbons are extracted most efficiently at each pressure. In the four separator oil displacements described here, low pressure gas samples differed little. CO_2 concentrations in the gas samples were high since no C_1 or C_2 was present and only small amounts of C_3 , C_4 , C_5 , C_6 , and C_7 were stripped from produced samples flashed to atmospheric pressure. Typical gas composition data for the 1400 psia run are plotted against dimensionless time in Figure 3.29. As the total amount of



a. P_1



b. P_2



c. P_3

Figure 3.28 Effect of increasing pressure on weight fractions of hydrocarbon liquids in upper (U) and lower (L) samples.

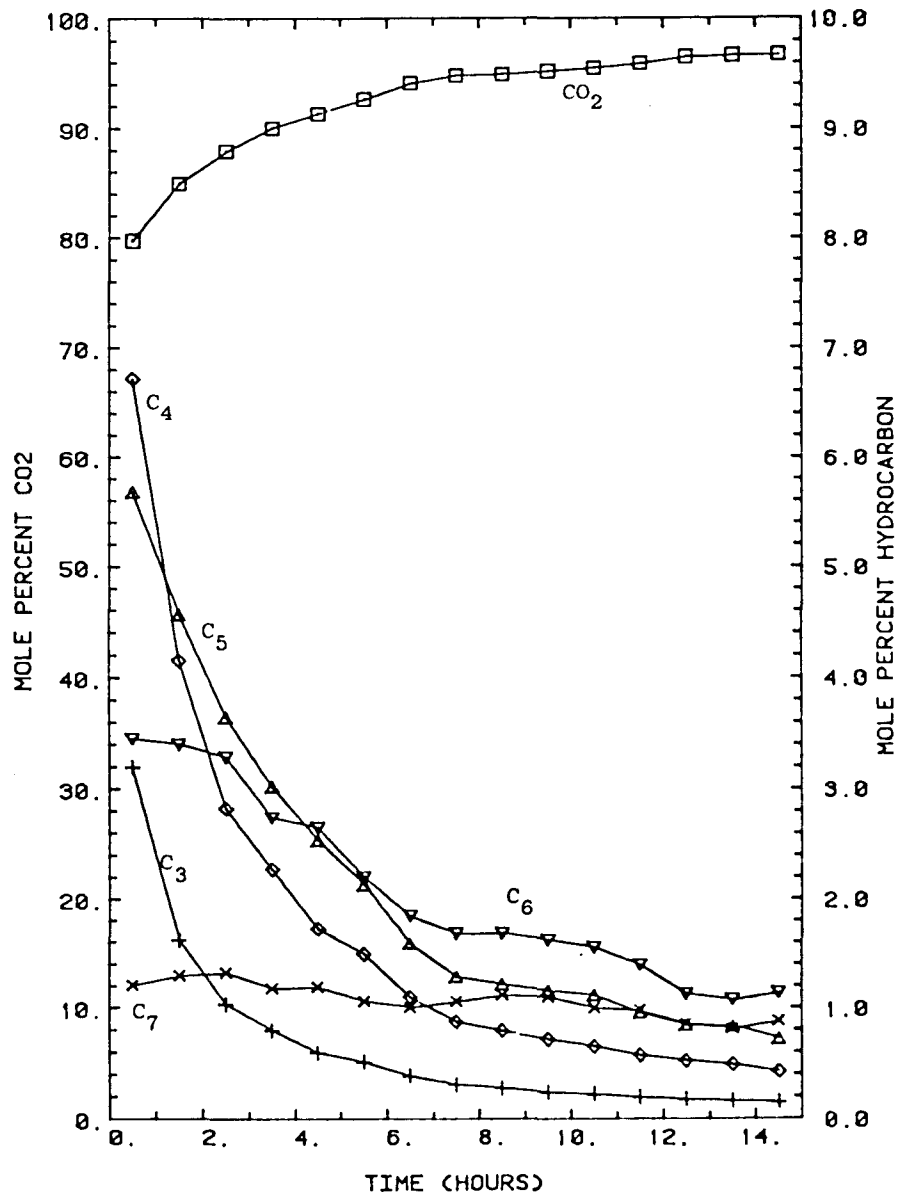
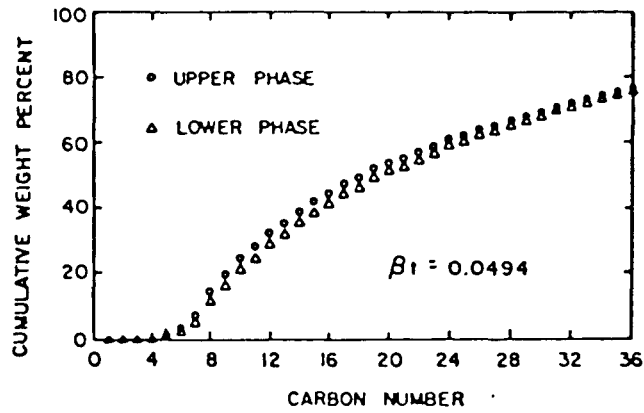


Figure 3.29 Smoothed compositions of upper phase gas samples from a CMC displacement of Maljamar separator oil by CO₂ at 1400 psia and 90°F.

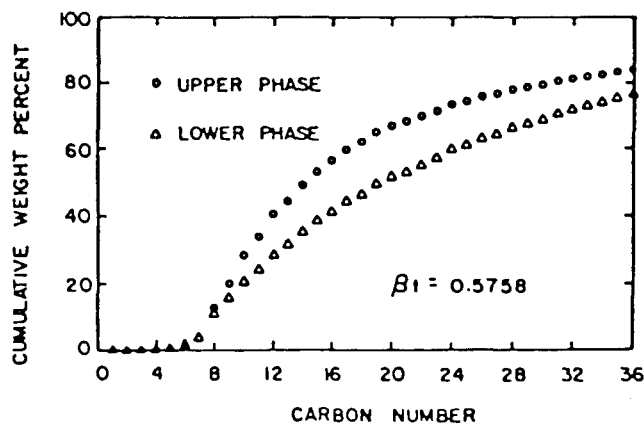
C₄-C₇ hydrocarbons present in the cell declined during the run, the mole fraction CO₂ in the low pressure gas climbed to well above 0.9 in both upper and lower samples. Typical liquid composition data for the 1200 psi run are shown in Figure 3.30. The upper and lower liquid samples taken at $\tau = .0494$ (Figure 3.30a), before the appearance of the CO₂-rich liquid phase, had compositions identical within experimental error. Compositions of liquid samples taken shortly after the phase split are shown in Figure 3.30b. The liquid from the upper phase sample was richer in hydrocarbons in the C₅-C₂₀ range than the liquids collected from the lower phase though both liquid samples contained significant amounts of hydrocarbons heavier than C₂₀. In all the displacements discussed here, upper liquid samples collected after the phase split were a clear yellow color which became lighter as the run progressed. Lower phase liquids retained the black color of the original crude oil. Liquid samples taken late in each run showed greater composition differences as illustrated in Figure 3.30c.

A comparison of the compositions of hydrocarbons extracted into the CO₂-rich phase is given in Figure 3.31. The compositions reported are for the first upper phase sample taken after the appearance of the CO₂-rich phase at each pressure. Thus, the compositions reported reflect the efficiency with which CO₂ extracts hydrocarbons of various molecular weights from the crude oil at the point when the CO₂-rich phase first appears. Figure 3.31 clearly establishes that the CO₂-rich liquid phases which formed in the runs at 1200 and 1400 psia extracted much heavier hydrocarbons than the CO₂-rich vapor phase present at 800 psia. In fact, essentially no hydrocarbons heavy enough to remain in the liquid phase after the flash to atmospheric pressure were collected from the vapor phase at 800 psia. Those present were all carried in the low pressure gas stream. At the higher pressures, substantial quantities of hydrocarbon liquids remained after the flash to low pressure, and as Figure 3.31 indicates, those liquids contained some remarkably heavy hydrocarbons. Thus, a CO₂-rich liquid phase extracts a much greater weight of hydrocarbons (Figure 3.27), and the hydrocarbons extracted are much heavier than those vaporized by a much lower density CO₂-rich vapor phase.

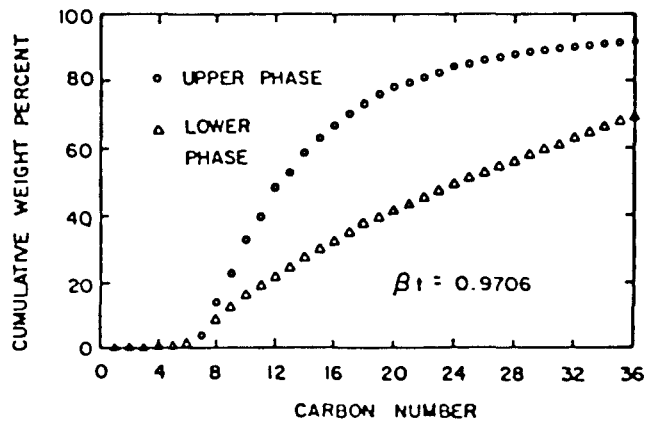
Phase compositions calculated from amounts and compositions of low pressure gas and liquid samples can be conveniently summarized on pseudo-ternary diagrams, though the limitations of representing mixtures containing large numbers of components in terms of only three components are well known. Figures 3.32-3.34 are ternary phase diagrams for CO₂ and Maljamar separator oil at the three pressures studied. Detailed gas, liquid, and phase composition data are available separately (Silva et al 1981b, 1981c, and 1981d). In the displacement at 800 psia, only a small portion of the phase diagram is scanned because only very small amounts of hydrocarbons were extracted into the upper (vapor) phase (Figure 3.32). The vapor phase was nearly pure CO₂ and hence, the composition of the oil in the cell hardly changed during the displacement. A CO₂ flood of Maljamar separator oil at 800 psi would clearly be immiscible. At 1200 psia (Figure 3.33), the displacement passed through the liquid-liquid region (see Figure 3.2) in which extraction of hydrocarbons was much more efficient. Similar behavior was observed at 1400 psia (Figure 3.34). The differences between the two displacements at the higher pressures were smaller because compositions of liquid-liquid systems are much less sensitive to pressure changes than are liquid-vapor systems.



a



b



c

Figure 3.30 Comparison of compositions of liquid hydrocarbon samples taken before, just after, and well after the appearance of the CO₂-rich phase in a CMC displacement of Maljamar separator oil by CO₂ at 1200 psia and 90°F.

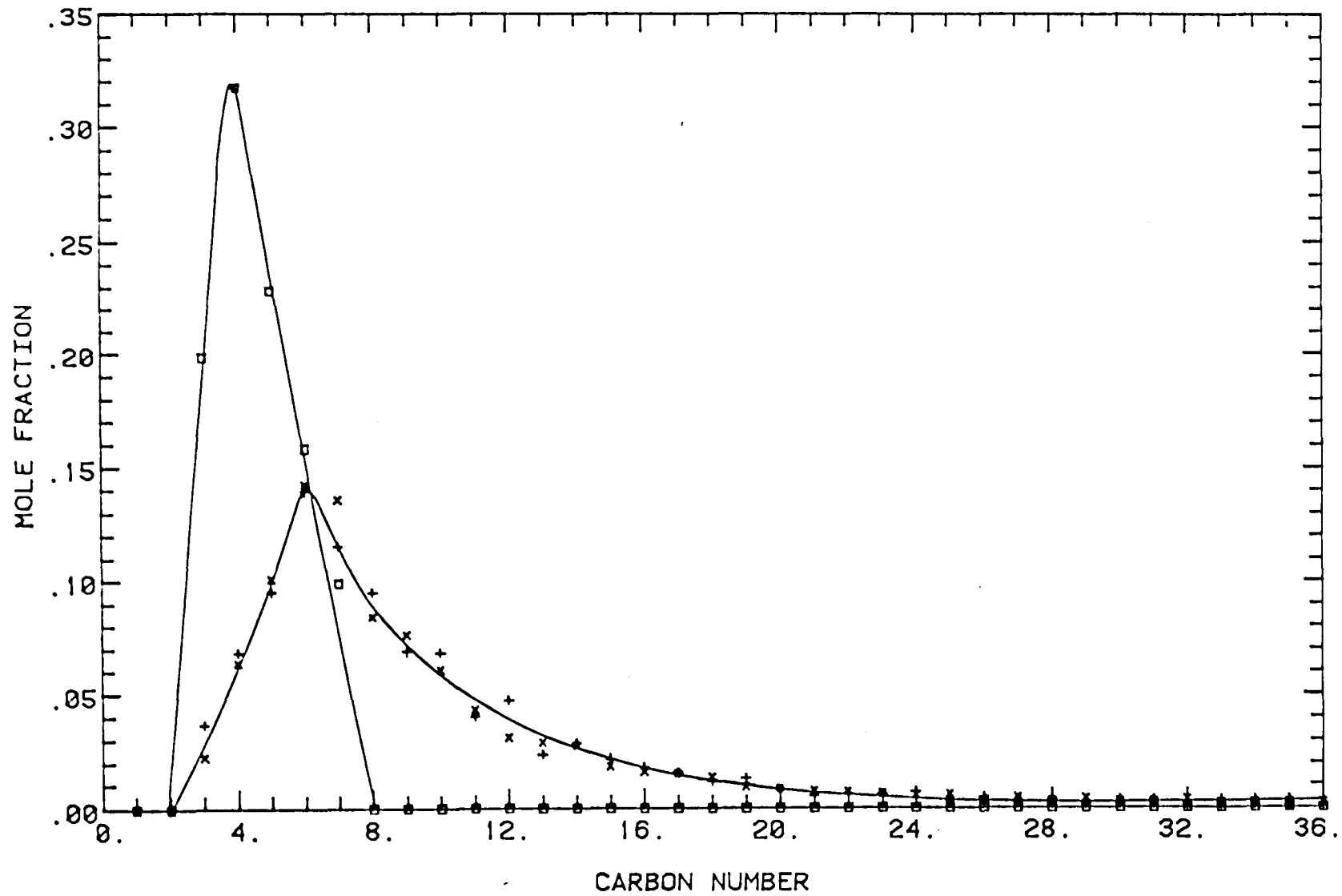


Figure 3.31 Comparison of compositions of hydrocarbons in upper phase samples taken just after the appearance of the CO₂-rich phase. Hydrocarbons vaporized from Maljamar separator oil by CO₂ at 800 psia (□) were much lighter than those extracted by CO₂-rich liquid phases at 1200 (+) and 1400 (x) psia.

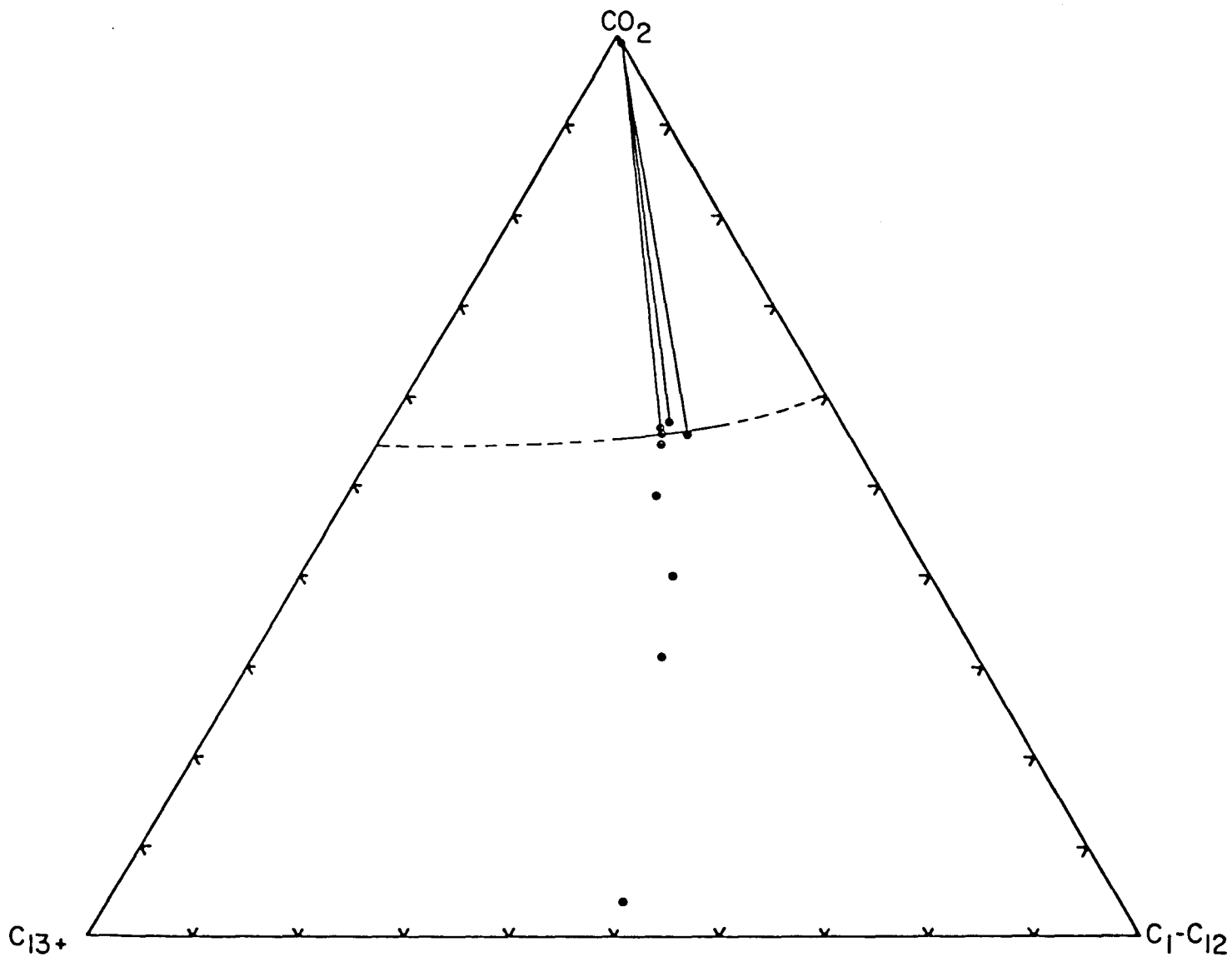


Figure 3.32 Pseudo-ternary representation of phase compositions of mixtures of CO₂ with Maljamar separator oil at 800 psia and 90°F.

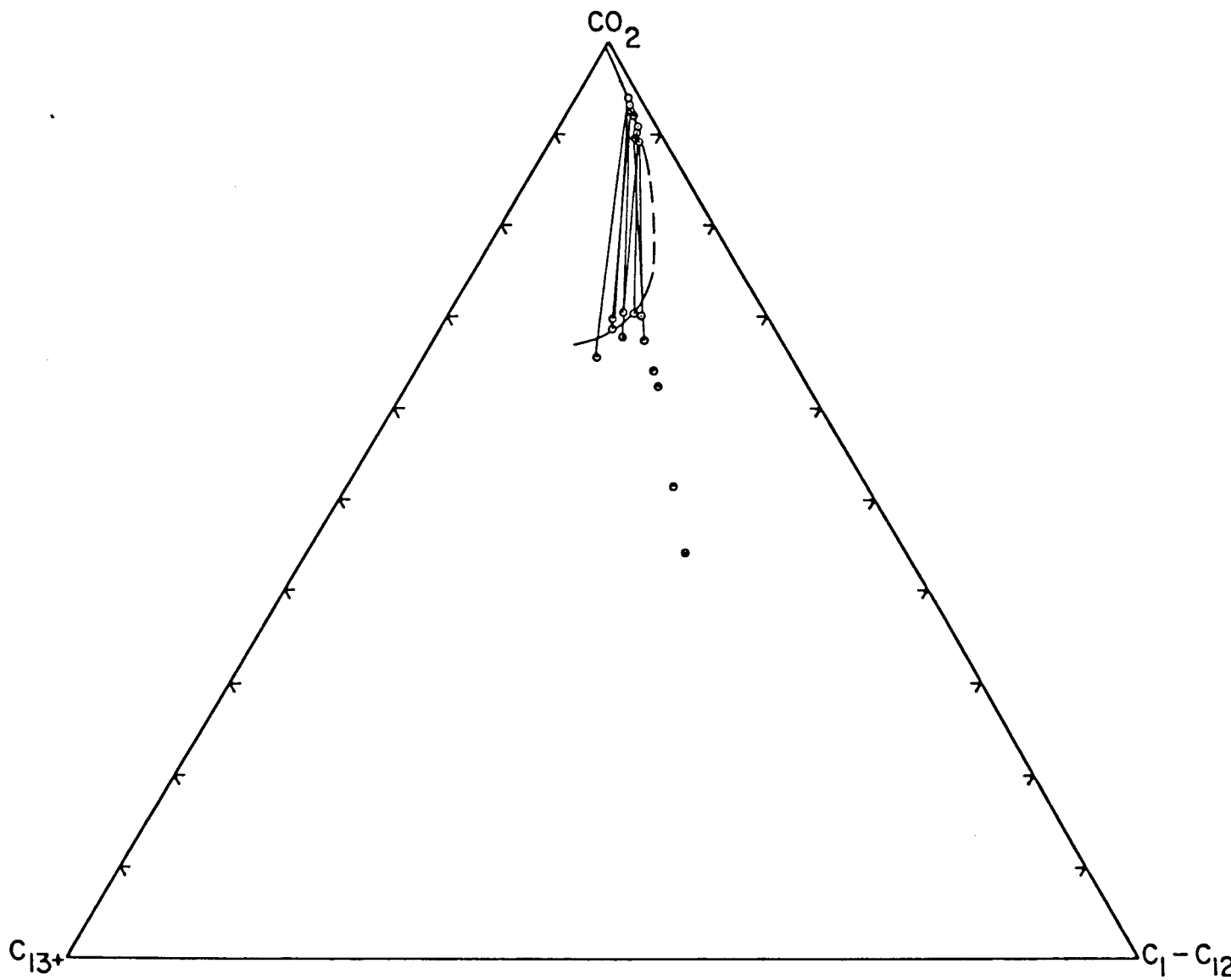


Figure 3.33 Pseudo-ternary representation of phase compositions of mixtures of CO_2 with Maljamar separator oil at 1200 psia and 90°F .

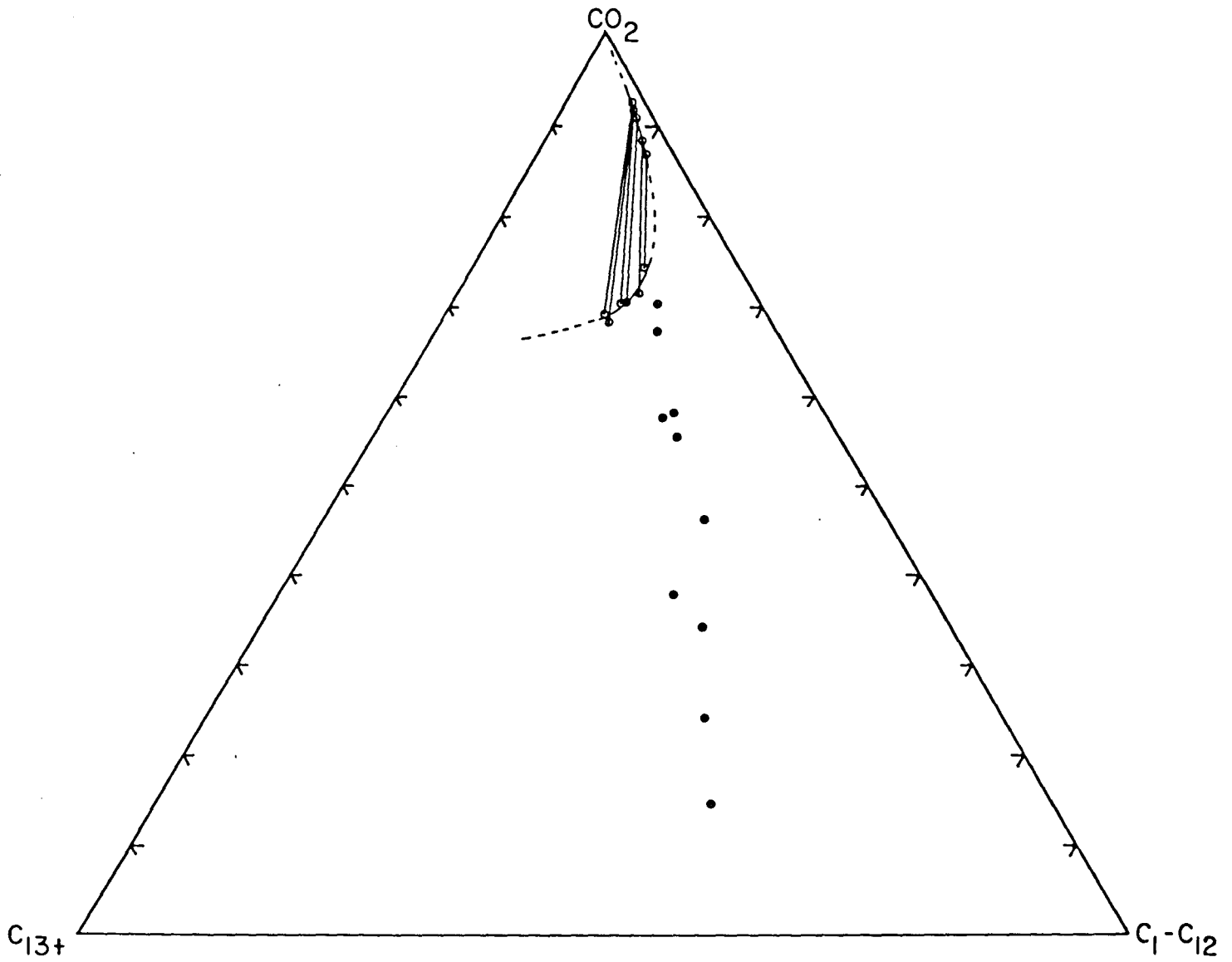


Figure 3.34 Pseudo-ternary representation of phase compositions of mixtures of CO_2 with Maljamar separator oil at 1400 psia and 90°F .

Indeed, the fact that the 1200 and 1400 psia phase diagrams are so similar is an indication of the repeatability of the experiment. The phase diagrams shown in Figures 3.32-3.34 are qualitatively consistent with the sequences of phase diagrams proposed by Orr, Yu, and Lien (1981) (see §4.1).

Phase densities for the four runs are reported in Figure 3.35. In the 800 psia displacement, the liquid phase density increased slightly as CO₂ dissolved in the oil and then remained essentially constant after the appearance of the CO₂-rich vapor phase. The vapor phase density was very close to that of pure CO₂, as it should have been since the amounts of hydrocarbons found in that phase were very small. The displacements at 1200 and 1400 psia showed more evidence of phase composition changes, which are reflected as phase density variations. In those runs, the density of the oil-rich phase also increased as CO₂ dissolved in the oil, but at the higher pressures, it continued to increase as CO₂ preferentially extracted lighter hydrocarbons from the oil remaining in the cell. Shortly after their appearance, the CO₂-rich liquid phases were significantly denser than pure CO₂ because they contained substantial quantities of hydrocarbons, some of which were quite heavy. With continued injection, however, the densities of the CO₂-rich phase declined as the amounts of light hydrocarbons remaining decreased and hence the amounts of hydrocarbons extracted decreased.

The phase composition and density results presented in this section are the most extensive available for any crude oil system described in the published literature, so far as we know. They represent substantial progress in our effort to investigate experimentally the variation of phase compositions and densities with variations in overall composition such as might occur in a CO₂ flood, and to understand how an increase in operating pressure affects those variations. It seems likely that the CMC technique will continue to be a valuable tool for detailed experimental investigations of compositional and fluid property behavior for CO₂-crude oil systems and, perhaps, others, and that the information obtained will contribute to the development of predictive tools for CO₂ flooding. For instance, the simultaneous phase density and composition data offer an opportunity for direct tests of the accuracy of equation-of-state predictions. In addition, the CMC experiment can be used to gather experimental data needed to support compositional reservoir simulations. If simultaneous phase viscosity measurements can be obtained, the technique will provide quantitative measures of fluid properties which can be used to assess the magnitudes and scales of viscous and gravitational instabilities.

CMC Displacement Results: CO₂-Maljamar Recombined Reservoir Fluid

Figure 3.36 compares results of two continuous multiple contact displacements performed at 90°F. The first was a displacement of Maljamar separator oil at 1200 psig and the second a displacement of Maljamar recombined reservoir fluid (RRF) at 2500 psig. The RRF had a bubble point pressure of 1525 psia and a gas-oil ratio of 650 SCF/BBL. The separator oil displacement was at a pressure high enough to be in the L₁-L₂ region (Orr, Yu, and Lien 1981; Orr and Taber 1981) and slightly above the MMP measured in slim tube displacements (Orr and Taber 1981). The RRF displacement was performed

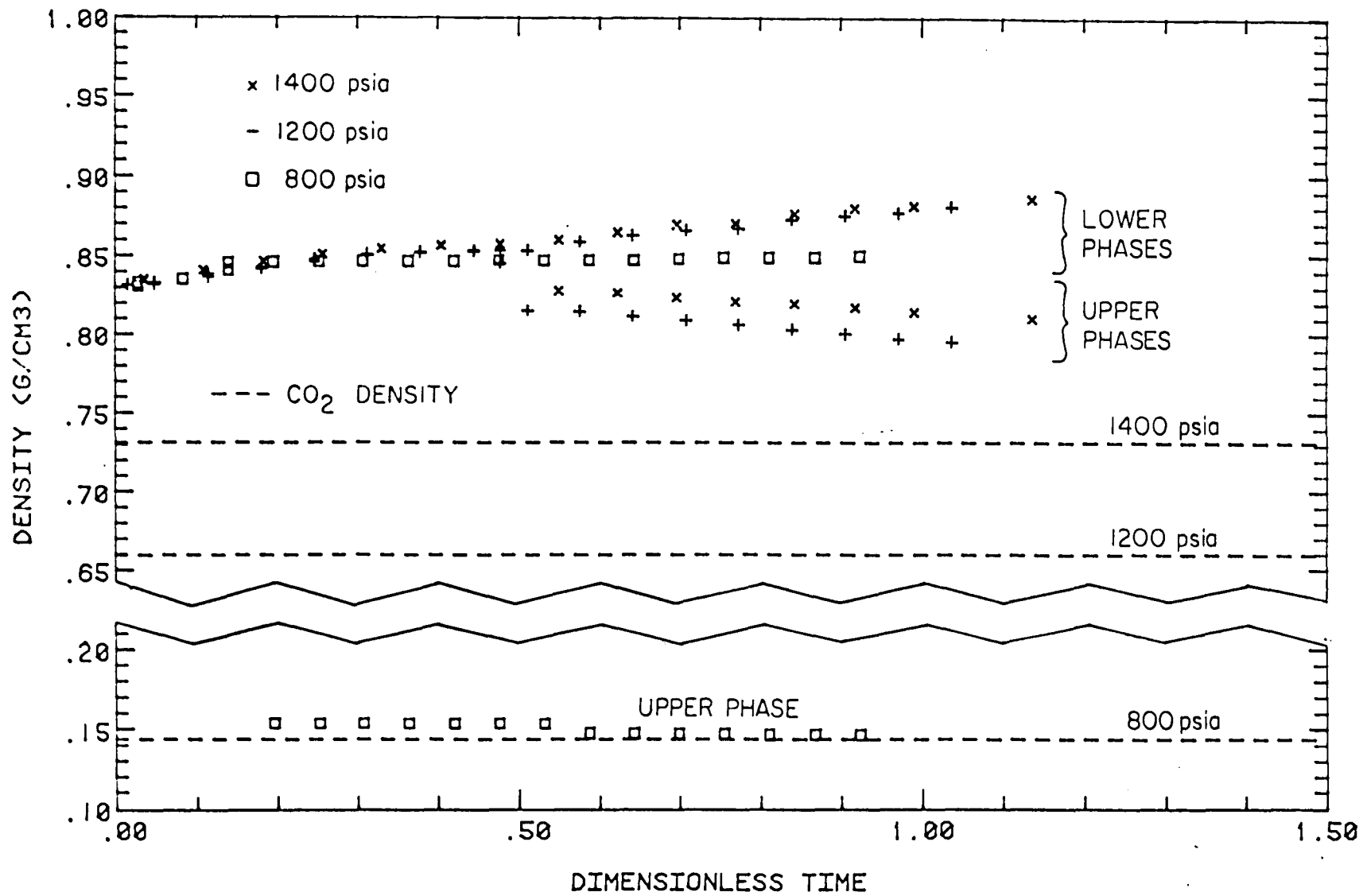


Figure 3.35 Densities of phases present during CMC displacements of Maljamar separator oil at 800, 1200, and 1400 psia and 90°F.

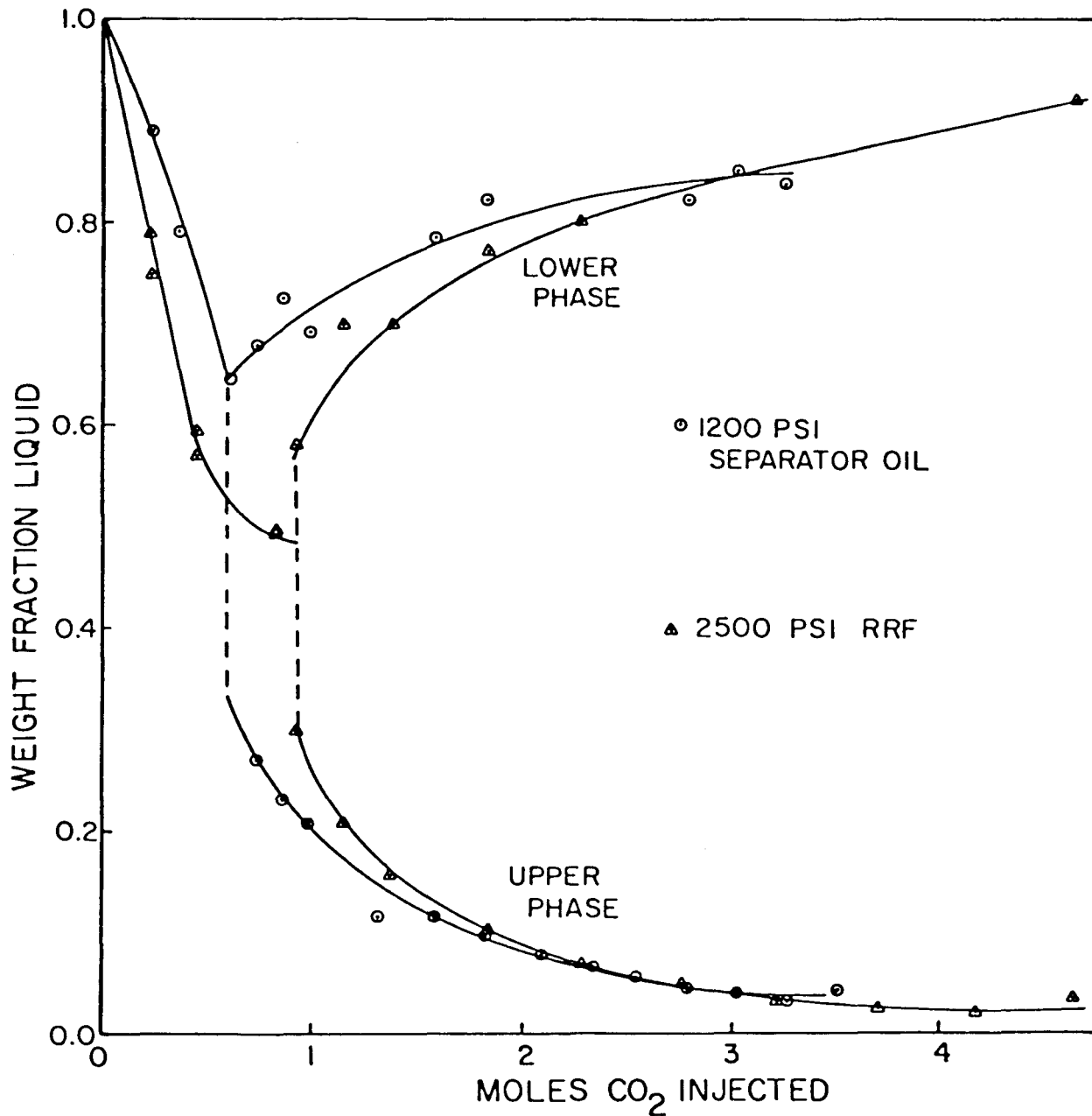


Figure 3.36 Comparison of weight fractions of hydrocarbon liquids in upper and lower samples for CMC displacements at 90°F of Maljamar separator oil at 1200 psia and Maljamar recombined reservoir fluid (RRF) at 2500 psia.

at a pressure close to the reservoir pressure of the area of the Maljamar field in which a pilot CO₂ flood will be performed. That displacement also passed through the L₁-L₂ region (see Figure 3.1). The liquid weight fractions given in Figure 3.36 are plotted against moles of CO₂ injected instead of dimensionless time since those displacements were performed before equipment for density measurements was installed. The behavior of the liquid weight fraction for the CO₂-RRF displacement was similar to that observed for the CO₂-separator oil systems described above. In both experiments, the CO₂-rich liquid phase extracted liquid hydrocarbons quite efficiently. In both cases, approximately 30% by weight of the upper phase was hydrocarbon components heavy enough to remain in the liquid phase on blowdown. As the displacements progressed, the amounts of hydrocarbon liquids extracted by the CO₂-rich upper phase declined as the lighter hydrocarbons, which were extracted more efficiently, were removed from the system. Also, the amount of CO₂ dissolved in the lower phase declined slightly as the hydrocarbons remaining became heavier and heavier.

Overall phase compositions were calculated for each phase from measured compositions and amounts of produced gas and liquid. Figures 3.37 and 3.38 summarize phase compositions for the two displacements. The oil is represented, in Figures 3.32-3.34, as a pair of pseudo-components, C₁-C₁₂ and C₁₃₊, though the actual composition data are much more detailed. A comparison of the CMC results for oils with and without solution gas with PVT results for similar systems is given in §4.

The results shown in Figure 3.37 were the first obtained with the CMC apparatus. It is interesting to compare Figure 3.37 with Figure 3.33 which gives results of a repeat experiment performed nearly a year later after numerous modifications and improvements of the apparatus had been made. Tie line slopes and upper phase compositions agree very well. Lower phase compositions also agree well although not as closely as the upper phase compositions, probably because measurements with a wet test meter of the smaller amounts of gas present in the lower phase samples showed more scatter.

3.3 Conclusions

Results of experiments performed to measure the volumetric, compositional, and fluid property behavior of CO₂-crude oil mixtures lead to the following observations and conclusions:

- (1) Constant composition PVT experiments indicate that the addition of solution gas to a dead oil enlarges the range of pressures and compositions in which mixtures of CO₂ and the recombined oil form two or more phases. Addition of solution gas also displaces the critical point on a pressure-composition (P-X) phase diagram to lower CO₂ concentrations and lower pressures. This alters partitioning of hydrocarbon components (see §4).
- (2) Volumetric behavior of a dead Wasson oil mixed with CO₂ at

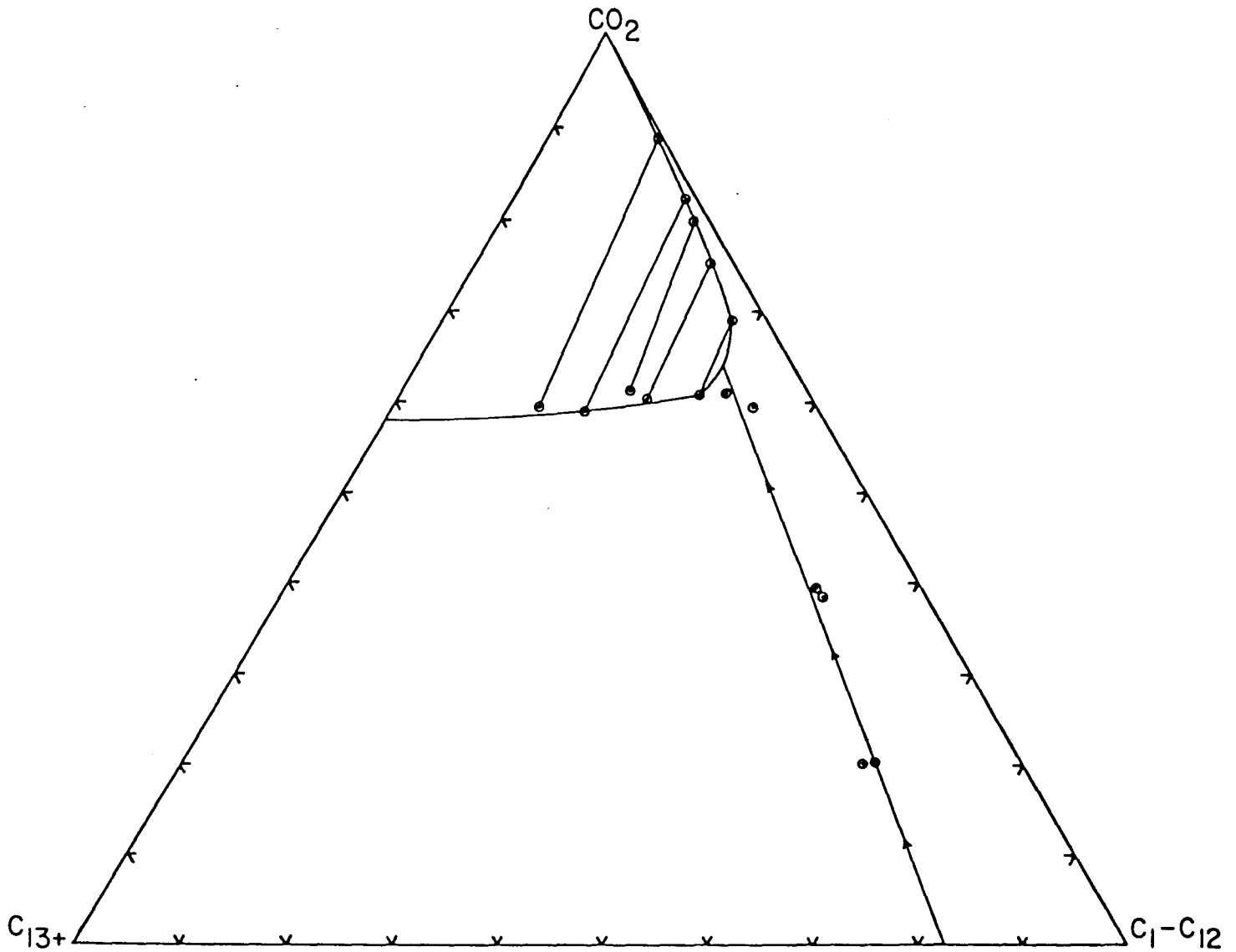


Figure 3.37 Pseudo-ternary representation of phase compositions of mixtures of CO₂ with Maljamar recombined reservoir fluid at 2500 psig and 90°F.

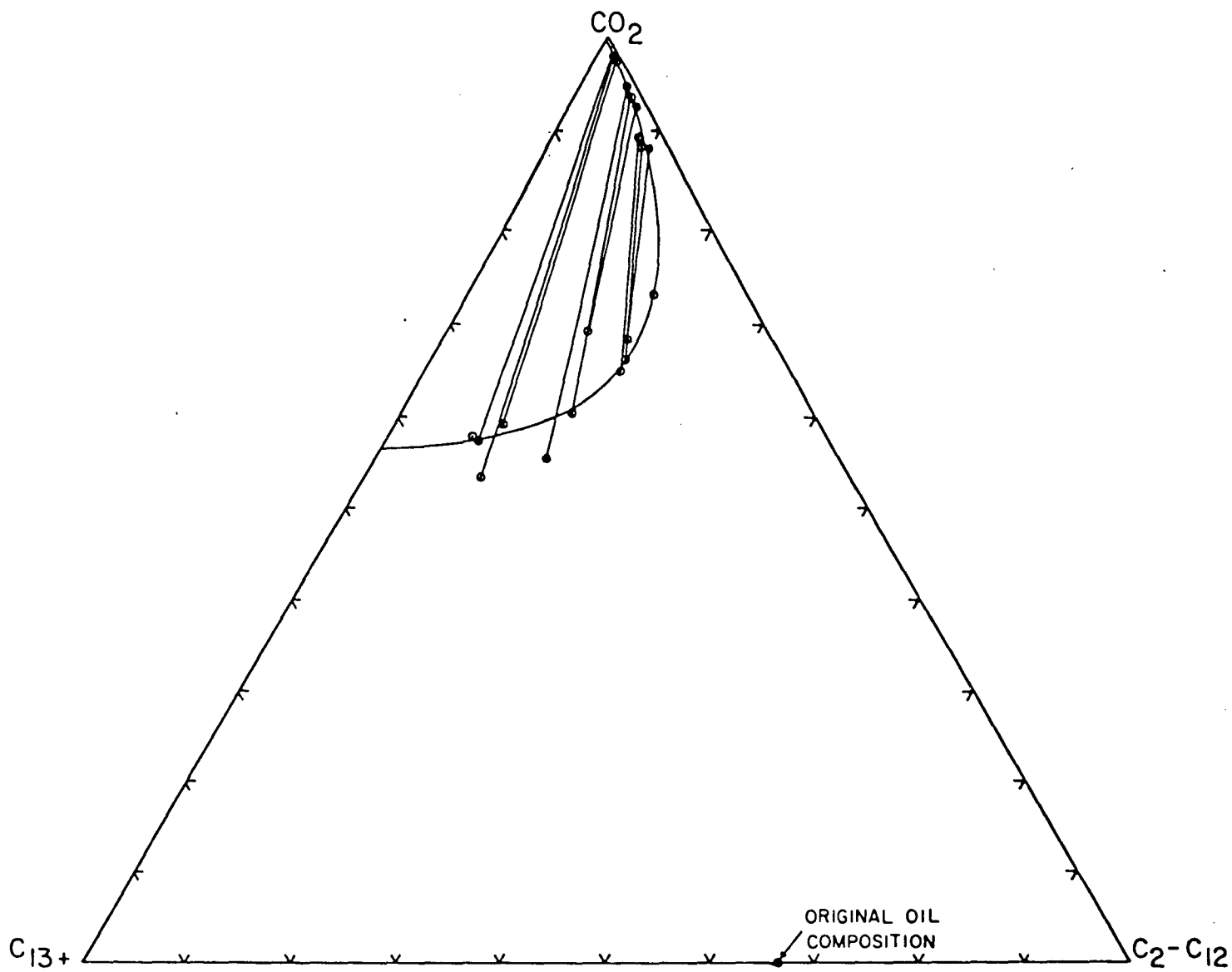


Figure 3.38 Pseudo-ternary representation of phase compositions of mixtures of CO_2 with Maljamar separator oil at 1200 psia and 90°F .

105°F is very similar to that of a dead Maljamar oil at 90°F despite the difference in temperature and the fact that the oils were from different fields. Compositions of the two San Andres oils are also similar. These results suggest that phase behavior experiments described here may give an indication of the behavior of other Permian basin oils.

- (3) Use of gold electrodes should be avoided in CO₂-crude oil systems where mercury use displaces fluids in the flow apparatus. Platinum electrodes appear to be unaffected by CO₂-crude oil mixtures and are not damaged by contamination with mercury.
- (4) A simple analysis of the operation of the CMC apparatus for binary systems indicates that effects of averaging of sample compositions can be controlled by selecting the sampling time and cell volume appropriately. The solutions presented are useful for estimating times required to perform CO₂-crude oil displacements.
- (5) CMC measurements of phase compositions and densities of CO₂-C₁₀ mixtures agree well with published values and with the simple analysis of the operation of the apparatus. Those results establish that the CMC experiment can be used to obtain phase composition and density data of acceptable accuracy.
- (6) For CO₂-crude oil systems, the CMC experiment provides direct evidence of the efficiency with which CO₂ extracts hydrocarbons from the oil, whether or not analyses of gas and liquid samples are performed. Extraction of hydrocarbons by a CO₂-rich liquid phase is much more efficient than that by CO₂-rich vapor at a similar pressure.
- (7) The differences between densities of CO₂-rich and oil-rich phases are smaller than those between pure CO₂ and original oil because the presence of extracted hydrocarbons in the CO₂-rich phase increases its density over that of CO₂. The density of oil saturated with CO₂ is slightly higher than that of the original oil, despite the fact that the density of pure CO₂ may be much lower than that of the oil.

4. INTERPRETATION OF EXPERIMENTS AND APPLICATION TO FIELD PROBLEMS

The experiments described in §2 and §3 were designed to isolate portions of the displacement process. In particular, effects of pore structure on displacement efficiency were examined, and the physical chemistry of CO₂-crude oil mixtures was studied. In this section, we consider aspects of the relationship between the physical behavior of the fluids and flow in porous rock. In §4.1, we examine the effects on CO₂ flood displacement efficiency of addition of solution gas to a dead oil by interpreting results of PVT and CMC experiments for live and dead oils in terms of pseudo-ternary diagrams. The analysis suggests an interpretation for the insensitivity of displacement results to the presence of solution gas. In §4.2, we consider a more comprehensive attempt to assess the importance of interactions of pore structure, phase and fluid property behavior, and flow instability.

4.1 Effect of Solution Gas on Local CO₂-Crude Oil Displacement Efficiency

Efficient displacement of crude oil by high pressure carbon dioxide is generally acknowledged to be the result of efficient extraction of hydrocarbons from the crude oil by dense CO₂ (Rathmell, Stalkup, and Hassinger 1971; Holm and Josendal 1974; Stalkup 1978; Metcalfe and Yarborough 1979; Gardner, Orr, and Patel 1979; Orr, Yu, and Lien 1981). While it is clear that adverse effects of viscous instability, gravity segregation and reservoir heterogeneity can partially offset the favorable effects of CO₂-crude oil phase behavior, it is really the transfer of components between the crude oil and the displacing phase which provides the potential for high displacement efficiency. Experimental investigations of the impact of phase behavior on displacement efficiency have relied on CO₂ floods in slim tubes, in which the effects of viscous fingering and heterogeneity are minimized. Effects of oil composition on the pressure required to obtain an efficient displacement in a slim tube were investigated by Holm and Josendal (1974), Yellig and Metcalfe (1980), Holm and Josendal (1980), and Johnson and Pollin (1981). Yellig and Metcalfe (1980) performed slim tube displacements with oils made by combining C₁, C₂-C₆ and C₇₊ fractions of fixed composition in varying amounts. They offered a correlation in which the "minimum miscibility pressure (MMP)" varied only with temperature as long as the predicted pressure was above the bubble point pressure of the oil. If not, the bubble point pressure was taken as the MMP. Holm and Josendal (1980) argued that the MMP correlated well with the density of CO₂ required to achieve efficient extraction, and that the effect of increasing temperature was to increase the pressure required to produce a CO₂ density high enough to extract hydrocarbons efficiently from the oil. They also reported that the presence of methane did not change the MMP appreciably. Rathmell, Stalkup, and Hassinger (1971) however, argued, based on pseudo-ternary and pseudo-quarternary phase diagrams, that the addition of methane to a reservoir oil should increase the minimum miscibility pressure.

The results presented by Holm and Josendal and by Yellig and Metcalfe

were based on slim tube displacement data but not upon detailed measurements of CO₂-crude oil phase behavior when the amount of solution gas present was varied. Hence, nothing could be said about the underlying physical reasons for the observed independence of the MMP on the amount of methane present. Rathmell, Stalkup, and Hassinger based their arguments on plausible phase diagrams but had limited phase composition measurements to test their arguments. In this section, we interpret, in terms of pseudo-ternary diagrams, comparisons of standard single contact PVT measurements for reservoir fluids with and without solution gas reported in §2.1. In addition, results of continuous multiple contact (CMC) displacements for the same systems are compared with the interpretation given. The results shed some light on the reasons behind the insensitivity of displacement results to the presence of solution gas in the oil.

Results of PVT experiments presented in §3.1 indicated that the addition of 672 SCF/BBL of solution gas (see Table 3.1) to Maljamar separator oil substantially altered the qualitative appearance of the pressure-composition (P-X) phase diagram, as comparison of Figures 3.1 and 3.2 indicates. Addition of solution gas enlarged the L₁-V, L₁-L₂, and L₁-L₂-V regions substantially and displaced the critical point on the P-X diagram to lower CO₂ concentration and pressure. Finally, comparison of phase volumes for mixtures with and without solution gas indicated that at high pressures, larger volumes of hydrocarbons were extracted into the upper liquid (L₂) phase when solution gas was present.

A qualitative explanation for the differences in volumetric behavior at different CO₂ concentrations and for the behavior with and without solution gas is given in terms of pseudo-ternary diagrams in Figures 4.1 and 4.2. The oil has been represented arbitrarily as heavy (H) and light (L) components. Figure 4.1 shows a sequence of pseudo-ternary diagrams for CO₂-RRF mixtures at pressures increasing from P₁ to P₆. The compositions labeled 1, 2 and 3 in Figures 4.1 and 4.2 represent mixtures containing 40, 60 and 80 mol % CO₂ in the original oil. At pressure P₁ (about 1000 psia, 6890 kPa, for the hydrocarbon system of Figure 3.1), all three mixtures form a liquid and a vapor as does the original oil. At P₂ (about 1075 psia, 7410 kPa, in Figure 3.1), which is just above the critical pressure of CO₂, a two-phase (L₁-L₂) region and a three-phase (L₁-L₂-V) region have appeared at the CO₂-H side of the diagram. With increasing pressure, the L₁-L₂-V triangle migrates toward the light (L) component apex. Thus, for the mixture at composition 3, the three-phase region occurs at lower pressures than for mixtures containing less CO₂ (see Figure 3.1). At P₃ (about 1250 psia, 8620 kPa, in Figure 3.1), mixture 3 is in the L₁-L₂ region while mixtures 1 and 2 remain in the L₁-V region. The three-phase region eventually disappears, with increasing pressure, at a critical tie line shown in the diagram for P₄. At a higher pressure, P₅, the mixtures rich in the light component (L) appear to be L₁-V mixtures, while those containing less (L) appear to be L₁-L₂ mixtures since both phases have densities and compressibilities typical of liquids. Thus, it is possible for a mixture like mixture 2 to pass, with increasing pressure, from an apparent L-V state to an apparent L₁-L₂ state without exhibiting three phases. That is evidently what happened for the mixture whose volumetric behavior is shown in Figure 3.3. In a situation like this, then, the CO₂-rich phase is a supercritical dense phase for which the distinction between liquid

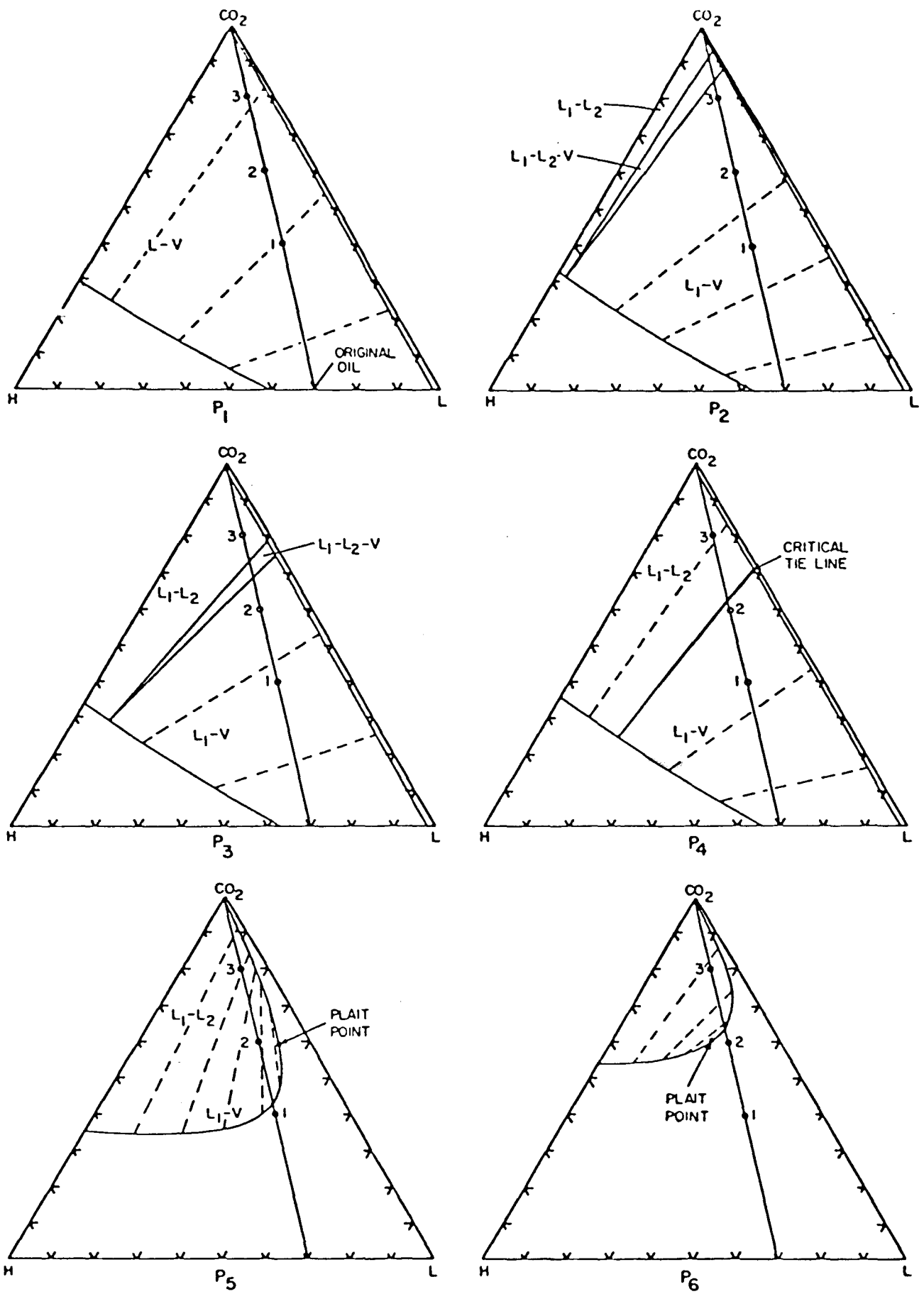


Figure 4.1 Phase behavior of a CO_2 -crude oil system with solution gas present.

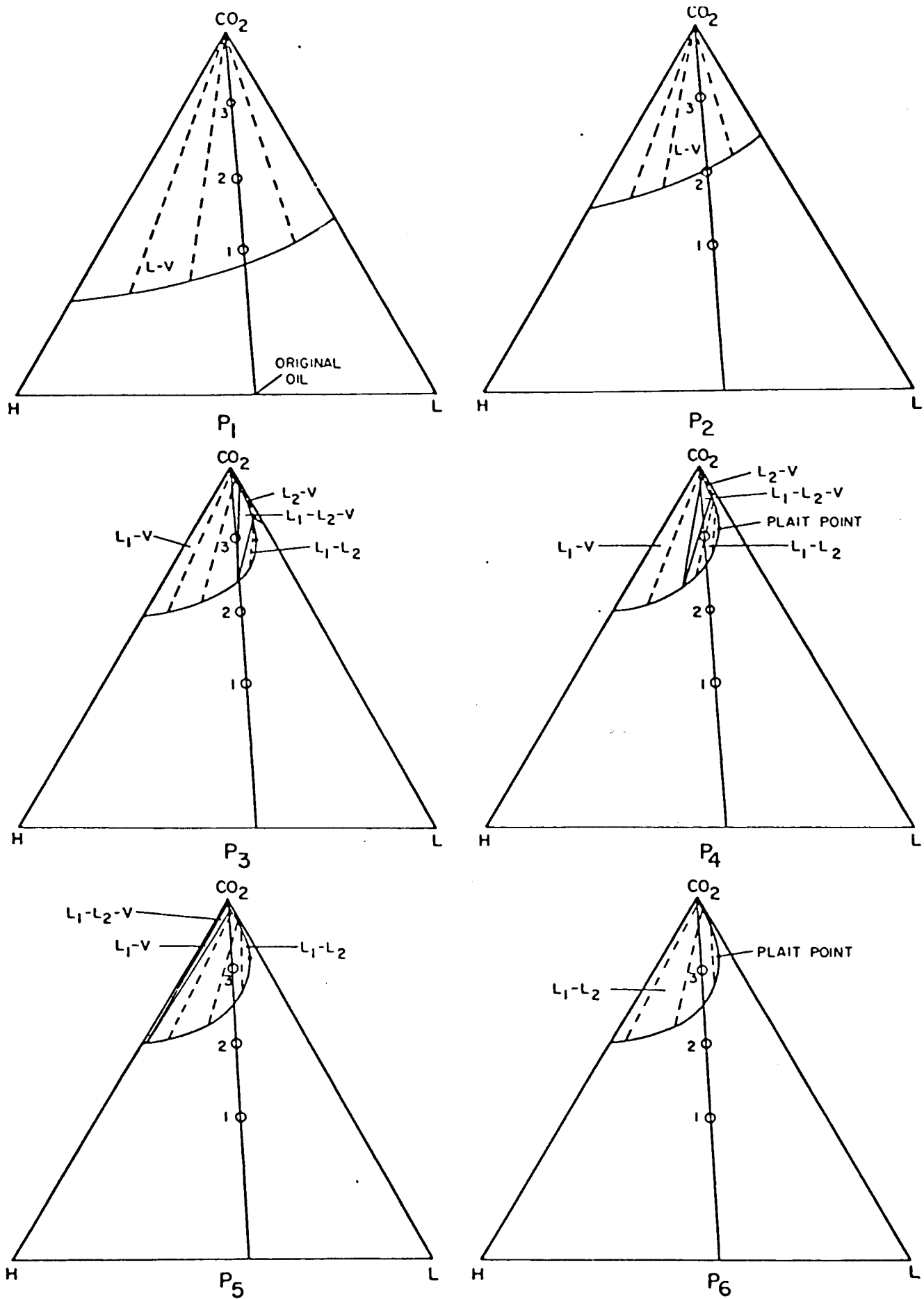


Figure 4.2 Phase behavior of a CO₂-crude oil system without solution gas.

and vapor is not clear. Similar behavior has been reported for mixtures of CO_2 , C_1 , and C_{16} (Orr, Lien, and Pelletier 1981).

Between P_5 and P_6 , the plait point for the remaining L_1 - L_2 region crosses the line of compositions on which mixtures of CO_2 and the original oil lie. The pressure at which the plait point crosses the binary mixture line is the critical pressure shown in Figure 3.1. Because the plait point lies to the left of the binary composition line at P_6 , then, the composition at which that line crosses the binodal curve is a dew point mixture. There must be a second dew point mixture, where the binary composition line crosses the binodal curve again, at a very high CO_2 concentration, since pure CO_2 must be a single phase above its critical temperature.

Figure 4.2 gives a similar sequence of ternary diagrams for CO_2 -separator oil mixtures. In this case, the light pseudo-component (L) contains no methane, ethane or propane, so it is miscible with the heavy pseudo-component. At pressure P_1 (about 500 psia, 3450 kPa, for the system in Figure 3.2), CO_2 is immiscible with both pseudo-components and the two-phase region is a band across the diagram. The solubility of CO_2 in the light component is somewhat higher than that in the heavy component, and the amount of either component extracted into the low density vapor phase is small. Hence, the tie lines shown as dashed lines in Figure 4.2 pass near the CO_2 apex. Mixture 1 (40% CO_2) is just inside the two-phase region. At a slightly higher pressure, mixture 1 would be at its bubble point pressure. At P_2 (around 800 psia, 5520 kPa, in Figure 3.2), CO_2 is soluble enough in the oil without solution gas that both mixture 1 and mixture 2 lie in the single phase region. At a higher pressure, P_3 (950 psia, 6550 kPa), the liquid phase rich in the light hydrocarbon component (L) has become so rich in CO_2 that it is immiscible with the L_1 phase which contains most of the heavy hydrocarbon component (Orr, Yu, and Lien 1981). Additional pressure increases cause the three-phase triangle to migrate toward the CO_2 -H side of the ternary diagram (P_4 and P_5). Thus, mixtures containing more than 80% CO_2 will exhibit three phases at pressures higher than those for which mixture 3 forms three phases (see Figure 3.2). A binary mixture can form three coexisting phases at one pressure at a fixed temperature. That pressure is just above 1100 psia (7580 kPa) for the CO_2 -H pseudo-binary mixture (Figure 3.2). At P_6 (say 1200 psia, 8270 kPa), the three-phase region has disappeared leaving a liquid-liquid region similar to, but smaller than that shown at P_6 in Figure 4.1. Because the liquid-liquid systems are much less sensitive to pressure changes than liquid-vapor systems, large pressure changes would be required to substantially alter the size of the two-phase region or the location of the plait point.

The phase diagrams presented in Figures 4.1 and 4.2 do not provide any direct indication of the displacement efficiency which might be observed in, say, a slim tube displacement. Computations such as those described by Gardner, Orr, and Patel (1979); Orr, Yu, and Lien (1981); and Orr and Taber (1981) indicate that the efficiency of the displacement process, in one dimension at least, is dominated by the slope of the tie lines. Helfferich proved that, in the absence of dispersion, a displacement will avoid the two-phase region, and hence be judged to develop or generate miscibility, if there exists no tie line which when extended passes through the two-phase region (Helfferich 1981). While real displacements always include some

dispersion (and probably some viscous fingering), in practice, the compositions of fluids present in the transition zone between oil and displacing CO₂ need only pass close to the dew point portion of the phase boundary. If so, the volume of residual oil left behind as the transition zone passes is small (Orr and Taber 1981), and the displacement is efficient.

As is apparent from Figures 4.1 and 4.2, tie line slopes are influenced strongly by the position of the plait point on the binodal curve. Phase volumes observed in single contact PVT experiments are also sensitive to the location of the plait point in relation to the line which represents binary mixtures of CO₂ and the oil. For instance, in Figure 4.2 the plait point for the L₁-L₂ region lies to the right of the binary composition line at all pressures at which two liquid phases are present (P₃-P₆). Thus with increasing pressure, mixtures of CO₂ with the separator oil pass from two-phase L₁-L₂ mixtures to single phase mixtures through a liquid-liquid bubble point, as was observed for the mixture containing 79.7 mol % CO₂ described in Figure 3.7a. Pressures up to 4000 psia (27580 kPa) were not sufficient to force the plait point to migrate enough to pass through the line of binary mixture compositions. Hence, no critical point was observed in the single contact PVT study for the separator oil. If a critical point occurs at any experimentally attainable pressure for the CO₂-separator oil system, it does so at pressures above the range shown in Figure 3.2. In contrast, the plait point in the CO₂-RRF system did cross the binary composition line, and hence, a critical point appears on the pressure-composition (P-X) diagram shown in Figure 3.1. At pressures above the critical pressure, L₁-L₂ mixtures enter the two-phase region through a liquid-liquid dew point. At such a dew point pressure, the criterion based on tie line extensions for developed miscibility would always be satisfied. Thus, the pressure required to satisfy the tie line extension criterion must be lower than the critical pressure on a P-X diagram.

If the picture given in Figures 4.1 and 4.2 is at least qualitatively correct, then the effect of adding solution gas to the separator oil is to enlarge the two-phase region, to shift the location of the plait point to lower CO₂ concentrations, and to displace the binary composition line toward the light hydrocarbon component. Displacement of the plait point alters tie line slopes in a favorable way, and displacement of the binary composition line moves the oil composition away from the region of tie line extensions. Those two effects partly compensate, therefore, for the adverse effects of enlargement of the two-phase region, which, in the absence of changes in tie line slope or oil composition would adversely affect displacement efficiency. Thus, the sequences of phase diagrams given in Figures 4.1 and 4.2 offer a possible explanation, qualitative at best, for the relatively small effect on minimum miscibility pressures of adding solution gas to the oil.

It is clear that the phase diagrams shown in Figures 4.1 and 4.2 cannot reflect completely the behavior of mixtures which contain as many components as a crude oil. Nevertheless, the sequences shown are qualitatively consistent with the essential features of the single contact phase diagrams shown in Figures 3.1 and 3.2. The results of CMC displacements with and without solution gas also appear to be consistent with the proposed sequences of phase diagrams. Comparison of Figures 3.37 and 3.38 confirms that the

two-phase region is larger for the CO₂-RRF mixture despite the higher pressure in that displacement, that the tie line slopes are more favorable in the CO₂-RRF system, that the binary composition line is displaced toward the light hydrocarbon component, and that the plait point occurs at lower CO₂ concentrations. Indeed, the CO₂-RRF displacement at 2500 psig (17320 kPa) entered the two-phase region near the plait point, which is consistent with the estimate of the critical pressure (2620 psia, 18060 kPa) from the single contact PVT experiments.

Thus, the experimental evidence available to date is in accord with the qualitative picture of the effect of pressure on CO₂-crude oil phase behavior given in Figures 4.1 and 4.2, though more experimental evidence would be desirable. In particular, phase composition measurements at pressures near the bubble point pressure of the CO₂-RRF mixture will be required to prove or disprove the proposed explanation for the insensitivity of slim tube displacement results to the presence of solution gas. Nevertheless, the results presented here suggest that pseudo-ternary diagrams, with all their limitations, can provide a useful conceptual framework for understanding CO₂-crude oil phase behavior and its impact on displacement processes.

4.2 Two-Dimensional Simulation of CO₂ Flood Performance

Numerical simulation programs applied to CO₂ flooding have concentrated on modeling either the effects of phase behavior (compositional simulators) or the effects of viscous fingering (miscible simulators), but there has been no attempt so far to examine interactions of phase behavior and viscous fingering (see §1 for a brief summary of approaches to simulation of field scale CO₂ floods). A simulator to be used to study relationships between CO₂ flood process mechanisms should include provision for modeling:

- (1) Phase behavior of CO₂-crude oil mixtures
- (2) Dispersion, longitudinal and transverse
- (3) Variation of phase viscosities with composition
- (4) Variation of phase densities with composition
- (5) Viscous and gravitational instability
- (6) Trapping and dead-end pore volume

A flow model which accounted for all the effects listed would be significantly more complex than any model currently available for CO₂ flooding. Reasons for the complexity are apparent from the equations which describe multiphase, multicomponent flow in porous media. The fundamental set of partial differential equations are those which result from a material balance for each component,

$$\sum_{j=1}^{n_p} \left\{ \phi \frac{\partial}{\partial t} \left[\rho_{jf} x_{ijf} S_{jf} + \rho_{jd} x_{ijd} S_{jd} + \rho_{jt} x_{ijt} S_{jt} \right] + \nabla \cdot \rho_{jf} x_{ijf} \tilde{v}_j - \nabla \cdot \phi \rho_{jf} \tilde{D}_{ij} \cdot \nabla x_{ijf} \right\} = 0, \quad i = 1, n_c \quad (4.1)$$

where ϕ is the porosity, n_c the number of components, n_p the number of phases, and \tilde{D}_{ij} the dispersion tensor for component i in phase j . The saturation of the j^{th} phase is divided into three parts: a flowing saturation, S_{jf} ; a fraction which communicates by some mass transfer mechanism with the flowing phase, S_{jd} ; and a trapped fraction, S_{jt} . Because the mole fractions of component i in each fraction of phase j , x_{ijf} , x_{ijd} and x_{ijt} will be different, there are, in general, three molar densities, ρ_{jf} , ρ_{jd} and ρ_{jt} , associated with each phase. In this generalization of the model given by Coats and Smith (1964), the lagging or dead-end saturation S_{jd} can exchange components with the flowing stream by a first order mass transfer mechanism driven by the difference in composition between flowing and stagnant but communicating fluid,

$$\phi \frac{\partial}{\partial t} \left(\rho_{jd} x_{ijd} S_{jd} \right) = K_j \left(\rho_{jf} x_{ijf} - \rho_{jd} x_{ijd} \right), \quad i = 1, n_c \quad (4.2)$$

The trapped saturation will be assumed to change only if the overall saturation of phase j changes, though the exact form of the dependence on phase saturations will be based on results of experiments described in §2.2. It is not obvious, for instance, how a portion of phase j , which is untrapped because the saturation of phase j rises, should be distributed between flowing and dead-end saturations; nor is it clear how the composition of a trapped phase should be modified by more of the same phase trapped later. It is clear, however, that some simplifying assumptions will be required if the problem is to be computationally tractable. The various fractions of a given phase must sum to the phase saturation

$$S_j = S_{jf} + S_{jd} + S_{jt}, \quad j = 1, n_p \quad (4.3)$$

and the phase saturations must sum to unity

$$\sum_{j=1}^{n_p} S_j = 1 \quad (4.4)$$

as must the mole fractions of each portion of each phase

$$\sum_{i=1}^{n_c} x_{ijf} = 1,$$

$$\sum_{i=1}^{n_c} x_{ijd} = 1, \quad j = 1, n_p \quad (4.5)$$

$$\sum_{i=1}^{n_c} x_{ijt} = 1,$$

The flow velocity of a phase is routinely assumed to be given by Darcy's equation

$$\underline{v}_j = - \frac{k k_{rj}}{\mu_j} \left(\nabla p_j + \rho_j \underline{g} \right), \quad j = 1, n_p \quad (4.6)$$

where k is the permeability, k_{rj} and μ_j the relative permeability and viscosity of phase j , p_j the pressure in phase j , and \underline{g} the gravity vector. Pressures in the phases are related by a set of capillary pressure relations, usually assumed to be functions of saturation.

$$p_j - p_k = p_{ckj} \left(S_j, S_k \dots \right), \quad j \neq k \quad (4.7)$$

If low interfacial tensions occur during a displacement, as would happen for compositions near a plait point, the capillary pressures would be functions of composition as well. Given the fact that there have been no measurements of capillary pressure relationships for the phases which occur for CO₂-crude oil mixtures, some of the functions p_{ckj} will be set to zero. Specification of the problem is completed by a set of equilibrium relations which gives the distribution of components between phases, and various functions which

describe the dependence of viscosity and density on phase compositions and of relative permeabilities on phase saturations.

Simple techniques for representation of essential features of CO₂-crude oil phase behavior were developed previously for use in a one-dimensional process simulator (Orr 1980). Given the complexity of any flow model which attempts to account for compositional effects combined with trapping and dead-end pore volume, the representation of phase behavior should be as simple as possible. In the one-dimensional model, longitudinal dispersion was modeled qualitatively by balancing time and space truncation errors so as to produce numerical dispersion levels similar to the magnitude of the physical dispersion to be modeled. The fully explicit, backward finite difference method used was particularly convenient for one-dimensional calculations. That approach is not suitable, however, for multidimensional calculations. In two-dimensional flow, for instance, the local flow velocity is a function of position, and it is not necessarily aligned with a coordinate axis. Furthermore, physical dispersion coefficients are functions of velocity (and probably saturation). Use of truncation error to model dispersion would not model effects of velocity variations and would inevitably introduce grid orientation effects. Hence, it appears desirable that dispersion be modeled explicitly.

Explicit modeling of dispersion requires that numerical dispersion, which arises out of truncation error in the finite difference representation of the differential equation, particularly the first derivative (convective) terms, be reduced to a magnitude significantly smaller than that of the physical values of longitudinal and transverse dispersion. The requirement for low numerical dispersion can be met by using very fine finite difference grids with the usual five point star or by using higher order (more accurate) representations of the derivatives. Fine grids can be useful since detailed resolution of small slugs or viscous fingers is possible, but the computational cost may be high. Higher order methods, such as those presented by Settari, Price, and Dupont (1977) appear to offer distinct advantages for simulation of unstable displacements, though at the cost of significant additional programming complexity over more standard finite difference methods. In this model, no special assumptions are made about the effects of viscous fingering. The viscous instability is inherent in the flow equations (Perrine 1961; Heller 1963, 1966), though of course, at least two space dimensions must be included.

Work continues on the implementation of the general model described above. Requirements of computational tractability will require additional simplifying assumptions. Nevertheless, as formulated, the model will allow numerical experiments to assess the relative importance of phase behavior, viscous fingering, gravity segregation, trapping and dead-end pore volumes, a computation which has not been attempted previously.

4.3 Conclusions

Analysis of results of single contact volumetric experiments as well as continuous multiple contact phase composition measurements suggests that:

- (1) Addition of solution gas to a dead oil displaces the critical point on a P-X diagram to lower CO₂ concentrations and lower pressures.
- (2) On a pseudo-ternary diagram, this corresponds to a displacement of the plait point to lower CO₂ concentrations and to the displacement of the binary composition line toward the light hydrocarbon pseudo-component. Displacement of the plait point alters tie line slopes in such a way that the region of oil compositions which are intersected by tie line extensions is reduced, while changing the oil composition by adding solution gas to the separator oil moves the oil composition away from the region of tie line extensions. Both effects act to compensate partly for the unfavorable effects of the enlargement of the two-phase region on CO₂ flood displacement efficiency.
- (3) Additional CMC displacements at one pressure of oils with and without solution gas should be performed to confirm or disprove the explanation given for the low sensitivity of displacement efficiency to the presence of solution gas.

A flow model has been formulated which will allow assessment of the importance of interactions of phase behavior, viscous fingering, and trapping. Work required to implement the model is in progress.

5. SUMMARY

This report describes progress in three research areas:

- (1) Development of experimental displacement techniques to study effects of pore structure and high water saturations on miscible displacement efficiency.
- (2) Measurement of phase behavior and fluid properties of CO₂-crude oil mixtures.
- (3) Interpretation of the effects of individual parts of the process mechanism on the performance of laboratory and field scale CO₂ floods.

In the first area, the difficulties inherent in the interpretation of miscible displacement mechanisms from effluent composition data have been reviewed. That review clearly indicated the need for displacement experiments with fluids of closely matched density and viscosity to isolate the effects of rock pore structure from those of viscous fingering and gravity segregation. Experimental procedures to study the effects of high mobile water saturations on the efficiency with which an injected fluid can contact and displace oil in place have also been outlined. Results of those experiments will shed additional light on the question of whether to use high mobile water saturations (alternating water and gas injection) to reduce the mobility of CO₂. The core flood experiments with simple fluid systems are part of a sequence of displacements which will culminate with CO₂ floods in the same cores. The independent measurements of the effects of pore structure and phase distributions will form the basis for interpretation of the far more complex CO₂ displacements.

The experimental results presented in the second area are also essentially independent measurements because the variations of phase compositions as a CO₂ flood progresses, along with attendant variations of phase densities and viscosities, strongly influence the local motions of the phases. Hence, they strongly affect the local displacement efficiency. Understanding of the competition between phase behavior, viscous instability, and flow heterogeneity requires some independent measurement of composition and fluid property variations which drive the process. Results of volumetric measurements have been presented for several systems which illustrate effects of variation of the amount of solution gas present. Because different oil fields have been subjected to widely varying pressure histories and because amounts of gas present initially vary widely, gas-oil ratios for fields to be CO₂ flooded will also vary widely. The results given here outline effects of a change in the gas-oil ratio for oils similar in composition.

Also given as part of research area (2) is a detailed description of the recent progress in the development of the continuous multiple contact experiment, which can be used to measure equilibrium phase compositions and

densities rapidly and efficiently. A simple theory of the operation of the apparatus is presented and tested for simple hydrocarbon systems, with excellent agreement between theory and experiment. The effect of increasing pressure on phase compositions and densities was investigated in a series of continuous multiple contact experiments for Maljamar crude oil. Results of those experiments document further the fact that a CO₂-rich liquid phase can extract hydrocarbons efficiently, more so than a CO₂-rich vapor phase if pressures and temperatures are such that CO₂-rich liquid and vapor phases can coexist. Progress on research to install equipment to make a simultaneous measurement of phase viscosities is also described. If successful, those measurements will provide information badly needed to predict the magnitude of effects of viscous instability in a transition zone between oil and CO₂. The results presented in this section demonstrate further the utility of the continuous multiple contact experiment.

In the third area, an interpretation of the results, phase volume, and phase composition experiments based on pseudo-ternary diagrams is given. The proposed sequences of diagrams with increasing pressure provide a possible explanation for observations that the presence of solution gas has little effect on experimentally determined minimum miscibility pressures. The analysis suggests additional experiments are needed to confirm or disprove the proposed explanation. Finally, formulation of a simulation model which would allow detailed calculation of the relative importance of competing process mechanisms such as phase behavior, viscous and gravitational instability, rock heterogeneity, dispersion and trapping of oil by mobile water, is outlined.

Thus, the research program reviewed here continues to concentrate on the mechanisms which act and interact to determine displacement efficiency in a CO₂ flood. The combination of experimental work and analysis is aimed, therefore, at development of better tools for prediction of CO₂ flood performance on a field scale.

ACKNOWLEDGEMENT

The research effort from which this report is drawn rests on the contributions of M.K. Silva, who shepherds the development of the CMC experiment; C.L. Lien, who has established dominance over a batch of unruly gas chromatographs; C.M. Jensen, who somehow manages to measure phase volumes despite oils blacker than night; M.L. Graham, whose careful core displacements have often lasted far into the night; M.T. Pelletier, who exuberantly tackles any design problem, electronic or mechanical, and makes things work when they don't; R.E. Bretz, who is busy establishing some semblance of order in our effort to flood cores with all manner of strange fluids; S.M. Linert, who patiently measures whatever needs measuring; B.T. Campbell, whose high pressure flow visualization apparatus is about to teach us how CO₂ floods really work; J.C. Franklin, who has convinced recalcitrant instruments to converse with each other, data to be transferred and calculated results to appear in usable form, all in a finite period of time; R.M. Specter, who is trying valiantly to teach a bunch of engineers and chemists to recognize a rock when they see one - may he yet succeed; and D.J. Callahan, who will be unchained from the drafting table upon completion of this report to resume mortal combat with the simulation programs. K.A. Grattan and P.L. Bradley deserve most of the credit for the fact that this report is composed mainly of complete English sentences. Many of the ideas and interpretations presented here have been molded and nurtured in endless discussions with J.P. Heller, N.R. Morrow, and I. Chatzis. We are grateful to Conoco, Inc., ARCO Oil and Gas, and AMOCO for equipment grants, and to Conoco, ARCO, and Shell Development Co. for oil and rock samples. Finally, we thank the U.S. Department of Energy and the New Mexico Energy and Minerals Department for the support which made this work possible. The sympathetic, active interest and encouragement of Leo Noll and Royal Watts of the U.S. DOE is much appreciated.

REFERENCES

- American Society for Testing and Materials 1976, "Proposed Test Method for Boiling Range Distribution of Crude Petroleum by Gas Chromatography," ASTM Standards, Part 25, Philadelphia, PA, 716-722.
- Aris, R. and Amundson, N. R. 1957, "Some Remarks on Longitudinal Mixing or Diffusion in Fixed Beds," AIChE J. 3, 280.
- Aronofsky, J. S. and Heller, J. P. 1957, "A Diffusion Model to Explain Mixing of Flowing Miscible Fluids in Porous Media," Pet. Trans. AIME 210, 345-349.
- Baker, L. E. 1977, "Effects of Dispersion and Dead-End Pore Volume in Miscible Flooding," Soc. Pet. Eng. J. 17, 219-227.
- Batycky, J. P., Maini, B. B., and Fisher, D. B. 1980, "Simulation of Miscible Displacement in Full Diameter Carbonate Cores," SPE 9233, presented at SPE 55th Annual Meeting of SPE of AIME, Dallas, September 21-24.
- Brenner, H. 1962, "The Diffusion Model of Longitudinal Mixing in Beds of Finite Length. Numerical Values," Chem. Eng. Sci. 17, 229-243.
- Brigham, W. E., Reed, P. W., and Dew, J. N. 1961, "Experiments on Mixing During Miscible Displacement in Porous Media," Soc. Pet. Eng. J. (March) 1-8.
- Coats, K. H. 1979, "An Equation-of-State Compositional Model," SPE 8284, presented at SPE 54th Annual Fall Meeting, Las Vegas, September 23-26.
- Coats, K. H. and Smith B. D. 1964, "Dead-End Pore Volume and Dispersion in Porous Media," Soc. Pet. Eng. J. 4 (March) 73-84.
- Collings, A. F. and McLaughlin, E. 1971, "Torsional Crystal Technique for the Measurement of Viscosities of Liquids at High Pressure," Trans. Faraday Soc. 67, 340-352.
- Deans, H. A. 1963, "A Mathematical Model for Dispersion in the Direction of Flow in Porous Media," Soc. Pet. Eng. J. 3, 49.
- De Bock, A., Grevendonk, W., and Awouters, H. 1967, "Pressure Dependence of the Viscosity of Liquid Argon and Liquid Oxygen, Measured by Means of a Torsionally Vibrating Quartz Crystal," Physica 34, 49-52.
- De Bock, A., Grevendonk, W., and Herreman, W. 1967, "Shear Viscosity of Liquid Argon," Physica 37, 227-232.
- Diller, D. E. 1980, "Measurements of the Viscosity of Compressed Gaseous and Liquid Methane," Physica 104A, 417-426.
- Dumore, J. M. 1964, "Stability Considerations in Downward Miscible Displacements," Soc. Pet. Eng. J. (December) 356-362.

Fussell, L. T. and Fussell, D. D. 1977, "An Iterative Sequence for Compositional Models Incorporating the Redlich-Kwong Equation of State," SPE 6891, presented at SPE 52nd Annual Fall Meeting, Denver, October 9-12.

Gardner, J. W., Orr, F. M., and Patel, P. D. 1979, "The Effect of Phase Behavior on CO₂ Flood Displacement Efficiency," SPE 8367, presented at SPE 54th Annual Fall Meeting, Las Vegas, September 23-26.

Gelhar, L. W., Gutjahr, A. L., and Naff, R. L. 1979, "Stochastic Analysis of Macrodispersion in a Stratified Aquifer," Water Resources Research 15 No. 6, 1387-1397.

Harrison, R. H., Moore, R. T., and Douslin, D. R. 1973, "Thermodynamic Properties of Compressed Gaseous Methane," J. Chem. Eng. Data 18 No. 2, 131-134.

Haynes, W. M. 1973, "Viscosity of Gaseous and Liquid Argon," Physica 67, 440-470.

Helfferrich, F. G. 1981, "Theory of Multicomponent, Multi-Phase Displacement in Porous Media," Soc. Pet. Eng. J. 21 (February) 51-62.

Heller, J. P. 1966, "Onset of Instability Patterns Between Miscible Fluids in Porous Media," J. Appl. Phys. 37, 1566-1579.

Heller, J. P. 1963, "The Interpretation of Model Experiments for the Displacement of Fluids Through Porous Media," AIChE J. 9 (July) 452-459.

Holm, L. W. and Josendal, V. A. 1980, "Effect of Oil Composition on Miscible-Type Displacement by Carbon Dioxide," SPE 8814, presented at 1st SPE/DOE Symposium on Enhanced Oil Recovery, Tulsa, April 20-23.

Holm, L. W. and Josendal, V. A. 1974, "Mechanisms of Oil Displacement by Carbon Dioxide," J. Pet. Tech. 16 (December) 1427-1438.

Johnson, J. P. and Pollin, J. S. 1981, "Measurement and Correlation of CO₂ Miscibility Pressures," SPE 9790, presented at SPE/DOE Symposium on Enhanced Oil Recovery, Tulsa, April 5-8.

Kazemi, H., Vestal, C. R., and Shank, G. D. 1978, "An Efficient Multicomponent Numerical Simulator," Soc. Pet. Eng. J. 18 (October) 355-368.

Lacey, J. W., Draper, A. L., and Binder, G. G., Jr. 1958, "Miscible Fluid Displacement in Porous Media," Trans. AIME 213, 76.

Mason, W. P. 1947, "Measurement of the Viscosity and Shear Elasticity of Liquids by Means of a Torsionally Vibrating Crystal," Trans. A.S.M.E. (May) 359-370.

McDonald, R. C. 1971, "Numerical Simulation with Interphase Mass Transfer," Report No. U7-71-a, Texas Petroleum Research Committee, Austin.

- Metcalf, R. S. and Yarborough, L. 1979, "The Effect of Phase Equilibria on the CO₂ Displacement Mechanism," Soc. Pet. Eng. J. 19 (August) 242-252.
- Michels, A., Botzen, A., and Schuurman, W. 1957, "The Viscosity of Carbon Dioxide Between 0°C and 75°C at Pressures up to 2000 Atmospheres," Physica 23, 95-102.
- Newitt, D. M., Pai, M. U., Kuloor, N. R., and Huggill, J. A. 1956, "Carbon Dioxide" in Thermodynamic Functions of Gases, Vol. 1., F. Din, Ed., Butterworths, London, 102-134.
- Nolen, J. S. 1973, "Numerical Simulation of Compositional Phenomena in Petroleum Reservoirs," SPE 4274, presented at SPE 3rd Symposium on Numerical Simulation, Houston, January 11-12.
- Orr, F. M., Jr. 1980, "Simulation of One-Dimensional Convection of Four Phase, Four Component Mixtures," Topical Report DOE/ET/12082-8, U.S. Department of Energy, Bartlesville, Oklahoma.
- Orr, F. M., Jr., Lien, C. L., and Pelletier, M. T. 1981, "Liquid-Liquid Phase Behavior in CO₂-Hydrocarbon Systems," Symposium on Chemistry of Enhanced Oil Recovery, American Chemical Society, Atlanta, March 29-April 3.
- Orr, F. M., Jr., Silva, M. K., Lien, C. L., and Pelletier, M. T. 1980, "Laboratory Experiments to Evaluate Field Prospects for CO₂ Flooding," SPE 9534, presented at Eastern Regional Meeting, Morgantown, November 5-7.
- Orr, F. M., Jr. and Taber, J. J. 1981, "Displacement of Oil by Carbon Dioxide," Final Report to the U.S. Department of Energy, Report No. DOE/ET/12082-9 (May).
- Orr, F. M., Jr., Yu, A. D., and Lien, C. L. 1981, "Phase Behavior of CO₂ and Crude Oil in Low Temperature Reservoirs," Soc. Pet. Eng. J. 21 (August) 480-492.
- Pelletier, M. T. 1981, "Compatibility of Gold and Platinum Electrode Materials with High Pressure CO₂-Crude Oil Mixtures," PRRC Report 81-34, Petroleum Recovery Research Center (September).
- Perkins, T. K. and Johnston, D. C. 1963, "A Review of Diffusion and Dispersion in Porous Media," Soc. Pet. Eng. J. 3 (March) 70-75.
- Perrine, R. L. 1961, "The Development of Stability Theory for Miscible Liquid-Liquid Displacement," Soc. Pet. Eng. J. (March) 17-25.
- Raimondi, P. and Torcaso, M. A. 1964, "Distribution of the Oil Phase Obtained Upon Imbibition of Water," Soc. Pet. Eng. J. (March) 49-55.
- Raimondi, P., Torcaso, M. A., and Henderson, J. H. 1961, "The Effect of Interstitial Water on the Mixing of Hydrocarbons during a Miscible Displacement Process," Mineral Industries Experimental Station Circular No. 61, The Pennsylvania State U., University Park (October 23-25).

Rathmell, J. J., Stalkup, F. I., and Hassinger, R. C. 1971, "A Laboratory Investigation of Miscible Displacement by Carbon Dioxide," SPE 3483, presented at SPE 46th Annual Fall Meeting, New Orleans, October 3-6.

Reamer, H. H. and Sage, B. H. 1963, "Phase Equilibria in Hydrocarbon Systems. Volumetric and Phase Behavior of the n-Decane-CO₂ System," J. Chem. Eng. Data 8 No. 4, 508-513.

Rose, W. 1964, "Dead-End Pore Volume and Dispersion in Porous Media: Discussion," Soc. Pet. Eng. J. (September) 282-283.

Saffman, P. G. and Taylor, G. I. 1958, "The Penetration of a Fluid into a Porous Medium or Hele-Shaw Cell Containing a More Viscous Liquid," Proc. 245, Royal Soc., London, 312.

Settari, A., Price, H. S., and Dupont, T. 1977, "Development and Application of Variational Methods for Simulation of Miscible Displacement in Porous Media," Soc. Pet. Eng. J. 17 (June) 228-246.

Shelton, J. L. and Schneider, F. N. 1975, "The Effects of Water Injection on Miscible Flooding Methods Using Hydrocarbons and Carbon Dioxide," Soc. Pet. Eng. J. 15 (June) 217-226.

Sigmund, P. M., Aziz, K., Lee, J. J., Nghiem, L. X., and Mehra, R. 1979, "Laboratory CO₂ Floods and Their Computer Simulation," World Petroleum Congress, Bucharest, Romania, September.

Silva, M. K., Lien, C. L., Pelletier, M. T., and Orr, F. M., Jr. 1981a, "Phase Compositions of Mixtures of CO₂ with Maljamar Recombined Reservoir Fluid at 90°F and 2500 psig," PRRC Report 81-8, Petroleum Recovery Research Center (March).

Silva, M. K., Lien, C. L., Pelletier, M. T., and Orr, F. M., Jr. 1981b, "Phase Compositions of Mixtures of CO₂ with Maljamar Separator Oil at 90°F and 1400 psig," PRRC Report 81-9, Petroleum Recovery Research Center (March).

Silva, M. K., Lien, C. L., Pelletier, M. T., and Orr, F. M., Jr. 1981c, "Phase Compositions of Mixtures of CO₂ with Maljamar Separator Oil at 90°F and 1200 psig," PRRC Report 81-10, Petroleum Recovery Research Center (March).

Silva, M. K., Lien, C. L., Pelletier, M. T., and Orr, F. M., Jr. 1981d, "Phase Compositions of Mixtures of CO₂ with Maljamar Separator Oil at 90°F and 800 psia," PRRC Report 81-30, Petroleum Recovery Research Center (July).

Spence, A. P. and Watkins, R. W. 1980, "The Effect of Microscopic Core Heterogeneity on Miscible Flood Residual Oil Saturation," SPE 9229, presented at 55th Annual Fall Meeting of SPE of AIME, Dallas, September 21-24.

Stalkup, F. I. 1978, "Carbon Dioxide Miscible Flooding: Past, Present and Outlook for the Future," J. Pet. Tech. 30 (August) 1102-1112.

Stalkup, F. I. 1970, "Displacement of Oil by Solvent at High Water Saturation," Soc. Pet. Eng. J. 10 (December) 337-348.

Taylor, G. I. 1953, "Dispersion of Soluble Matter in Solvent Flowing Slowly Through a Tube," Proc. 219, Royal Soc., London, 186.

Thomas, G. H., Countryman, G. R., and Fatt, I. R. 1963, "Miscible Displacement in a Multiphase System," Soc. Pet. Eng. J. 3 (September) 189-196.

Todd, M. R. 1979, "Modeling Requirements for Numerical Simulation of CO₂ Recovery Processes," SPE 7998, presented at the California Regional Meeting of SPE, Ventura, April 18-20.

Todd, M. R. and Longstaff, W. J. 1972, "The Development, Testing and Application of a Numerical Simulator for Predicting Miscible Flood Performance," J. Pet. Tech. 24 (July) 874-882.

Watkins, R. W. 1978, "A Technique for the Laboratory Measurement of Carbon Dioxide Unit Displacement Efficiency in Reservoir Rock," SPE 7474, presented at SPE 53rd Annual Fall Meeting, Houston, October 1-3.

Webeler, R. W. H. 1961, "Viscosity X Density Measurements for Normal Liquid Hydrogen and Various Ortho-Para Mixtures," Ph.D. Thesis, University of Cincinnati.

Welber, B. 1960, "Damping of a Torsionally Oscillating Cylinder in Liquid Helium at Various Temperatures and Densities," Physical Review 119 No. 6 (September) 1816-1822.

Yellig, W. F. and Baker, L. E. 1980, "Factors Affecting Miscible Flooding Dispersion Coefficients," presented at the 31st Annual Technical Meeting of the Petroleum Society of CIM in Calgary, May 25-28.

Yellig, W. F. and Metcalfe, R. S. 1980, "Determination and Prediction of CO₂ Minimum Miscibility Pressures," J. Pet. Tech. 32 (January) 160-168.

RESEARCH PRESENTATIONS

"Laboratory Experiments to Evaluate Field Prospects for CO₂ Flooding," by F.M. Orr, Jr., Eastern Regional Meeting of SPE of AIME, Morgantown, WV, November 7, 1980.

"Laboratory Experiments to Evaluate Field Prospects for CO₂ Flooding," by F.M. Orr, Jr., Production Technology Symposium of SPE of AIME, Hobbs, NM, November 11, 1980.

"Enhanced Oil Recovery by CO₂ Flooding," by F.M. Orr, Jr., Carlsbad Section of AIME, Carlsbad, NM, November 18, 1980.

"Enhanced Oil Recovery by CO₂ Flooding," by F.M. Orr, Jr., Roswell Geological Society, Roswell, NM, November 20, 1980.

"Experimental Investigations of the Phase Behavior, Properties and Flow Behavior of CO₂-Crude Mixtures at Reservoir Conditions," by F.M. Orr, Jr., United Kingdom Atomic Energy Establishment, Winfrith, Dorchester, England, January 6, 1981.

"Experimental Investigations of the Phase Behavior, Properties and Flow Behavior of CO₂-Crude Mixtures at Reservoir Conditions," by F.M. Orr, Jr., Department of Petroleum Engineering, Heriot-Watt University, Edinburgh, Scotland, January 8, 1981.

"Experimental Investigations of the Phase Behavior, Properties and Flow Behavior of CO₂-Crude Mixtures at Reservoir Conditions," by F.M. Orr, Jr., Societe Nationale Elf Aquitaine, Pau, France, January 15, 1981.

"Continuous Measurement of Phase Compositions for CO₂-Crude Oil Mixtures," by F.M. Orr, Jr., Research and Development Department, ARCO Oil and Gas, Plano, Texas, February 9, 1981.

"Liquid-Liquid Phase Behavior in CO₂-Hydrocarbon Systems," by F.M. Orr, Jr., C.L. Lien and M.T. Pelletier, Division of Petroleum Chemistry, Symposium on Enhanced Oil Recovery, American Chemical Society, Atlanta Meeting, March 31, 1981.

"Phase Behavior of CO₂-Crude Oil Mixtures," by F.M. Orr, Jr., Department of Petroleum Engineering, University of Texas, Austin, Texas, April 21, 1981.

"Phase Behavior of CO₂-Hydrocarbon Systems: Measurement by Continuous Multiple Contacts," by F.M. Orr, Jr., Department of Chemical Engineering and Materials Science, University of Minnesota, Minneapolis, Minnesota, May 29, 1981.

"Dispersion, Trapping and Dead End Pores," by F.M. Orr, Jr., Department of Petroleum Engineering, Heriot-Watt University, Edinburgh, Scotland, June 5, 1981.

RESEARCH PARTICIPANTS

<u>Name</u>	<u>Title</u>	<u>Background</u>	<u>Research Activities</u>
F.M. Orr, Jr.	Principal Investigator	B.Sc., Ph.D. Chemical Engineering	Overall project supervision, analysis and simulation of multicomponent multiphase flow in porous media
J.J. Taber	Principal Investigator	B.Sc., Ph.D. Chemistry	Senior Advisor on all aspects of project
C.L. Lien	Research Chemist	B.Sc., Ph.D. Chemistry	Sampling and analytical techniques for CO ₂ -crude oil systems
R.E. Bretz	Research Engineer	B.Sc. Chemical Engineering Ph.D. Bio-Engineering	Core flood measurements of effects of trapping, dispersion, and dead-end pores
M.K. Silva	Research Assistant	B.Sc., Basic Science	Continuous multiple contact measurements of phase compositions and fluid properties
C.M. Jensen	Research Assistant	B.Sc., Chemistry	PVT experiments for CO ₂ -crude oil systems
M.L. Graham	Research Assistant	B.Sc., Biology	Core flood experiments
M.T. Pelletier	Undergraduate Research Assistant	Senior, Metallurgy	Instrumentation, high pressure equipment design and construction
B.T. Campbell	Graduate Research Assistant	B.Sc., Geology	Flow visualization for CO ₂ -crude oil displacements
S.M. Linert	Undergraduate Research Assistant	Sophomore, Petroleum Engineering	Preparation of hydrocarbon samples for analysis
J.C. Franklin	Undergraduate Research Assistant	Senior, Computer Science	Software for data acquisition, microprocessor control of laboratory equipment
D.J. Callahan	Graduate Research Assistant	B.Sc., Geology	Simulation of CO ₂ flood performance
R.M. Specter	Graduate Research Assistant	B.Sc., Geology	Evaluation of reservoir core material